PART I: EFFECT OF NANOMICELLE SIZE ON TRANS-SCLERAL PERMEABILITY OF DEXAMETHASONE.

AND

PART II: STRATEGIES TO MINIMIZE OCTREOTIDE ACYLATION DURING SUSTAINED RELEASE FROM BIODEGRADABLE POLYMERS.

A DISSERTATION IN
Pharmaceutical Sciences
and
Chemistry

Presented to the Faculty of University
of Missouri - Kansas City in partial fulfillment of
the requirements for the degree

DOCTOR OF PHILOSOPHY

By

RAVI D. VAISHYA

B. Pharm. Hemchandracharya North Gujarat University, India, 2007
Kansas City, Missouri
2015

PART I: EFFECT OF NANOMICELLE SIZE ON TRANS-SCLERAL PERMEABILITY OF DEXAMETHASONE.

Ravi D. Vaishya, Candidate for the Doctor of Philosophy Degree

University of Missouri-Kansas City, 2015.

ABSTRACT

Our primary aim was to determine the effect of nanomicelle size on dexamethasone (DEX) transport across the sclera. Nanomicelles of various sizes were developed and characterized. Low molecular weight diblock co-polymers, $mPEG_{750}$-PCL_{700} (DB1), $mPEG_{2000}$-PCL_{1500} (DB2) and $mPEG_{5000}$-PCL_{4000} (DB3) were synthesized by ring opening polymerization. Polymers were characterized by H^1 NMR (structure), gel permeation chromatography (molecular weights and polydispersity), critical micelle concentration (CMC) and *in vitro* cytotoxicity studies in corneal, conjunctival and retinal cell-lines. Newly synthesized polymers were purified and characterized for their structure and molecular weights by H^1-NMR and GPC, respectively. The CMCs were found to be 0.13, 4.48 and 6.04 μg/mL for DB1, DB2 and DB3, respectively. In order to understand the factors and interactions influencing drug solubilization in micelle core, an exploratory 2-factors 3-level response surface methodology was generated using SAS 9.02 (exploratory model). The independent factors were polymer amount (X1) and DEX amount (X2). Solubility of DEX in micelle solution was taken as response variable (Y). Micelle preparation method was modified based on the results obtained from exploratory model. The optimal drug:polymer ratio was identified by another response surface design (optimization model) to achieve DEX solubility of 1mg/mL for all the nanomicellar formulations. The optimized formulation was characterized for solubility of DEX, micelle size and polydispersity, morphology, *in vitro* release and *in vitro* transport across conjunctival cell line. Nanomicellar formulations

(referred to as DEXM) containing >1mg/mL DEX were developed for all three polymers using design of experiment. The optimized nanomicelle formulation exhibited mean size in range of 10nm, 30nm and 60nm with unimodal size distribution and low polydispersity for DB1, DB2 and DB3 polymers, respectively. The formulation was also subjected to *ex vivo* transport across excised rabbit sclera to determine influence of micelle size on DEX transport across the static barrier. DEX permeability across the excised rabbit sclera for DEXM and DEX suspension (control) were found to be $2.7x10^{-6}$, $3.0x10^{-6}$, $1.5x10^{-6}$ and $1.2x10^{-6}$ cm/sec, respectively. There were 2.2, 2.5 and 1.3-fold increase in DEX permeability with nanomicelles of mean sizes 10 nm, 25 nm and 60 nm, respectively.

The permeability studies across the sclera, static barrier, indicates that the nanomicelles with average sizes 10nm and 30nm may have potential to deliver therapeutic agents to the back of the eye following topical administration. Therefore, nanomicellar formulation may provide therapeutic levels in the back of the eye following topical administration.

PART II: STRATEGIES TO MINIMIZE OCTREOTIDE ACYLATION DURING SUSTAINED RELEASE FROM BIODEGRADABLE POLYMERS.

Ravi D. Vaishya, Candidate for the Doctor of Philosophy Degree

University of Missouri-Kansas City, 2015.

ABSTRACT

Overall aim of this research was to minimize acylation of octreotide during sustained release from biodegradable polymers. Polymeric microparticle (MPs)-in-gel formulations for extended delivery of octreotide were developed. Polymer modification and reversible hydrophobic Ion-Pairing (HIP) complex strategies were investigated to achieve-mentioned goals. Polycaprolactone (PCL), polylactic acid (PLA) and polyglycolic acid (PGA) based triblock (TB = PCL10k-PEG2k-PCL10k) and pentablock (PB; PBA = PLA3k-PCL7k-PEG2k-PCL7k-PLA3k and PBB = PGA3k-PCL7k-PEG2k-PCL7k-PGA3k) polymers were synthesized and characterized for structure, molecular weight and physical state. Octreotide was encapsulated in TB, PBA and PBB MPs using methanol-oil/water emulsion solvent evaporation method. Sodium dodecyl sulfate (SDS), dextran sulfate (DS; Mw 9-20kDa (DSA) and Mw 36-50kDa (DSB)) were used as ion-pairing agents to prepared reversible HIP complex with octreotide. Mechanics of HIP complex formation and dissociation were investigated. DSA-octreotide and DSB-octreotide complex encapsulated PLGA (50/50) microparticles (MPs) were prepared using S/O/W emulsion method. MPs were characterized for size, morphology, encapsulation efficiency, drug loading and *in vitro* release. Release samples were subjected to LC analysis for quantitation and LC-MS analysis for identification of native and chemically modified species. A significant fraction of released octreotide was acylated from lactide and glycolide based PBA (53%) and PBB (92%) polymers. Substantial amount of peptide was not released from PBB polymers after 330 days of incubation.

Complete release of octreotide was achieved from TB polymer over a period of 3 months with minimal acylation of peptide (~13%). Release of octreotide was sustained for 55 days for HIP complex-encapsulated MPs. A large fraction of peptide was released in chemically intact form (m/z 1019.3 and m/z 510.3) and <7% peptide was acylated from DSA-octreotide and DSB-octreotide encapsulated MPs. Polycaprolactone based polymers may be appropriate for extended peptide delivery. Conversely, polymers having PLA and PGA blocks may not be suitable for peptide delivery due to acylation and incomplete release. Reversible HIP complex is a viable strategy to maintain chemical stability of peptide during long-term delivery from PLA and PGA based polymers.

APPROVAL PAGE

The faculties listed below, appointed by the Dean of the School of Graduate Studies have examined a dissertation titled "Effect of Nanomicelle Size on Trans-scleral Permeability of Dexamethasone and Strategies to Minimize Octreotide Acylation during Sustained Release from Biodegradable Polymers." presented by Ravi D. Vaishya, candidate for the interdisciplinary Doctor of Philosophy degree and certify that in their opinion it is worthy of acceptance.

Supervisory Committee

Ashim K. Mitra, Ph.D., Committee Chair
Department of Pharmaceutical Sciences

Simon Friedman, Ph.D.
Department of Pharmaceutical Sciences

Kun Cheng, Ph.D.
Department of Pharmaceutical Sciences

J. David Van Horn, Ph.D.
Department of Chemistry

Russell B. Melchert, Ph.D., R.Ph
Department of Pharmacology and Toxicology

TABLE OF CONTENTS

LIST OF ILLUSTRATIONS

PART I: EFFECT OF NANOMICELLE SIZE ON TRANS-SCLERAL PERMEABILITY OF DEXAMETHASONE.

Figures

Figures

Figures

Figures

Figures

PART II: STRATEGIES TO MINIMIZE OCTREOTIDE ACYLATION DURING SUSTAINED RELEASE FROM BIODEGRADABLE POLYMERS.

Figures

Figures

LIST OF TABLES

PART I: EFFECT OF NANOMICELLE SIZE ON TRANS-SCLERAL PERMEABILITY OF DEXAMETHASONE.

Tables

Tables

PART II: STRATEGIES TO MINIMIZE OCTREOTIDE ACYLATION DURING SUSTAINED RELEASE FROM BIODEGRADABLE POLYMERS.

ACKNOWLEDGEMENTS

I would like to express my immense gratitude towards my mentor Dr. Ashim K. Mitra for his exceptional support and motivation during my graduate studies. His guidance was critical in solving a number of scientific challenges. I deeply appreciate him for encouragement and believing in me that helped me to develop critical thinking as a scientist. I would also like to extend my gratitude to members of my supervisory committee Drs. Kun Cheng, J. David Van Horn, Simon Friedman and Russell B. Melchert for their constant support, discussions on my research and valuable critics on my dissertation. It is my honor to have such extraordinary scientists and researchers as a part of my supervisory committee. I am greatly thankful to Dr. Dhananjay Pal for support in the laboratory and scientific discussions. I would also like to extend my appreciation to Mrs. Ranjana Mitra for her continuous support and timely help during my stay at UMKC. My special thanks to Dr. Jacob Marszalek, who served on my committee and explained me interpretation of statistical design of experiments, which gave me confidence to present my research data at various international conferences. I am grateful to Dr. Russell B. Melchert for being supportive and agreeing to serve on my supervisory committee on a short notice.

I am greatly thankful to Dr. Sulabh Patel, Dr. Varun Khurana, Dr. Mitan Gokulgandhi, Dr. VK Chaithanya Ponnaluri, Dr. Divya Teja Vavilala, Dr. Kalpesh Patel, Dr. Deep Kwatra, Rakesh Awasthi, Saurabh Goyal, Ashwin Parenky and Sujay Shah for being supportive friends. I thankful to my colleagues Dr. Mitesh Patel, Animikh Ray, Mary Joseph, Vibhuti Agrahari, Dr. Ashwani Dutt Vadlapudi, Xiaoyan Yang and Kishore Cholkar for their timely help and creating such a cheerful environment in the lab throughout my studies. My special thanks to Drs. Ripal Gaudana, Deep Kwatra, Sriram Gunda and Nanda Kishore Mandava for their valuable suggestions on my research projects.

I sincerely appreciate constant support of Joyce Johnson, Sharon Self, Ashley Ismert, Tamica Lige, Shana Eisentrager and Nancy Bahner in administrative assistance throughout my stay at UMKC. I appreciate support from Nancy Hoover from School of Graduate Studies and National Institute of Health for financial support. I would also like to thank Dr. James B. Murowchick (School of Geological Sciences) for helping in XRD analysis. I would also like to thank Elise Chapline from UMKC Counseling Center for her time in my personal development.

My special gratitude towards my parents Anandi Vaishya and Dhirajlal Vaishya and brother Himanshu Vaishya for their support and love. At last, I would like to thank Rutva Trivedi for being patient with me, sharing happiness and sorrows, great food, encouragement and advice.

Dedicated to My Family

PART I: EFFECT OF NANOMICELLE SIZE ON TRANS-SCLERAL PERMEABILITY OF DEXAMETHASONE.

CHAPTER 1

1. LITERATURE REVIEW[1]

1.1. Ocular anatomy

The eye can be broadly divided into two sections, (i) anterior segment and (ii) posterior segment (Figure 1-1). The anterior segment encompasses the cornea, conjunctiva, iris, ciliary body and lens. The posterior segment consists of the sclera, choroid, retina and vitreous humor. A brief description of these ocular tissues is provided in following section.

Cornea: It is the outermost transparent multilayered membrane of the eye. It is devoid of blood vessels and obtains its nourishment from aqueous humor and limbal blood capillaries. Thickness of human cornea is around 0.5 mm and it comprises of five layers i.e. corneal epithelium, Bowman's membrane, stroma, Descemet's membrane and endothelium (arranged in the order of outermost to innermost) [2]. The epithelial layer comprises of five to six layers of columnar cells. The first layer is composed of non-keratinized squamous cells. These cells have intercellular tight junctions. The innermost layer of columnar cells is known as germinal layer. Bowman's layer and stroma (substantia propria) are mostly composed of collagen fibrils. Descemet's membrane is a thick basal lamina sandwiched between stroma and endothelium. The endothelium represents a monolayer of squamous cells [2].

Iris: It consists of pigmented epithelial cells and circular muscles (constrictor iridial sphincter muscles). These muscles cause miosis or constriction of the pupil by the action of cholinergic nerves. Iris also contains the dilator muscles , responsible for dilation of the pupils upon sympathetic stimulation [3].

Ciliary body: It is comprised of ciliary muscles and processes. Ciliary muscles have fibrous bundles and are highly flexible. Non-pigmented epithelial cells form the blood-aqueous barrier, which restricts the movement of proteins and colloids into the aqueous humor [3].

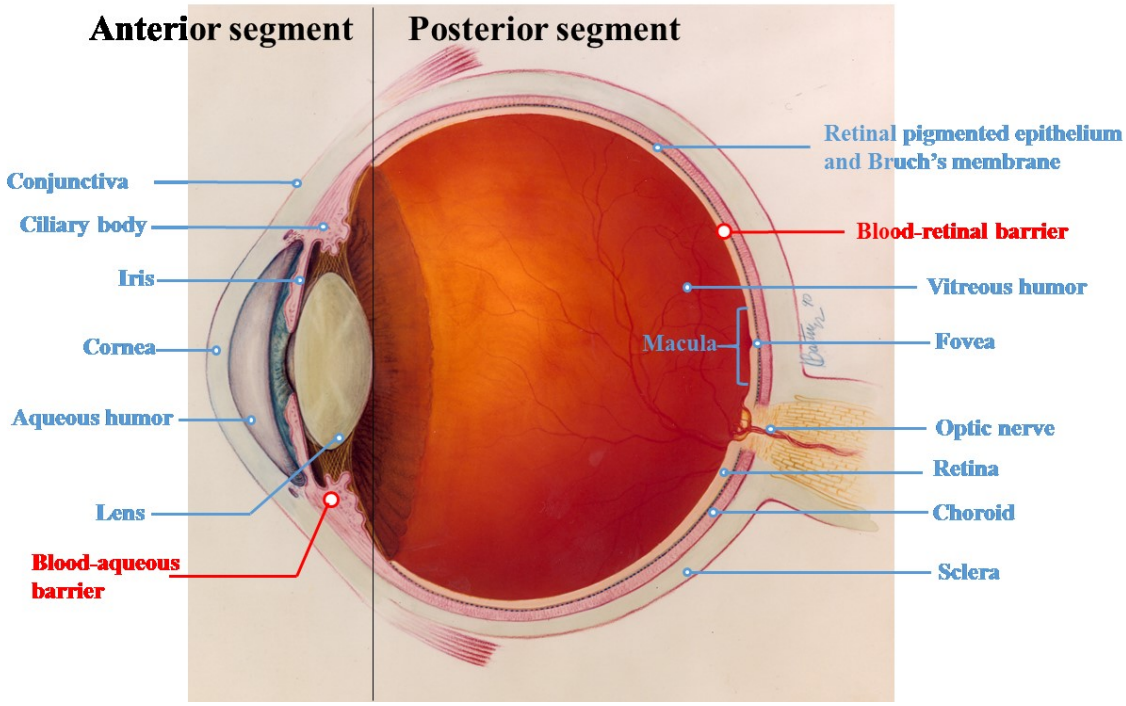

Figure 1-1 Anatomy of the EYE. Credit: *National Eye Institute*.

Conjunctiva: It consists of a clear mucous membrane. This layer is divided into three parts i.e. palpebral, fornical, bulbar, and an underlying basement membrane. The tissue lines the inside of eyelids and spreads from the anterior surface of sclera (white part of the eye) up to the limbus. It is composed of non-keratinized stratified columnar epithelial cells. It helps lubricate the eye by producing mucus and tears [3].

Sclera: It represents a matrix above the choroid, which principally shields the internal organs of the eye. Its thickness varies from 0.5 to 1 mm and mainly consist of collagen bundles with dispersed melanocytes and elastic fibers [4]. The sclera is a porous tissue and hence permeability of molecules have been observed to be inversely proportional to molecular weight[5]. In addition, as these porous channels are filled with water, transport of hydrophilic molecules is favored over hydrophobic ones[5].

Choroid: It is sandwiched layer between retina and sclera. This layer is a highly vascularized tissue. It is further sub divided into vessel layer, choriocapillaries and Bruch's membrane. The vessel layer comprises of arteries and veins, whereas choriocapillaries, as the name suggests is a dense network of capillaries. Bruch's membrane is situated between choroid and retinal-pigmented epithelium (RPE). It is composed of basal lamellae of RPE and the endothelial cells of choroid [6].

Retina: It is a light sensitive tissue comprising of two major layers i.e. (RPE) and neurosensory retina. RPE is directly in contact with the light sensing neural cells rods and cones. These cells are further associated with bipolar and ganglionic cells. The optic nerve is linked with the ganglionic cells, which are further coupled to amacrine cells. RPE functions as a nutrient source to the retina via the choroid. It forms a tight junction flanked by the choroid and retina. RPE cells also aid in the elimination of damaged photoreceptors via phagocytosis. Inner part of the neurosensory retina mainly obtains its blood supply from the

retinal artery, whereas the outer portions fulfill their nutritional requirements by the choriocapillaries [6a].

Vitreous humor: It is a hydrogel matrix, localized between retina and lens. This matrix is separated from the anterior segment by anterior hyaloids membrane and is linked through ligaments to the retina. The vitreous consists of hyaluronic acid and collagen fibrils. However, cortical region contains dispersed hyalocytes. Vitreous humor is about 98 to 99.7% water and pH is around 7.5 [7].

1.2. Barriers to ocular drug delivery (ODD) [8]

Bioavailability of a dosage form in general is the percentage of the drug that absorbs and reaches the potential site of action regardless of the route of administration. The US Food and Drug Administration defines bioavailability as "the rate and extent to which the active ingredient or active moiety is absorbed from a drug product and becomes available at the site of action. For drug products that are not intended to be absorbed into the bloodstream, bioavailability may be assessed by measurements intended to reflect the rate and extent to which the active ingredient or active moiety becomes available at the site of action." Since pharmacological response is related to the amount of drug at the site of action, the availability of a drug from a formulation plays a critical role in deciding its clinical efficacy. However, the amount of drug normally cannot be measured directly at the site of action. Hence, most of the bioavailability studies involve the determination of drug concentration in the blood or urine assuming that the drug at the site of action is in equilibrium with the drug in the blood [9]. Even though bioavailability is often interpreted as the percentage of the drug absorbed into the bloodstream, the blood levels in topical delivery (such as ophthalmic and dermatologic delivery) are generally used only to monitor side effects and toxicities and not as an indication of therapeutic efficacy.

For ocular considerations, both systemic and ocular bioavailability is important as ophthalmologists use both systemic and topical medications. However, a number of medications given orally to treat ocular infections is considerably less as most of the dosage forms are given either topically or by other drug delivery systems like site-specific injections. Some of the medications given intravenously suffer from poor ocular bioavailability and result in systemic side effects. Ocular drug delivery can be broadly classified into anterior segment drug delivery and posterior segment drug delivery. Understanding of the anatomical features of both these segments of the eye is vital in enhancing the efficacy of the drug product and bypassing the ocular barriers, which can negatively affect the bioavailability of the formulation.

In spite of continued investigation of new drug delivery systems and frequent introduction of novel ophthalmic drugs, ocular drug delivery does not seem to progress at the same pace, which is typical of other delivery systems, such as oral, transdermal or transmucosal. The ocular delivery systems normally suffer from low bioavailability, poor patient compliance and systemic side effects. Poor bioavailability of formulations delivered topically to the anterior segment of the eye is due to efficient protective mechanisms, which ensure the proper functioning of the eye. It is also due to other concomitant factors such as short residence time as a result of rapid and efficient drainage by the nasolacrimal apparatus; non-corneal absorption; and relative impermeability of the cornea to both hydrophilic and hydrophobic molecules. Because of these mechanisms and factors, the rate of drug loss from the ocular surface can be 500 to 700 times greater than the rate of absorption into the anterior chamber, and 1-5% or less of the drug from the topically applied solutions reaches the anterior segment. Drug delivery to the posterior segment itself is a great challenge along with ocular bioavailability considerations.

Inefficiency of the current ocular drug products and an increased understanding of ocular drug absorption mechanisms have spurred researchers to design novel ways to enhance ocular bioavailability. Various approaches to increase the ocular bioavailability following topical instillation can broadly be divided into two categories. The first one is based on the use of sustained and novel drug delivery systems, such as implants, microspheres, nanoparticles, liposomes, *in-situ* gels, collagen shields, etc. These carriers prolong the precorneal residence time and provide the continuous and controlled delivery of drugs. The second approach involves maximizing corneal drug absorption/penetration by different strategies such co-administration of therapeutic agents and rational prodrug derivatization, which can improve the physicochemical properties of the active moiety and has the potential to bypass the efflux pumps. Prodrugs can further be targeted to influx transporters present on the ocular surfaces.

Entry of drugs into the ocular tissues is restricted because of its unique anatomy and physiology. Several factors such as precorneal clearance of drugs, low corneal permeability and blood ocular barrier (BOB) deter the ocular bioavailability. These factors will be discussed in the following section.

Precorneal factors

Topically instilled conventional dosage forms have a very short precorneal residence time and poor ocular bioavailability (less than 5%). It is attributed to precorneal factors such as tear film, tear drainage, dilution by tear flow, reflux blinking and drainage of the formulation due to gravity. Upon instillation, the drug solution is diluted due to lachrymal secretion and tear flow. As most of the drugs cross the cornea by simple diffusion, the tear dilution decreases the concentration gradient, which is the driving force for passive absorption of drugs. Therefore, repeated administration is desired to maintain therapeutic drug level. Tears deliver the majority of nutrition and oxygen to cornea and remove the

metabolic waste of avascular corneal epithelium and anterior stroma [10]. In an anatomical perspective, tear film is composed of three layers namely the inner most mucin film, middle aqueous layer and the outer oily layer that retards the evaporation of the water from tear film. Lachrymal gland contributes to the aqueous portion of tear film, goblet cells of conjunctiva provide mucin and meibomian gland in the eyelid supplies oil. The action of blinking continuously maintains tear film and drainage ducts present in the eye removes the excess tear. Aston et al. studied permeability of β-blockers across cornea and conjunctiva and found that the conjunctival permeability was higher for all the drugs used than the corneal permeability [11]. It was inferred that tear film, in conjunction with cornea, limits the permeability of drugs[12].

While using topical instillation, a considerable amount of drug is lost through reflux blinking and reflux tearing. This phenomenon occurs because of some discomfort or irritation to the eye when the patient instills the formulation. The reasons for this discomfort or irritation can be a component of the formulation, pH of the formulation, osmolarity difference etc. When the drop volume is high, the nasolacrimal drainage and drainage due to gravity are the major pathways by which the drug is lost.

Cornea as a barrier

Cornea is 1 mm thick near limbus and 0.5 mm thick in the center [13]. For the drugs instilled topically, the corneal route is considered as a major route for the absorption, despite of its poor permeability. Steroids, like dexamethasone are used for various ocular diseases, and have a poor corneal permeability. In an *in vitro* transport experiment, using excised rabbit corneas, the permeability of dexamethasone was found to be $5x10^{-6}$ cm/sec. Poor permeability is due to the corneal epithelium, which has inter-cellular tight junctions. However, dexamethasone acetate, which is a prodrug, had permeability of $3.7x10^{-5}$ cm/sec [14] [15]. Most drugs cross the cornea by simple diffusion via paracellular or transcellular route.

However, there are distinct pathways for drug transport for hydrophilic and lipophilic drugs. Hydrophilic drugs were found more in intercellular spaces and lipophilic drugs were found more in lipid structures of the cells. This means that hydrophilic molecules prefer the paracellular route and the lipophilic molecules prefer the transcellular route [16]. Cornea consists of five different layers, namely corneal epithelium, bowman's membrane, corneal stroma, Descemet's membrane and endothelium [13]. The paracellular resistance across rabbit cornea is reported to be 12-16 $k\Omega cm^2$ [17]. Presence of these tight junctions makes the cornea a formidable barrier for the ionized molecules [18]. The Bowman's membrane is an acellular layer and divides epithelium and stroma. It is made up of collagen fibers and has a thickness of 8 to 14 μm. This layer makes a strong barrier. The corneal stroma is also composed of collagen fibers and has greatest thickness of all the layers. Unlike the Bowman's membrane and the corneal epithelium, this layer is hydrophilic and porous allowing rapid movement of hydrophilic molecules. Nevertheless, for the macromolecules and lipophilic drugs, it is a considerable barrier. Descemet's membrane is a basement membrane for corneal endothelium which is a one cell layer thick (5-10 μm) with phospholipids as a major content. The endothelium is in direct contact with the aqueous humor and control the movement of molecules from aqueous humor to the stroma. The cells of this layer also have high enzymatic activity. Due to phospholipids as a major constituent, endothelium is permeable to lipophilic molecules and nearly impermeable to ions.[18-19]

In summary, the corneal stroma is hydrophilic and allows the free passage of hydrophilic molecules and the epithelium is lipophilic and permits the passage of lipophilic molecules. The Descemet's membrane prefers hydrophobic molecules. Overall, the cornea as a whole is a formidable barrier for transport of drug, as it comprises of multiple layers with hydrophilic and hydrophobic character. Molecule must possess optimal solubility in both oil and water as well as should be in non-ionized form to be able to permeate through cornea.

Blood ocular barrier

The blood ocular barrier is a major barrier for the entry of the drug in to the eye and removal of the drug from the eye after systemic administration. BOB is comprised of blood aqueous barrier (BAB) and blood retinal barrier (BRB). These barriers are present to provide an immune privilege site to the delicate eye tissues. They restrict the entry of the pathogenic molecules into the eye and protect from the possibility of inflammation and tissue damage to the sensitive structures like retina and neurons. Overall, they control the movement of nutritional products, metabolic wastes and *exogenous* molecules and maintain an environment in which the visual cycle can work efficiently. The BAB is present in the anterior segment. The non-pigmented cell layer of ciliary epithelium and endothelial cells of blood vessels supplied to the iris, together constitute the BAB. Both these cellular layers have intercellular tight junctions. BAB is not considered as a complete barrier like BRB because of the fenestrated capillaries present on the ciliary processes. These capillaries are highly permeable and allow the passage of molecules with molecular weight 40 kDa, which cannot pass through the iris blood vessels[20]. The permeation of substances across the iris blood vessel from the aqueous humor is less restrictive and the iris tissue is quite porous. Therefore, the drugs present in the aqueous humor, especially small and lipophilic ones can easily enter the circulation and be eliminated from the anterior chamber[21].

BRB is present in the posterior segment and prevents the entry of the drug molecules from the blood circulation into the retina. The BRB is further divided into inner BRB and outer BRB. The outer BRB is formed by the monolayer of retinal-pigmented epithelium (RPE), which separates the neural retina from the choroidal blood circulation (Figure 1-2) [22]. Neural retina is firmly attached to the RPE that plays a major role in maintaining the viability of the retinal photoreceptors.

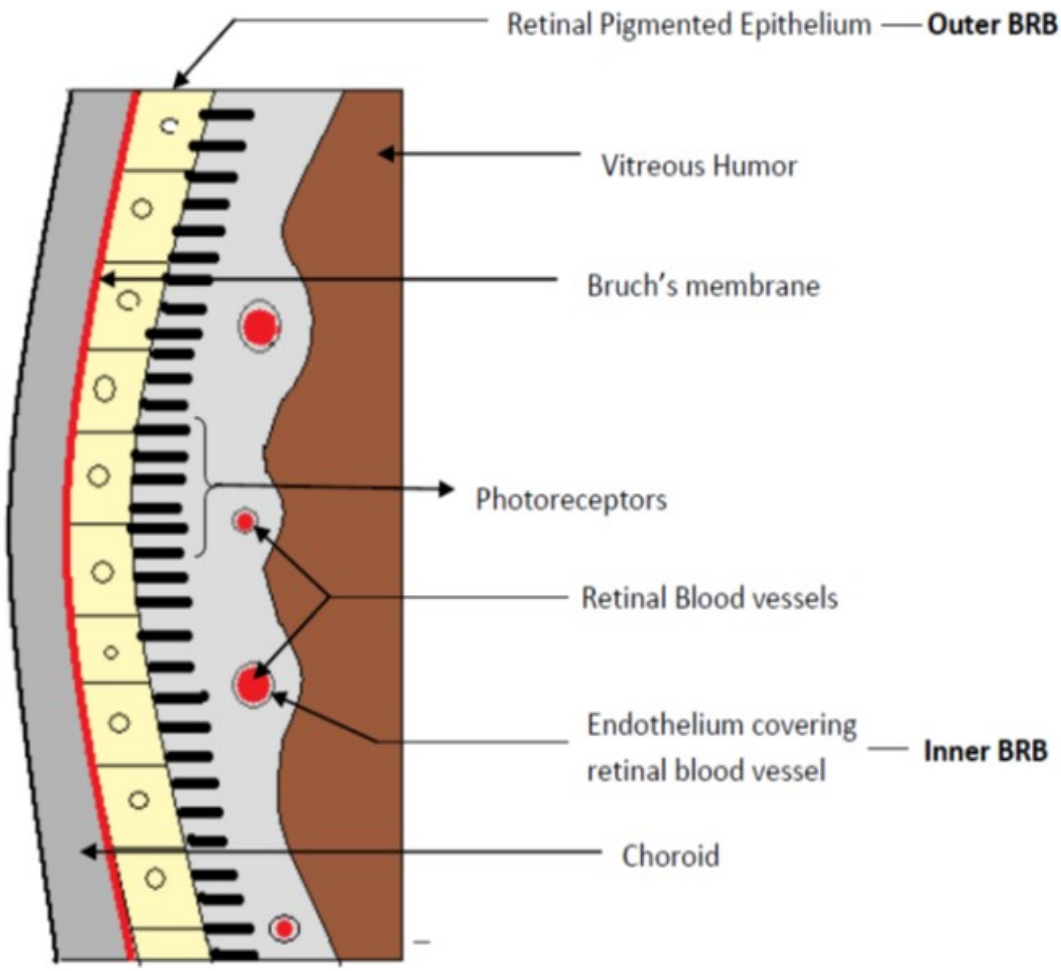

Figure 1-2 Schematic representation of inner BRB and outer BRB.

In nutshell, RPE is responsible for removal of the waste product of retina from subretinal space, retinoid transport and metabolism, absorption of light, synthesis of growth factors, enzymes and pigments, immunological role and very selectively allow the passage of nutritional molecules to retina from choroidal circulation.

The inner BRB is composed of the tight junctions between the endothelial cells of the retinal blood vessels (Figure 1-2). These endothelial cells separate the blood and the neural retina. The tight junctions are made up of proteins like zonulae occludente present between the endothelial cells [23]. The glial cells like Müller cells and astrocytes also cover the retinal blood vessels and generate the signals to stimulate the barrier properties of endothelial cells [24]. Anatomically, the inner BRB is quite similar to the blood brain barrier (BBB). In comparison to BBB, the inner BRB has more density of tight junctions and pericytes [25]. Due to presence of higher amount of pericytes, the retinal blood vessel permeability was 4 times more than that of brain [25]. The glial cells and the tight junctions of the endothelial cells together limit the entry of drugs into the retina through paracellular route and protect the neural retina [26]. BAB and BRB play an important role in limiting the bioavailability of systemic or periocular routes such as subconjunctival route, which are usually employed to overcome the limitations of topical route. Apart from acting as a physiological barrier, these ocular structures (especially cornea, inner BRB and RPE) also express some influx transporters, like peptide transporter, and efflux transporters like ATP binding cassette proteins. Transporters can increase or decrease the drug permeation and modulate the bioavailability and will be discussed in a separate section.

1.3. Routes of drug delivery [8]

Four modes of administration can be employed for drug delivery to the eye: topical, systemic, intraocular and periocular (including subconjunctival, Sub-Tenon's, retrobulbar and peribulbar) [27]. Figure 1-3 shows the various routes for Ocular drug delivery.

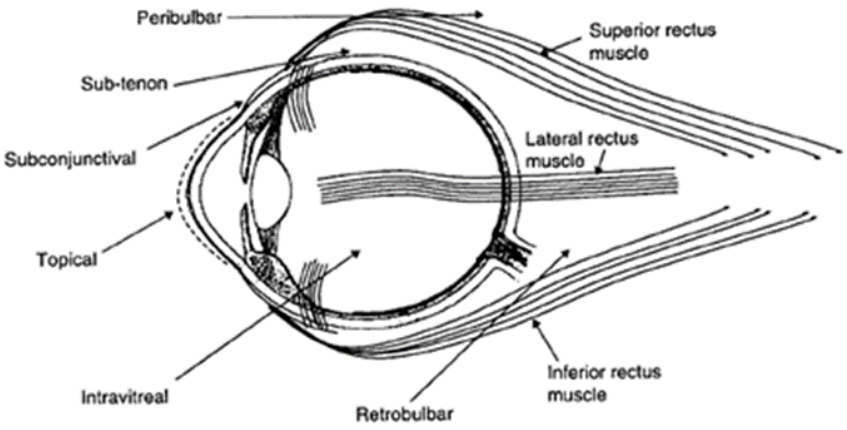

Figure 1-3 Schematic representation of local routes for ocular drug delivery.

Topical route

Topical route is the most common route to deliver medications for treating both surface and intraocular conditions. This route is often preferred over other routes for management of various pathological diseases affecting anterior chamber (i.e. cornea, conjunctiva, sclera, anterior uvea). Three reasons account for this: (a) convenience in administration (b) higher ratio of ocular to systemic drug level and (c) cost affordability. Solutions, emulsions, suspensions, ointments, and rate-control release systems (devices) are commonly used dosage forms administered by topical route [28]. Drug levels in intraocular tissues such as uveal track (choroid, iris and retina) is low due to precorneal factors and barrier properties of the cornea. Corneal and non-corneal (trans-scleral) are the two common routes of drug absorption following topical administration. Non-corneal/trans-scleral route specifically involves drug movement across the conjunctiva and sclera [28]. Corneal absorption is the main pathway for most ophthalmic drugs and it is considered to be a rate-limiting process due to the presence of corneal epithelium [29]. Lipophilicity and presence of tight junctions around the corneal epithelium cells reduces the entry of hydrophilic drug molecules into the corneal stroma. However, breaking tight epithelium junctions (e.g. by benzalkonium chloride) is one possible way of increasing hydrophilic drug penetration inside the stroma by paracellular pathway. On the other hand, lipophilic drug substances cross the corneal epithelium with ease but penetration into the hydrophilic corneal stroma is difficult [29]. However, in most of the pathological conditions, like intraocular inflammation and glaucoma, drug penetration into intraocular tissues is desirable [30].

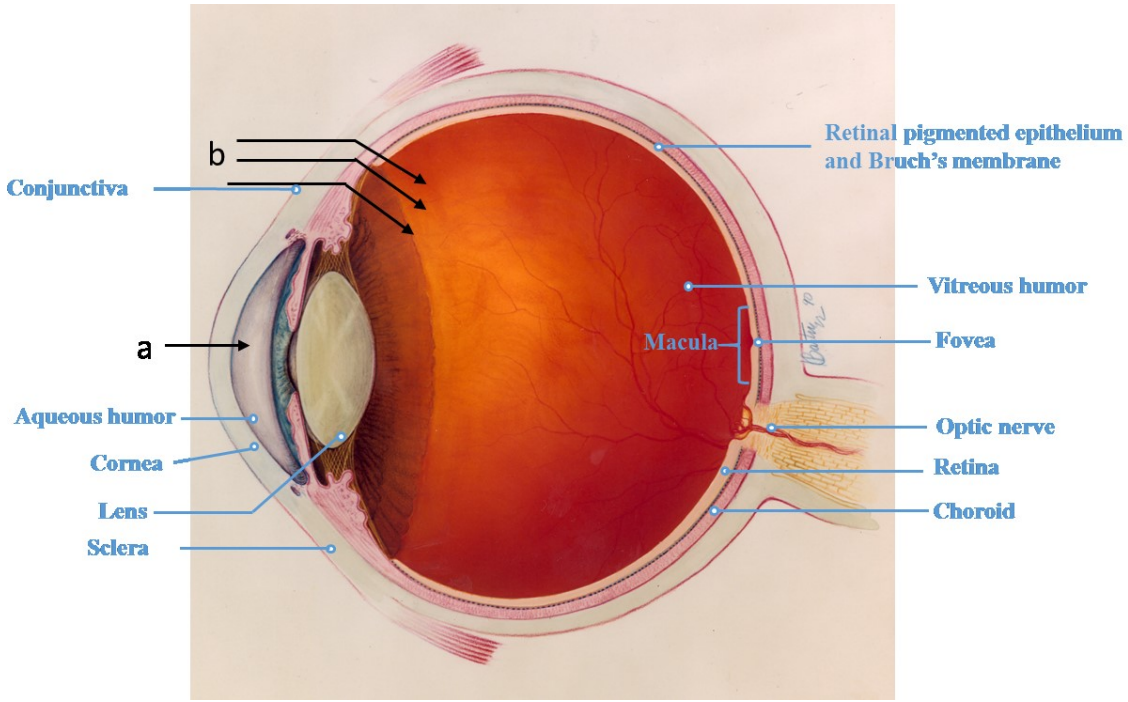

Figure 1-4 Pathways of absorption of drug into the eye following topical instillation. (a) Corneal pathway. Drugs transport through the cornea via passivie diffusion. Molecule must possess a balanced lipophilicity and hydrophilicity to have higher permeability. The drug transported across the cornea enters the aqueous humor, which is eliminated due to high aqueous humor turnover. Moreover, les is known to be lease permeable to drugs. (b) trans-corenal pathway. The conjucntiva and sclera are more permeable tissues compared to the corena. Once the drug crosses the sclera and enters the intraocular tissues, it may distribute in the surrounding tissues by diffusion.

Another path involves penetration across the conjunctiva and sclera (non-corneal route) into the intraocular tissues. However, it is a minor absorption pathway compared to the corneal route due to the presence of the local capillary beds that remove the drug from target sites into the blood circulation [31]. The conjunctival epithelium is a weaker barrier compared to the corneal epithelium. The rest that enters the sclera seems to have rather good access into the eye. The poorly vascularized sclera is significantly more permeable than the cornea. In general, the sclera does not form a very tight barrier to penetration of the solutes even of relatively large molecular weight [30-31]. Thus, ophthalmic drugs can be absorbed from conjunctiva and delivered to the eye via the sclera. However, drainage loss through blood vessels of the conjunctiva can greatly affect the conjunctival/scleral pathway. Nevertheless, it should be noted that the conjunctival epithelium is the most viable route for ocular delivery of peptides and oligonucleotides [32]. It is much harder to deliver drugs to the posterior segment because of membrane barriers. These barriers, in conjunction with nasolacrimal drainage of administered drops, drug metabolism, protein binding, lens barrier and long diffusional path lengths result in poor drug delivery to the retina following topical administration [33]. Moreover, the passage of drugs from the anterior segment to the posterior segment does not appear to be an efficient strategy because of the continuous drainage of the aqueous humor (i.e. a turnover of 2-3 mL/min). Thus, locally used ophthalmic therapies failed to provide an efficient pharmacological effect in the posterior segment (e.g. retina and vitreous) [31]. Many efforts have been directed towards enhancing the corneal permeability of the drug following topical administration. The application of high concentrations of penetration enhancer to increase the bioavailability may cause mucosal irritation and corneal abrasion, leading to toxicological complications.

The volume of the solution that can be instilled in the precorneal area is also limited. The eyelid and the conjunctival sac can take up a limited amount of the instilled solution. The

volume that the precorneal area can accommodate is ~50 µL. When instilled volume is more than 50 µL, the excess solution is removed from the precorneal area via nasolacrimal duct and the amount of drug in that volume of fluid is lost. Both in the nasolacrimal duct and in the nasopharynx, the drug can be absorbed systemically through the mucosa, avoiding presystemic hepatic first-pass metabolism[34]. Moreover, when the volume is more than the maximum volume, the reflux blinking and tearing remove the excess volume. The normal tear volume is restored within 2-3 min and the excess volume is lost within 20-30 sec by precorneal factors[35]. Higher the volume of drop instilled, more rapidly it will be lost via nasolacrimal duct system[34b, 34c, 36]. As the instilled volume is increased, more amount of drug is removed through nasolacrimal duct. When the instilled volume is very low, it may be diluted in the tear fluid, decreasing drug effect. 0.5% tropicamide, at drop volume of 5 µL produced less mydriasis than the one with 16 µL [37].

In summary, drug absorption is limited to 5% at best following topical application due to precorneal and corneal barriers. Nonetheless, it is most patient compliant route. As ocular barriers and the physicochemical properties of drug molecules govern drug availability in the anterior and posterior segment, research should be directed towards surpassing these barriers by novel routes of administration and/or altering the properties of drug molecules [27].

Systemic route

Drugs administered systemically (e.g. through the oral or intravenous route) also have poor access to the aqueous humor and the vitreous [30]. Ocular bioavailability of systemically administered drugs depends on the drug concentration gradient between serum and ocular tissues and as well as blood-ocular barrier characteristics. The limitations of this route for drug delivery are poor ocular bioavailability due to BOB and systemic toxicity.

Intraocular injection

Intraocular injections may be either intracameral or intravitreal. Injections that are made into the aqueous humor of the eye may be referred to as intracameral injection, whereas injections into vitreous humor are referred to as intravitreal injection.

Intracameral injection:

This route may be sought for intraocular antibiotic therapy. Up to 100 µL volume in human can be injected in this route. Intracameral injections are used in cataract surgery and for the management of disease afflicting the anterior segment. This route of administration fails to deliver significant concentrations of drugs to the posterior segment. Since the trauma associated with this injection may severely damage the eye, this can be the last resort in controlling severe infections of the eye[28, 33].

Intravitreal injection:

Drug access into the vitreous is desirable in various infections and inflammations. Examples of such situations are infection of the vitreous in endophthalmitis and various vitreoretinopathies. However, access of drugs into the vitreous is usually poor because there is virtually no penetration through the crystalline lens or between the ciliary process and crystalline lens. In addition to this, there is no satisfactory access from the blood vessels into the retina due to the pigment epithelium [30]. Thus, the only remaining route will be by direct injection of drug into the posterior segment through the pars plana, evading all the barriers. Studies have been carried out to evaluate the pharmacokinetic parameters of intravitreal injections of antiviral agents such as: ganciclovir, foscarnet and sidofovir; antibiotics such as cefazolin, amikacin, moxifloxacin, ceftizoxime, ceftrioxone, ceftazidime and monoclonal antibodies such as rituximab, bevacizumab [27].

It is noteworthy that the elimination half-life of drugs increases with molecular weight in the vitreous [33]. Large molecules (linear molecules > 40kDa and globular molecule

>70kDa) tend to have longer retention times due to the tight barrier that surround the vitreous humor. This route of administration is more suitable for drugs with high molecular weight (>500Da) and longer half-life [27]. On the other hand, in the plasma, peptide and protein drugs exhibit short elimination half-life [33]. Due to this unique vitreal clearance property, drug therapy via intravitreal injection seems to be a viable option, as reported for treatment of age-related macular degeneration (AMD) with the anti-vascular endothelial growth factor (VEGF) therapies, using pegaptanib (Macugen®), ranibizumab (Lucentis®) and bevacizumab (Avastin®) [31]. Although drug delivery through intravitreal injection can achieve higher concentration in the neural retina, adverse effects such as retinal detachment from repeated injections, retinal hemorrhage, endophthalmitis, cataracts and other retinal toxicities due to high concentration upon bolus dose administration may result in patient incompliance. Ausayakhun et al. studied the efficiency and complications of intravitreal ganciclovir (2 mg in 0.1 mL per injection) to control CMV retinitis. The results indicated that 60% of the treated eyes remained stable, 13% showed improvement and 26% showed a decrease in visual acuity. Moreover, retinal detachment was observed in 6%, intravitreal hemorrhages in 1% and endophthalmitis in 1% of treated eyes. This study clearly demonstrates the complications of the intravitreal injection that should be taken into consideration. Several studies were carried out on similar lines, which suggest that intravitreal injection, although useful, may not be ideal strategy for posterior segment diseases. Advancement in drug delivery system design and surgical techniques have led lead to the development of intravitreal implants that can be placed inside the vitreous to deliver constant drug levels over prolonged periods. Unlike single intravitreal injections administered 2 or 3 times a week, intravitreal implants can be conveniently replaced every 6 months. More about ocular implants will be discussed separately in this chapter.

Periocular injection

Periocular region is the region surrounding the eye. Among existing routes, it is the most efficient and least painful route of drug delivery. Periocular injection is used when eye drops alone are not effective enough for treatment of eye inflammation and additional help is required. The drug is usually injected in close proximity to sclera in the posterior segment. Drugs delivered by this route can reach to the sclera, choroid, vitreous, retinal pigment epithelium, and neural retina. Peribulbar, retrobulbar, subconjunctival and Sub-Tenon's injections are frequently used approaches offered by periocular route for drug delivery in to the eye. Time to reach drug vitreal level depends on available drug concentration and the intermittent barrier layers between target site and site of drug administration[27, 33]. Lack of efficacy, convenience and safety are few drawbacks of periocular route due to which it is yet not considered as a first line treatment and still serve as an additive to topical drug therapy [38].

Subconjunctival injection:

The outer sclera is covered by conjunctival membrane. Drug injection beneath the conjunctiva is a less invasive localized delivery technique for posterior eye segment. The potential reasons to give subconjunctival injection is to achieve high drug concentration at the target site along with better drug diffusion into the conjunctival, subconjunctival and scleral tissues. Larger surrounding area can be treated by subconjunctival injection rather than the wound margin alone which prevents migration of cell to the sclerectomy site from the surrounding area in filtering procedure.[39] Pinilla et al. have demonstrated that low dose of mitomycin C by subconjunctival injection delays the fibroblastic proliferation from Tenon's capsule and scleral biopsies [39]. It is easier and safer to perform subconjunctival injections as compared to Sub-Tenon's. Routinely, subconjunctival injections of antibiotics are used to treat intraocular and severe corneal infections.

Sub-Tenon's injection:

The Tenon's capsule is a facial sheath of connective tissue sandwiched between the conjunctiva and episcleral plexus. The episcleral or subtenon's space is a void between the Tenon's capsule and sclera. Subtenon's injection places the drug in contact with sclera for longer period due to its avascular nature. The posterior Tenon's capsule has the tendency to degenerate with age, thus helping the diffusion of anesthetic into the retrobulbar cone. A drug solution administered by subtenon's injection has the disadvantage of decreased molecular penetration through the sclera and choroid. Moreover, rapid removal of the drug by the choroidal circulation can result in shortened duration of action. It is considered to be the most promising route of targeting posterior segment [40]. In sub-Tenon's injections, the needle tip passes through the conjunctiva and Tenon's capsule in the inferior *cul-de-sac*, entirely out of your view. Risk of perforating the globe with subconjunctival injections is minimal in well-trained hands and with a cooperative patient. However, given the closer proximity to the interior of the eye, and the fact that it is a "blind" injection, a sub-Tenon's injection carries a higher risk of globe penetration.

Retrobulbar injection:

Injections through the lower eyelid into muscles surrounding the eye are frequently employed for administration of anesthetic agents or for corticosteroid therapy in severe inflammation to the posterior segment of the globe [28]. With retrobulbar injection, higher local concentrations can be achieved for anesthesia or akinesia of the globe during surgery, and there is little to no influence on intraocular pressure [33]. Retrobulbar injection involves deposition of drug solution into retrobulbar space within the muscle cone. This route is preferred when the medication needs to be in direct contact with macular region. Such injections are usually given with a special 23-gauge sharp 1.5-inch needle with a rounded tip and a 100 bend. The needle is introduced in the quadrant between the inferior and the lateral rectus muscles and directed posteriorly until orbital septum resists its penetration; the needle

is directed towards the apex of orbit and penetrated until it meets the resistance of intermuscular septum. Following penetration through this structure, the needle reaches the retrobulbar space, which can take 2-3 mL of solution. Care should be taken to minimize needle movement to prevent possible laceration of the blood vessels. Pressure should be applied on the globe to distribute the anesthetic effect and to ensure homeostasis [41]. Retrobulbar injection of drugs may result in penetration through the sclera but the highly vascularized choroid will be a physiological barrier and finally the pigment epithelium will hinder the movement of drug into the retina and the vitreous [30].

Peribulbar injection:

Peribulbar injection has been devised to lower the risk of injury to intraorbital structures associated with retrobulbar administration during cataract surgery. The injection is made in the inferior lateral quadrant of the orbit using a 26-gauge half-inch disposable needle [42]. Peribulbar injection can be classified as circum-ocular (sub-tenon's, episcleral); peri-ocular (anterior, superficial); peri-conal (posterior, deep) and epical (ultra deep); based on the depth of the needle [43]. Comparable clinical efficacy using the retrobulbar and peribulbar techniques have been reported [44]. A total of 8-10 mL of anesthetic solution (mixture) can be injected in both sites. The peribulbar route is less effective than the retrobulbar route in anesthetizing the globe. However, it is the safer mode of administration. Although, peribulbar and retrobulbar injections are proven to be useful in analgesia, akinesia, the control of intraocular pressure and postoperative analgesia, complications such as diplopia, orbital hemorrhage, artery occlusion, brainstem anesthesia, optic nerve trauma and apoptosis have been reported [27].

1.4. Micelles for topical ocular drug delivery[45]

Micelles consists of amphiphilic molecules that, generally, self-assemble in aqueous media to form organized supramolecular structures. Micelles are formed in various size

(10nm to 1000nm) and shapes (spherical, cylindrical and star-shaped, etc.) depending on the molecular weights of the core and corona forming blocks. The self-assembly take place above certain concentration, referred to as critical micelle concentration (CMC). A schematic representation of micelle formation with amphiphilic polymers or surfactants is shown in the Figure 1-5. The force driving the self-assembly and maintenance of supramolecular assembly is hydrophobic interactions of core forming blocks, for typical micellar structures. The corona-forming block is water-soluble that renders micelles soluble in aqueous phase. Taking the advantage of hydrophobic core, these nanocarriers can been utilized to enhance the water solubility of hydrophobic molecules. Nanomicelles investigated for topical ODD thus far can be divided into two broad categories i.e., polymeric and surfactant micelles. The typical surfactant micelles are characterized by higher CMC where a dynamic equilibrium exists between micelle aggregates and unimers in the solution. Micellar aggregates formed by surfactants are weak and susceptible to physical instability upon dilution. In contrast, polymeric nanomicelles exhibit lower CMC and better stability against dilutions. Hydrophobic drugs are encapsulated in the nanomicelle core by hydrophobic interaction. Other interactions, such as van der Waals' forces and hydrogen bonding may also contribute to the encapsulation in micelle core. Selection of the type of nanomicelle carrier is dependent on the physicochemical properties of drug molecule, drug:polymer or drug:surfactant interactions, site of action, rate of drug release, biocompatibility and physical stability. A summary of micellar formulation investigated for ODD is presented in Table 1-1.

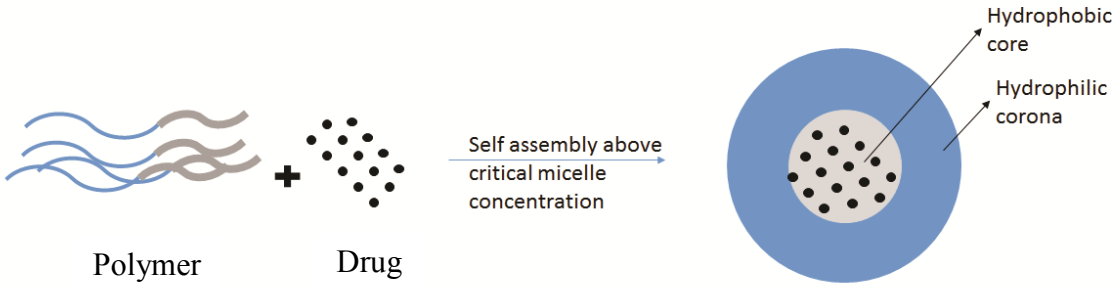

Figure 1-5 Schematic representation of micelle formation with amphiphilic polymers or surfactants. Hydrophobic block is driving force behind aggregation and hydrophilic block forms corona aiding solubilization of supramolecular assembly. Hydrophobic agents may be entrapped inside the core of micelle.

1.4.1. Polymeric Nanomicelles

Polymeric nanomicelles are formed by amphiphilic polymers with distinct hydrophobic and hydrophilic segments. The polymer self-assemble to form micelles in aqueous solution, wherein water insoluble segment forms the core and hydrophilic segment forms the corona. In some cases, the self-assembly is not spontaneous and micelle formation is assisted by additional means, such as temperature[46]. The self-assembly occurs above the CMC. The hydrophilic segments forming corona aid the solubilization of entire supramolecular structure. Polymeric micelles are characterized by their low CMC in addition to excellent kinetic and thermodynamic stability in solution. Ideally, the polymers utilized to prepared nanomicelles should be biodegradable and/or biocompatible. The most widely studied core-forming polymers are poly(lactide), poly(propylene oxide) (PPO), poly(glycolide), poly(lactide-co-glycolide), and poly(ε-caprolactone) (PCL). Poly(ethylene glycol) (PEG) is the most frequently utilized hydrophilic segment due to its excellent water solubility and biocompatibility. Other polymers exploited for ODD include poloxamine [47], chitosan [48], chitosan/F127 [49] and poly(ethylene glycol)–poly(hexyl-lactide) (mPEG-hexPLA) [50]. Biodegradation of polymer ensures elimination of inactive polymer from ocular tissues. However, the degradation products should not be toxic or inflammatory to the sensitive ocular tissues particularly the neural retina.

Table 1-1 Summary of nanomicelle/micelle systems investigated thus far for ocular drug delivery.

Polymer/ Surfactant	**Therapeutic agent**	**Size**		**PDI**	**Surface charge**	**Remarks**	**Reference**
Pluronic F127	Pilocarpine	23.3 ± 0.5 nm (in DDI water), 30.3 ± 0.3 nm (in buffer, pH 7.4)		NR	NR	64% increase in AUC along with significantly prolonged miotic activity with nanomicelles.	[51]
Poloxamine (Tetronic® 1107)	α-Tocopherol	30–40 nm		0.475	NR	Micelles were stable for months at 4 ºC	[52]
Poloxamines (Tetronic® T908, T1107 and T1307)	Ethoxzolamide	Multimodal size distribution		NR	NR	Tunable drug release profile was achieved with mixed micelle system.	[47]
MPEG–hexPLA	Cyclosporin A	54 ± 1 nm		0.229 ± 0.008	NR	The polymer well tolerated in in rabbits. *In vivo* transcorneal permeability was improved and nanomicelle formulation was significantly efficacious in preventing corneal graft rejection.	[53]
mPEG-PDLLA	Pirenzepine hydrochloride	PEG/PLA wt ratio	Size (nm)	NR	NR	*In vivo* biocompatibility study in rabbits exhibited on significant toxicity for 9 months. Intraoculer levels of Pirenzepine hydrochloride following topical instillation were enhanced with nanomicelles.	[54]
		80/20	152.5				
		50/50	89.6				
		40/60	50.2				
Pluronic F127 with Chitosan	Dexamethasone	25.4 - 28.9nm		0.39-0.54	+9.3 to +17.6 mV	*In vitro* permeability increased with increase in chitosan concentration. Improved *in vivo* bioavailability.	[48]

Table 1-1 Summary of nanomicelle/micelle systems investigated thus far for ocular drug delivery.

Pluronic F127 with Chitosan (0.3-0.8%)	metipranolol	123–232 nm	0.117-0.157	+6.1 to +9.2 mV	Pharmacological response significantly improved upon incorporation of chitosan.	[55]
Crosslinked micelles made of NIPAAM, VP, and MAA with MBA and TEGDMA as cross linking agents	Dexamethasone	300–450 nm	NR	NR	Micelles exhibited very high entrapment efficiency and bioadhesive properties. It also resulted in higher anti-inflammatory activity for an extended duration.	[56]
mPEG-PCL	Dexamethasone	28 nm	NR	0.135	Aqueous solubility of dexamethasone was increased up to 1.36mg/mL. The nanomicelle enhanced dexamethasone permeability across the excised rabbit sclera by 2.5-fold.	[46]
Crosslinked micelles made of NIPAAM, VP and AA having cross-linked with MBA	Ketorolac (free acid)	35 nm	NR	NR	A 2-fold increase in permeability was observed across excised rabbit cornea. Nanomicelles significantly improved *In vivo* ocular anti-inflammatory activity.	[57]
Quaternary ammonium palmitoyl glycol chitosan	Prednisolone	10-100 nm	NR	NR	A significantly higher aqueous humor levels were achieved with formulation following single topical instillation.	[58]
Flt1 peptide-hyaluronate (HA) conjugates	Genistein	172.0 ± 18.7 nm	0.25 ± 0.11	–23.4 ± 5.1 mV	A significant suppression of corneal neovascularization was observed in silver nitrate cauterized corneas of rats. The retinal vascular hyper-permeability was reduced in diabetic retinopathy model rats.	[59]

Table 1-1 Summary of nanomicelle/micelle systems investigated thus far for ocular drug delivery.

PEG-P(Asp)	FITC-P(Lys)	50.7 nm	0.046	NR	PIC micelles specifically accumulated in CNV lesions following tail Injection in rat CNV model.	
PEO-PPO-PEO	Mechanistic study with model plasmid DNA with *lacZ* gene	155 ± 44 nm	NR	-4.4 ± 2.0 mV	Micelle significantly enhanced *In vivo* gene transfer efficiency to ocular tissues in rabbit and nude mice models. Endocytosis was delineated as major transport mechanism for micelles.	[60]
Polyethylene glycol 40 stearate	Cyclosporine A	200 nm	NR	NR	A significantly higher Cyclosporine A level in the cornea, conjunctiva, and lacrimal gland were found with micelles.	[61]
Sympatens AS	Cyclosporine A	9.7 ± 0.05 nm,	<0.1	−0.4 ± 0.1 mV	Nanomicelles enhanced corneal levels of cyclosporine A following topical dose compared to Restasis®.	[62]
PHEA-PEG_{5000}-C16	Dexamethasone alcohol	10-30 nm	NR	NR	Nanomicelle formulation enhanced *in vivo* bioavailability of dexamethasone alcohol in rabbits.	[63]
Sympatens AS and Sympatens ACS	Cyclosporine A	9-12 nm	<0.16	neutral	In the porcine in situ model (*ex vivo*), remarkably high cyclosporine A levels in the cornea were observed for the nanomicellar solution	[64]

NR= Not reported
mPEG-PDLLA = Methoxy poly(ethylene glycol)–poly(D,L-lactide)
mPEG–hexPLA = Methoxy poly(ethylene glycol)-hexylsubstituted poly(lactide)
mPEG-PCL = Methoxy poly(ethylene glycol)-polycaprolactone
AUC = Area under curve
NIPAAM = N-isopropylacrylamide
AA = Acrylic acid
MBA = N,N'-methylene bis-acrylamide
TEGDMA = Triethyleneglycol dimethacrylate
Flt1 peptide = Sequence GNQWFI
PHEA= Polyhydroxyethylaspartamide
PEG = Poly(ethylene glycol)
FITC-P(Lys) = Fluorescein isothiocyanate-labeled poly-L-lysine

Table 1-1 Summary of nanomicelle/micelle systems investigated thus far for ocular drug delivery.

VP = Vinyl pyrrolidone MAA = Methacrylate	PEG-P(Asp) = polyethylene glycol-block-poly-K,L-aspartic acid)

Several important attributes must be deliberated to design a nanomicellar formulation for ODD rationally. Some of the important factors are site of action, polymer composition, drug loading, release rate, nanomicelle-tissue interaction, size and surface charge. Hydrophobic drug is encapsulated in the micelle core during or after micelle formation depending on the preparation method. The process involves hydrophobic interactions and/or hydrogen bond formation between drug and polymer. The most commonly used methods of micelles formation are direct dissolution, solvent evaporation, film hydration and dialysis method [65]. Encapsulation efficiency in the micelle core depends on the method used to prepare the micelles and extent of drug-polymer interactions. Generally, methods like solvent evaporation and film hydration result in higher encapsulation efficiency than direct dissolution and dialysis methods [65-66]. For example, aqueous solubility of biphenyl dimethyl dicarboxylate in $mPEG_{2000}$-PLA_{1000} carrier system with film hydration method was 13.2 mg/mL compared to 2 mg/mL with dialysis method [67]. Direct dissolution is the simplest method of preparation and may be easy to scale up. Depending on the type of polymer and drug-polymer interaction, this method may also be modified to eliminate the use of organic solvents like acetone or DMF that must be removed before clinical use. For example, honokiol was encapsulated in nanomicelles using direct dissolution methods without using organic solvents. Triblock co-polymer PCL-PEG-PCL was dissolved in water to form micelles by heating at 50 ^{o}C followed by entrapment of honokiol [68]. Film hydration method can also be an alternative to direct dissolution method. Exposure of polymer-drug film for extended duration under vacuum could completely remove volatile organic solvents [35b].

Stability of nanomicelles is very important for efficacious ODD. As mentioned earlier, polymeric nanomicelles are kinetically and thermodynamically more stable compared to low molecular weight surfactant micelles. The rate of dissociation of unimers from polymeric

micelles is slower making the micelles kinetically stable [69]. Thermodynamic stability is achieved by interactions of core-forming blocks as well as the ability of hydrophilic block to solubilize the supramolecular structure. In addition, stability of nanomicelles may also improve upon incorporation of hydrophobic drug molecules [13].

The mechanism of drug release from nanomicelles is dependent on the nature and strength of interactions between core-forming polymer and drug molecules, micelle stability in ocular tissues, polymer degradation and rate of diffusion of drug molecules from micelle core. Drug release should be tailored keeping the site of action in mind. For example, if the site of action is at precorneal area such as conjunctiva or cornea, drug release must take place in the precorneal space and the released drug may be absorbed, following topical administration. Nevertheless, nanomicelles must provide good precorneal retention time to avoid loss of formulation via precorneal clearance mechanisms. In a more productive absorption scenario, topically administered nanomicelles may be absorbed followed by release in the target tissue. Stability of nanomicelles in the precorneal environment and cell-micelle interactions may determine length of precorneal residence time. Volume of lachrymal fluid is 7 μL and normal tear turnover rate is 0.66 μL/min[70]. On the other hand, vitreous humor is relatively stagnant compartment and the release rate could be dependent on physically stability, polymer degradation rate and drug-polymer interaction. However, no nanomicelle systems has been able to provide sustained release for more than a few days. Thus, nanomicelles delivery via IVT route would require frequent administrations. Frequent IVT injections are not patient compliant and associated with various side effects such as endophthalmitis, retinal detachment and retinal haemorrhage. Hence, nanomicelle systems should be avoided for IVT administration.

Size of the nanomicelles are critical aspects of designing an ODD system. For polymeric micelles, size may be controlled by the molecular weight of the polymer and drug loading. Ocular disposition of nanomicelles following topical instillation may be influenced by the size of nanomicelles [71]. Transport of nanocarriers such as nanoparticles have been reported to be dependent on the size i.e., smaller the size higher is the permeability of nanocarrier [71]. Paracellular transport of nanomicelles across the conjunctiva and the sclera may result in higher drug levels in the intraocular tissues following topical administration. Nanomicelles of pilocarpine were developed with amphiphilic pluronic (F127, Mw 12,600) polymer[72]. Pluronic polymers are triblock co-polymers having hydrophilic PEG flanking the hydrophobic PPO. Above CMC, F127 forms nanomicelles of size ~17nm and ~23nm in DDI water and PBS buffer, respectively. In addition, incorporation of hydrophobic agents into micelle core also increased the micelle size. Nanomicelle size of ~30nm was observed for pilocarpine base loaded nanomicelles in PBS, pH 7.4. When these nanomicelles were examined for miotic response in female albino rabbits, a higher effect and longer duration of mitotic response was observed for pilocarpine base-loaded pluronic micelles. Such augmentation in mitotic response may be due to productive absorption of drug-loaded nanomicelles or released hydrophobic pilocarpine base form.

The eye is a specialized and isolated organ where most nutrients are supplied via specialized transporter mechanisms. Sterility and biocompatibility are very important aspects that must be studied thoroughly before selecting the type of polymers and excipients. Polymeric micelles have been recently investigated for their potential as ODD. One advantage with nanomicellar carrier is that it can be easily filter sterilized to lower the endotoxin/microbial burden.

1.4.2. Surfactant Nanomicelles

Amphiphilic molecules having a hydrophilic head and hydrophobic tail are commonly referred to as surfactants. Hydrophilic head of surfactant molecules can be dipolar/zwitterionic, charged or anionic/cationic, or neutral/non-ionic. Commonly used surfactants for nanomicellar formulation are sodium dodecyl sulphate (SDS, anionic surfactant), dodecyltrimethylammonium bromide (DTAB, cationic surfactant), ethylene oxide (N-dodecyl; tetra, C12E4), Vitamin E TPGS (d-alpha tocopheryl polyethylene glycol 1000 succinate), octoxynol-40 (non-ionic surfactants) and dioctanoyl phosphatidyl choline (zwitterionic surfactants). A hydrophobic tail commonly comprises of a long chain hydrocarbon and rarely includes a halogenated/oxygenated hydrocarbon/siloxane chain.

Micelles are formed when surfactants are dissolved in water at concentration above CMC. A balance between intermolecular forces such as Van der Waals interactions, hydrogen bonding, hydrophobic, steric and electrostatic interactions are vital for nanomicellar formulation. Shape of nanomicelles i.e. spherical, cylindrical or planar/discs/bilayers depends on the non-covalent aggregation of surfactant monomers. Alteration in the chemical structure of surfactant and conditions such as surfactant concentration, pH, temperature, ionic strength may determine the shape and size of nanomicelles. Transformation of nanomicelles can take place from one dimension into cylindrical micelles or two-dimension into bilayers/discoidal nanomicelles, which can be controlled by surfactant heads. Such transformation results from reduced forces of repulsion between the charged head groups.

Nanomicellar formulation for the topical delivery of small as well as macromolecules has been exploited by several investigators. Surfactant nanomicellar formulation has been utilized for improving the diffusion of topically delivered drugs through cornea thus improving ocular

bioavailability. Luschmann C et al., developed a nanomicelle solution of cyclosporine A (CyA) containing non-ionic surfactants (Sympatens AS)[62]. The average size of formulated nanomicelles ranges between 9.7 and 10.1 nm. Nanomicelle solution showed no signs of ocular irritation. It may be considered as a seamless drug delivery system for administration of CyA to the anterior segment. It also exhibited high levels of CyA in cornea. The nanomicelle solution exhibited high levels of CyA (826±163 ng/g_{cornea}), which exceeded the tissue levels reported for cationic emulsion of CyA (750 ng/g_{cornea}) and Restatsis® (350 ng/g_{cornea}). Therefore, nanomicelles of CyA promises an efficient method of treatment for inflammatory corneal diseases and may improve the patient compliance by reducing the number of instillations per day**.**

Vadlapudi et al., developed a clear, aqueous nanomicellar formulation of biotinylated lipid prodrug for the treatment of corneal herpetic keratitis[73]. Non-ionic surfactants – vitamin E TPGS and octxynol-40 were selected to formulate micellar formulation of biotin-12Hydroxystearic acid-acyclovir (B-12HS-ACV). TEM analysis suggested that nanomicelles were spherical, homogenous and devoid of aggregates. The average size of formulated nanomicelles was 10.78 nm. No significant burst effect we reported for the release of B-12HS-ACV from nanomicellar formulation. A sustained release of B-12HS-ACV from its nanomicellar formulation was observed for a period of 4 days as compared to 100% release of B-12HS-ACV in ~6 h from its ethanolic solution.

Mitra et al. reported application of nanomicellar formulation for posterior segment delivery via topical administration[74]. Vitamin E TPGS and octoxynol-40 of different hydrophilic lipophilic balance (HLB) values were used to prepare aqueous mixed nanomicellar formulation of voclosporin in order to carry out initial studies. Rapamycin and DEX were also encapsulated in an aqueous nanomicellar formulation. Size of nanomicelles encapsulating voclosporin,

rapamycin and DEX were in the range of 10-25 nm. Voclosporin aqueous mixed nanomicellar formulation (0.2%) efficacy was compared with Optimmune® (CyA ophthalmic ointment) in canine keratoconjuntivitis sicca model utilizing Schirmer tear test (tear production in an eye) and corneal observation as end points. The control values were found way below the threshold value (>15mm/min) whereas nanomicellar formulation maintains the value well above the threshold. No side effects were noticed with voclosporin nanomicellar formulation administered twice daily indicating its safety in animal model. Tolerability studies of nanomicellar formulations (0.02 and 0.2%) against Restasis® was investigated in New Zealand White (NZW) rabbits. Ocular irritation was reported highest in Restasis® compared to voclosporin nanomicelle formulation. These results confirmed that voclosporin aqueous nanomicelle formulation is well tolerated and induce significantly less ocular irritation as compared to Restasis®. Voclosporin (0.2%) nanomicelle formulation showed no dose dependent side effect on particular function and histopathological ocular indices in 2 and 13-week studies carried out in NZW rabbits and beagle dogs. No toxicity with minimal systemic exposure and accumulation were observed with nanomicelle formulation. Anterior and posterior tissues were analysed for voclosporin levels following single and once daily drop instillation of nanomicellar formulation in NZW rabbits. High drug concentrations were reported in the posterior ocular tissues in relative to minimal and/or non-detectable drug levels in aqueous humor, lens and vitreous humor. Adverse effects such as increased intraocular pressure or cataract formation can be avoided with nanomicelle formulation due to the minimal drug levels in aqueous humor, lens and vitreous humor. Mixed nanomicellar aqueous formulations can be utilized to deliver therapeutic agents to the posterior ocular tissues via topical instillation.

Recently, DEX and rapamycin topical nanomicellar formulations were utilized for posterior ocular tissues delivery via non-invasive route [75]. Encapsulation of DEX and rapamycin in nanomicellar formulation resulted in improved solubility of DEX and rapamycin by 6.7 and 1000 times, respectively. Ocular tissue distribution studies revealed that 50 ng/g and 370 ng/g of DEX and rapamycin, respectively were detected in retina-choroid whereas minimal or no drug levels were detected in aqueous ocular chamber suggesting a non-corneal route of drug absorption to the posterior segment.

CHAPTER 2

2. HYPOTHESIS AND RATIONALE

2.1. Statement of the problem and Hypothesis

Topical administration is the most patient compliant route. Nonetheless, drug delivery to intermediate and posterior segment via topical drops is a significant challenge. Less than 5% of topically administered dose reaches ocular segments (such as retina and vitreous) owning to static and dynamic barriers [76]. Typical instillation volume for topically administered formulation is usually less than 40-50 μL, to avoid drug loss via reflux tearing and nasolacrimal drainage. Low instillation volume entails steroidal agents to be solubilized at higher concentration in aqueous solution in order to achieve therapeutic drug level in intermediate and/or posterior segments. However, steroids are hydrophobic in nature with poor aqueous solubility and cannot be dissolved at higher concentrations in aqueous solution.

Nanocarriers such as liposomes and nanomicelles are capable of solubilizing highly hydrophobic drugs in aqueous medium [77]. Micelles represent supramolecular arrangement of amphiphilic polymeric systems with typical size in range 10-100 nm. They have been investigated extensively to solubilize hydrophobic drugs. Polymeric micelles can be prepared with various di-block polymers consisting of hydrophobic and hydrophilic units. Transport of nanocarriers across the static and dynamic barriers may depend on the particle size [71]. Recently, Inokuchi *et al.* have illustrated that the liposome size of ~110 nm resulted in higher coumarin-6 accumulation in posterior segment following topical administration [78]. A few examples of micelle for ODD are also available which delivered drug to the intraocular tissues following topical administration. Mixed micelle formulation of dexamethasone from our laboratory also resulted in significantly higher concentrations in the intraocular tissues. It was theorized that the

nanomicelle preferably follows transscleral pathway due to its hydrophilic surface to achieve higher concentrations in the posterior segment. Nanomicelles are gaining attention as potential drug delivery vehicle to deliver drugs to the intraocular tissues such as uvea following topical administration. The size of the nanocarrier, nanomicelles in this case, may be a major factor influencing the permeability of encapsulated therapeutic agents following topical administration. Therefore, it is important to delineate influence of nanomicelles size on permeability of drug across the sclera as trans-scleral may be the major route of permeation. We hypothesize that nanomicelles of mean size less than 50 nm may effectively overcome the conjunctival and scleral barriers to provide therapeutic drug concentration in the intermediate and posterior uvea.

Rationale for using statistical design of experiments

Recently, there has been a growing interest in utilizing design of experiment (DOE) to optimize formulation parameters. Experimental designs such as a 3-level response surface methodology may explain the influence of individual factors and their interactions on response variables. Typically, DOE is utilized to optimize formulation process parameter within a set range for individual factor. However, in our case we aim to use DOE methodology to identify the factors and interactions (drug-drug, polymer-drug and polymer-polymer) that may enhance or lower drug loading in nanomicelles. Based on information from exploratory model, we will modify the nanomicelle preparation method to optimize process thereby achieving higher aqueous solubility.

Rationale for using dexamethasone (DEX)

Uveitis is an intraocular inflammatory disease responsible for 10-15% blindness in developed countries [79]. It affects intermediate and/or posterior segments involving sections of choroid and retina, which often results in blindness. Steroids have been a mainstay treatment

option for this inflammatory condition [76a, 80]. Traditionally, steroids are administered by systemic routes. However, systemic administrations of steroid are not well tolerated by all patients [80c, 81]. Topical drops of steroids are well tolerated but drug levels achieved in intermediate and posterior ocular segments are often subtherapeutic [80c, 81]. In the past decade, clinically recalcitrant uveitis has been treated by steroids administered as intravitreal (IVT) injections [80b, 82]. IVT injections are associated with numerous side effects including retinal detachment, endophthalmitis, cataract and elevated intraocular pressure [82a, 83].

2.2. Objectives

To test above-mentioned hypothesizes, we propose following specific aims.

1. To synthesize and characterize di-block poly(ε-caprolactone)-block-monomethoxy-poly(ethylene glycol) (PCL-mPEG) polymers of various molecular weight of PCL and PEG segments. An mPEG of molecular weight 750, 2000 and 5000 gm/mol will be employed in the synthesis of di-block polymers. Molecular weights of PCL block will be varied to control average nanomicelle size of ~10, 30 and 60 nm. The newly synthesized polymers will be characterized for proton-NMR (structure, micelle forming behavior), gel permeation chromatography (purity, molecular weighs, molecular weight, polydispersity), powder X-ray diffraction (physical state), and critical micellar concentration.
2. To prepare nanomicelle encapsulating dexamethasone using film hydration method. To utilize DOE methodology (response surface design) to identify the process parameters (factors and interactions) influencing the drug loading for film hydration method. To modify the film-hydration method to achieve better drug loading i.e. aqueous solubility of dexamethasone in nanomicelles.

3. To develop dexamethasone-loaded nanomicelles of mean sizes 10, 30 and 60 nm using polymers developed in Aim-1 by modified film-hydration method. To characterize dexamethasone-encapsulated nanomicelles for drug loading (solubility), size, polydispersity, location of drug and *in vitro* release of drug.
4. To determine permeability of dexamethasone from nanomicelles *in vitro* across human conjunctival cells and *ex vivo* across excised rabbit sclera. Compared the permeability of dexamethasone from nanomicelles of various sizes to delineate influence of nanomicelles size of trans-scleral permeability.

CHAPTER 3

3. POLYMER SYNTHESIS AND CHARACTERIZATION[84]

3.1. Materials

Dexamethasone (purity ≥99%) was obtained from Enzo Life Sciences (Farmingdale, NY). ε-Caprolactone, stannous octoate and methoxy poly(ethylene glycol) (mPEG; Mw 2000) were procured from Sigma Chemicals (St. Louis, MO). Acetonitrile, methanol, d_6-chloroform, d_6-DMSO, anhydrous diethyl ether, tert-butyl methyl ether (TBME) were also obtained from Sigma Chemicals (St. Louis, MO) and used without further purification. Human conjunctival epithelial cell (HCE cell, Chang cell, CCL-20.2) was procured from ATCC (American type culture collection). Human corneal epithelial cell (SV40) was a generous gift from Dr. Araki-Sasaki (Kinki Central Hospital, Japan). Lactate dehydrogenase (LDH) and CellTiter 96® AQ_{ueous} Non-Radioactive Cell Proliferation (MTS) assay kits were purchased from Fisher Scientific Inc. and Promega corp., respectively. Millipore™ Millex™ Sterile Syringe Filters made of Durapore® hydrophilic polyvinylidene fluoride (PVDF) (pore size 0.22 μm) were obtained from Fisher Scientific Inc.

3.2. Methods

3.2.1. Synthesis

The di-block polymer were synthesized by ring opening polymerization by following published protocol with necessary modifications [85]. Synthesis scheme is illustrated in (Figure 3-1).

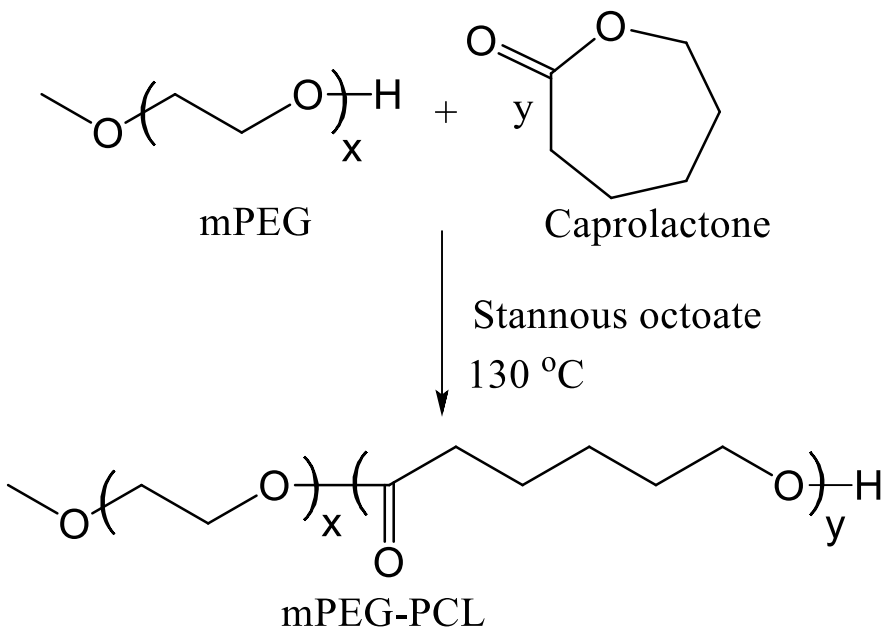

Figure 3-1 General synthesis scheme for di-block mPEG-PCL polymers.

Briefly, monomer ε-caprolactone, initiator mPEG and catalyst stannous octoate (0.5% w/w of reactants) were added in a reaction vessel prefilled with nitrogen. Toluene (5 mL) was added to reactants, followed by heating at 100 ^{o}C under vacuum until the total volume was reduced to initial volume. The temperature was then raised to 130 ^{o}C. After 12 h, the reaction mixture was cooled down to room temperature (RT). The reaction mixture was dissolved in dichloromethane and precipitated in cold anhydrous ether. The final product was filtered and dried under vacuum. The polymer was characterized by ^{1}H-NMR (Varian 400 MHz), and gel permeation chromatography for structure and molecular weight determinations.

3.2.2. NMR

To perform ^{1}H-NMR spectroscopy, samples were dissolved in $CDCI_3$ and spectra were recorded with Varian-400 NMR instrument. NMR data was processed using VNMRJ or ACD labs software.

3.2.3. Gel permeation chromatography

Purity, molecular weights and polydispersity of polymers were further confirmed by GPC analysis. Polymeric samples were analyzed with refractive index detector (Waters 410). Briefly, samples were prepared by dissolving 5 mg of polymeric material in tetrahydrofuran (THF) whereas THF was utilized as eluting agent at the flow rate of 1 mL/min. Separation was carried out on Styragel HR-3 column and polystyrene samples with narrow molecular weight distribution were utilized as standards.

3.2.4. Critical micelle concentration (CMC)

CMC was determined using pyrene as a hydrophobic fluorescent probe following a previously published method with modifications [86]. Briefly, serial dilutions of polymer from 1000 µg/mL to 0.27 µg/mL were prepared in chloroform. Each dilution was added with 30 µg

pyrene in chloroform. The chloroform solution, containing polymer and pyrene, were vortexed and dried under vacuum. DDW was added to the dried samples and vortexed for 1 min. Solutions were incubated at 37 °C for 12 h, then syringe-filtered (0.22 μm) to remove undissolved pyrene. Filtrates were measured for pyrene fluorescence. Samples were excited at 330 nm and emissions were measured at 372 nm (I_2) and 392 nm (I_1). A ratio of emission intensities (I_2/I_1) was plotted against polymer concentrations to calculate CMC. The polymer concentration here we observed a sharp increase in I_2/I_1 ratio was considered as CMC for the polymer.

3.2.5. Cell culture

Human conjunctival epithelial cells (HCE cells) were maintained in cell culture flask containing Minimum Essential Medium (MEM) Earle's Balanced Salt Solution (BSS) medium supplemented with 10% fetal bovine serum (FBS), 100 U/L of penicillin, 100 mg/L of streptomycin, sodium bicarbonate (2.2 mg/mL), and 2 mM L-glutamine. Human corneal epithelial cells (SV40 cells) were cultured in DMEM/F-12 medium supplemented with 15% (v/v) heat inactivated FBS, 22 mM NaHCO3, 15 mM HEPES and 5 mg/L insulin, 10 μg/L human epidermal growth factor, 100 mg penicillin and 100 mg streptomycin each. Both cell lines were incubated at 37 °C, 5% CO_2 and 98% humidity.

3.2.6. In vitro cytotoxicity

Cytotoxicity studies were performed for newly synthesized polymer by MTS and LDH assays. Polymer concentrations of 25, 50, and 100 mg/mL were examined for cytotoxicity in both conjunctival (HCE cells) and corneal (SV40 cells) cell lines. The polymer concentrations were chosen such that it would cover the highest concentration of polymer in the final formulation obtained by DOE. We went up to 100 mg/mL concentration of polymer to make certain that there is no toxicity even at higher concentration.

MTS assay: MTS assay was performed according to previously published protocol with minor modifications [87]. Polymer solutions were prepared in culture medium and sterilized by filtration with 0.2 μm syringe filters. In brief, HCE or SV40 cells at a density of 10^4 per well were cultured in 96-well plate and incubated for 24 h. Polymer solutions were prepared in culture medium and sterilized by filtration with 0.2 μm syringe filters. Following incubation, medium was removed and cells were exposed to three different concentrations of polymer solution i.e., 25, 50 and 100 mg/mL (n = 6). Cells without treatment were selected as positive control whereas cells treated with triton-X 100 (0.1% v/v) as negative control. Following 48 h of incubation, culture medium from the 96-well plate was substituted by 100 μL of serum free medium containing 20μL of MTS solution. Cells were then incubated at 37 °C and 5% CO_2 for 4 h. After incubation, absorbance of each well was measured at 450 nm. Cell viability (%) was calculated by equation 3.1.

Cell viability (%) = ((Abs of sample-Abs of negative control)/(Abs of positive control-Abs of negative control))*100 ... (3.1)

LDH Assay: HCE or SV40 cells were seeded in 96-well plate at a density of 10^4 cells per well and incubated at 37 °C, 5% CO_2, and 98% humidity for 24 h. Polymer solutions were prepared in culture medium and sterilized by filtration with 0.2μm syringe filters. Following incubation period, cells were exposed to various concentrations of polymer (25, 50 and 100 mg/mL, n = 6) and incubated for 48 h. Cells without treatment were selected as negative control whereas cells treated with Triton-X 100 (0.1% v/v) as positive control. According to the protocol provided by manufacturer, LDH release in cell supernatant was quantified by LDH assay kit (Takara Bio Inc., Japan). Samples were analyzed at absorbance wavelength of 450 nm with 96-well plate reader. LDH (%) release was calculated by equation 3.2.

LDH released (%) = ((Abs of sample-Abs of negative control)/(Abs of positive control-Abs of negative control))*100 … (3.2)

3.3. Results and discussion

Di-block polymer was synthesized by anionic ring opening polymerization using stannous octoate as the catalyst and mPEG as the initiator. A summary of polymers synthesized in this project is given in Table 3-1. Polymer was purified by cold ether precipitation and dried under vacuum. Structure of the polymer was confirmed by ^{1}H-NMR (Figure 3-2). Proton NMR showed all the characteristic peaks for the polycaprolactone and mPEG residues. Weight and number average molecular weights (Mw and Mn) and PDI were determined by gel permeation chromatography (Table 3-1). GPC chromatogram represented only one peak associated with DB polymer (Data not shown). All newly synthesized polymers possessed molecular weight close to the feed ratio and acceptable polydispersity.

Critical micelle concentration (CMC) was obtained by pyrene method in aqueous polymer solution (Figure 3-3). CMC for the polymer was 0.13, 4.48 and 6.04 μg/mL for DB1, DB2 and DB3, respectively. Such low CMC values indicate greater stability against dilutions following topical instillation in tear fluid.

Table 3-1 Summary of polymer molecular weights and polydispersity for di-block polymers for nanomicelle preparation.

Code	Block co-polymer composition	Mn[a] (gm/mol)	Mn[b] (gm/mol)	Mw[b] (gm/mol)	PDI[b]
DB1	$mPEG_{750}$-PCL_{700}	1450	1627	1972	1.21
DB2	$mPEG_{2000}$-PCL_{1500}	3500	3155	4586	1.45
DB3	$mPEG_{5000}$-PCL_{4000}	9000	9060	10950	1.21

Mn-Number average molecular weight, Mw-Weight average molecular weight.

PDI-polydispersity index.

[a]Theoretical value, calculated according to the feed ratio.

[b]Determined by GPC analysis.

Value in subscript represents molecular weight (gm/mol)

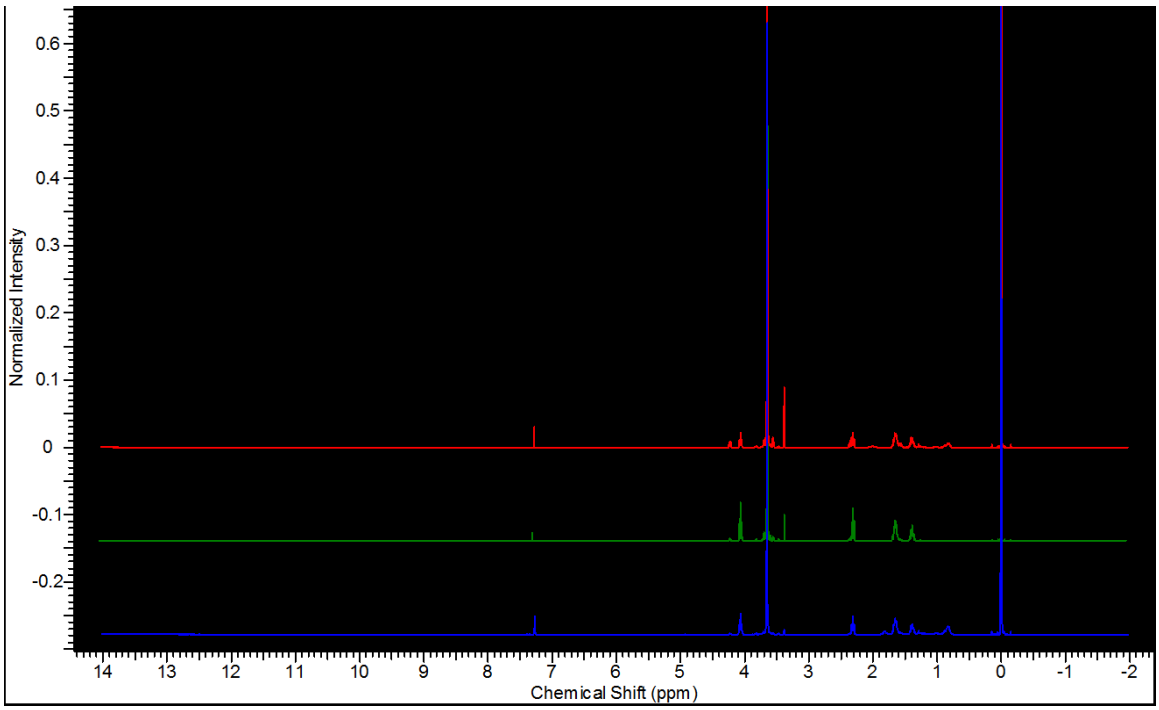

Figure 3-2 Proton NMR for DB1, DB2 and DB3 polymers.

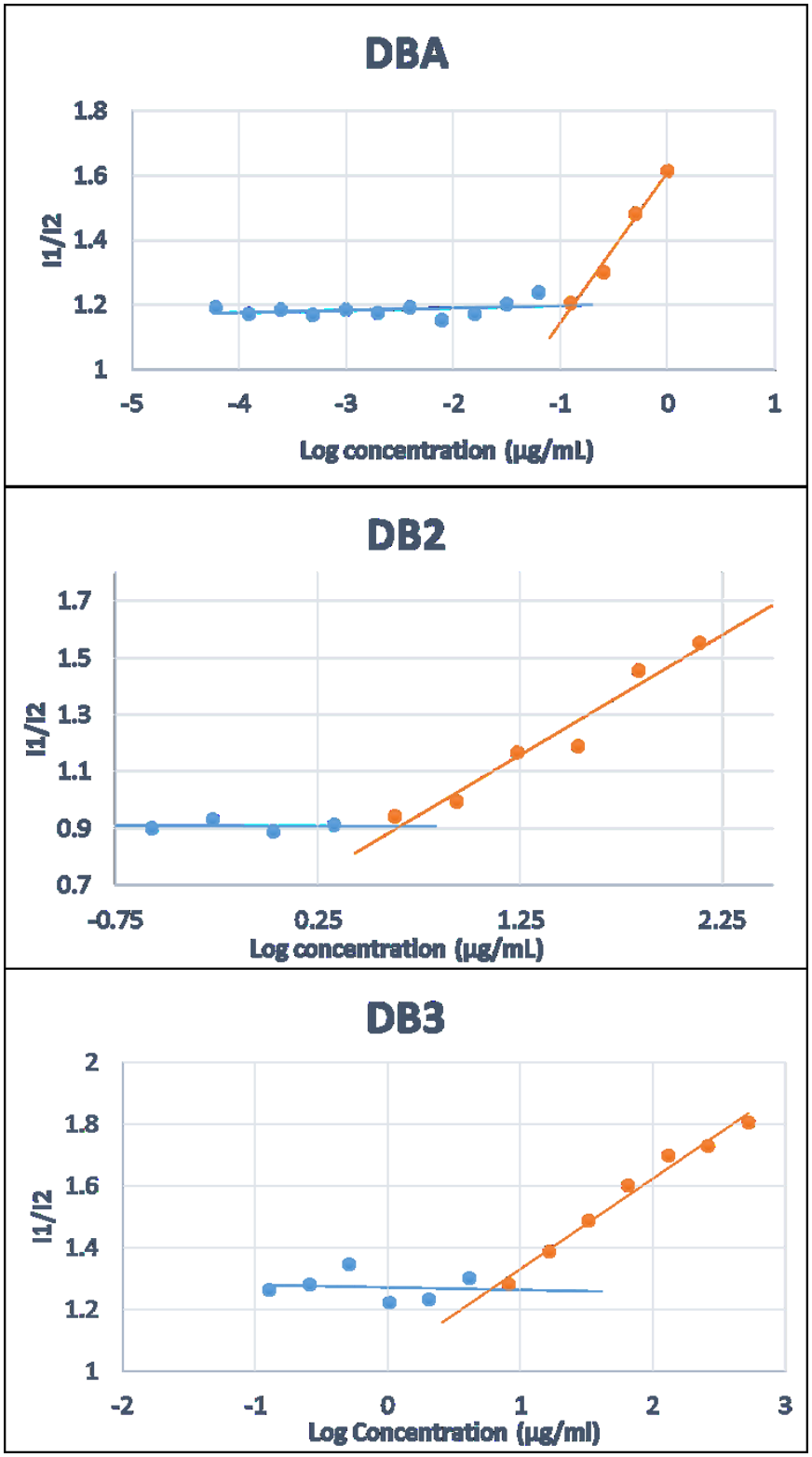

Figure 3-3 Critical micelle concentration measurement. Intensity ratio I2/I1 verses log polymer concentration (µg/ml) profile for the mPEG-PCL polymers. Where, I2 and I1 is ratio of emission intensities at 372nm and 392nm, respectively.

Cytotoxicity studies of DB polymers were conducted on conjunctival and corneal cells, by MTS and LDH assays, prior to development of formulation. Percent cell viability was calculated based on amount of formazione released for both HCE and SV40 cells (MTS assay) (Figure 3-4). Positive control (medium) and test groups were compared by ANOVA. No significant difference in %cell viability was observed at all polymer concentrations (ANOVA $p>0.05$). In addition, cytotoxicity study was also performed by LDH assay to confirm results obtained from the MTS assay. Polymers interact with cells via cell membrane, and therefore estimating the amount of LDH released in culture medium could be a preferred way to estimate the cell wall damage and thus cytotoxicity of polymers. LDH release for cells treated with polymer was compared to negative control (blank, medium). Based on ANOVA analysis, no significant difference in %LDH release was observed between blank and treatment groups, in both HCE and SV40 cells (Figure 3-5). These cytotoxicity studies suggests that the polymers are safe to use in the given concentration range for ODD.

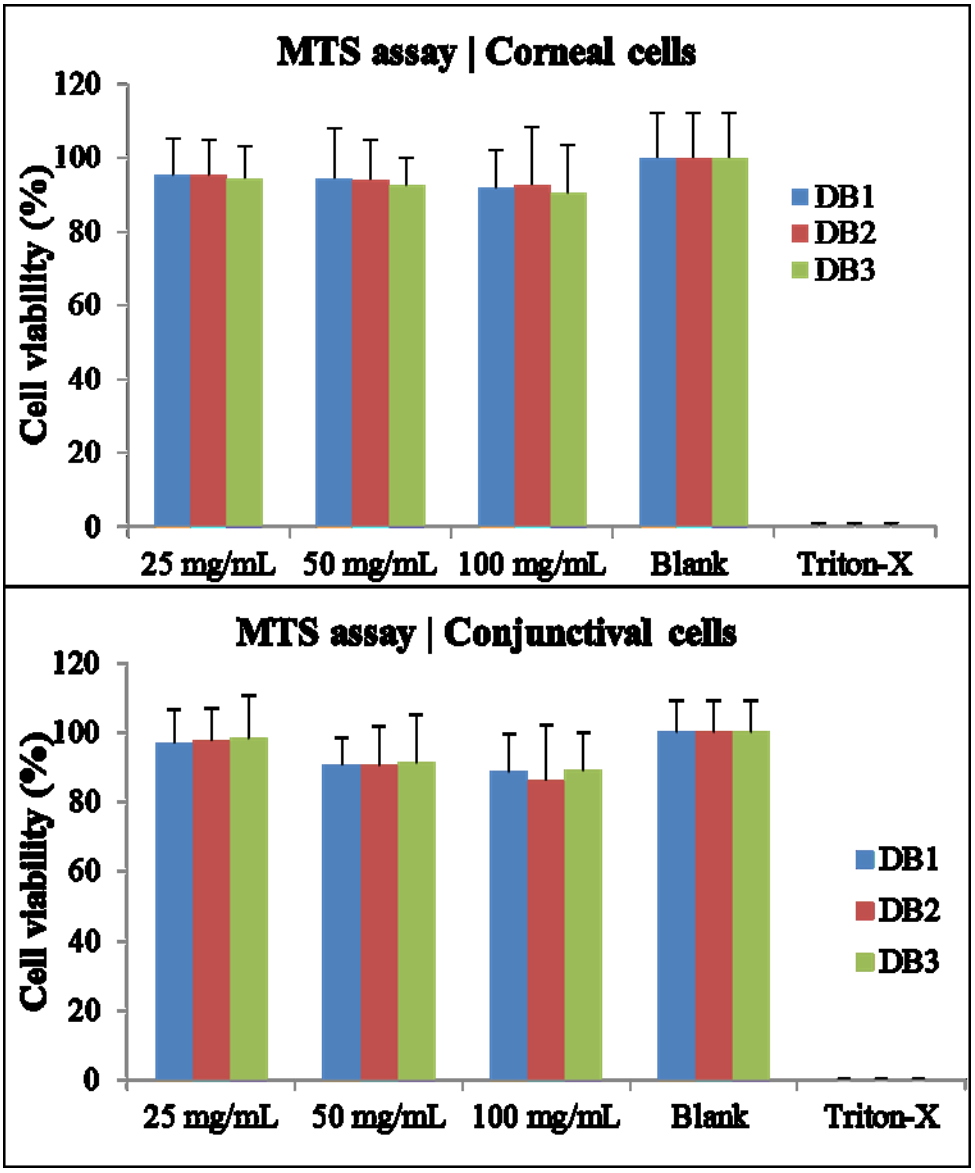

Figure 3-4 Cytotoxicity study by MTS assay in Corneal and Conjunctival epithelual cells. Blank (medium alone) is negative control. Triton-X is positive control.

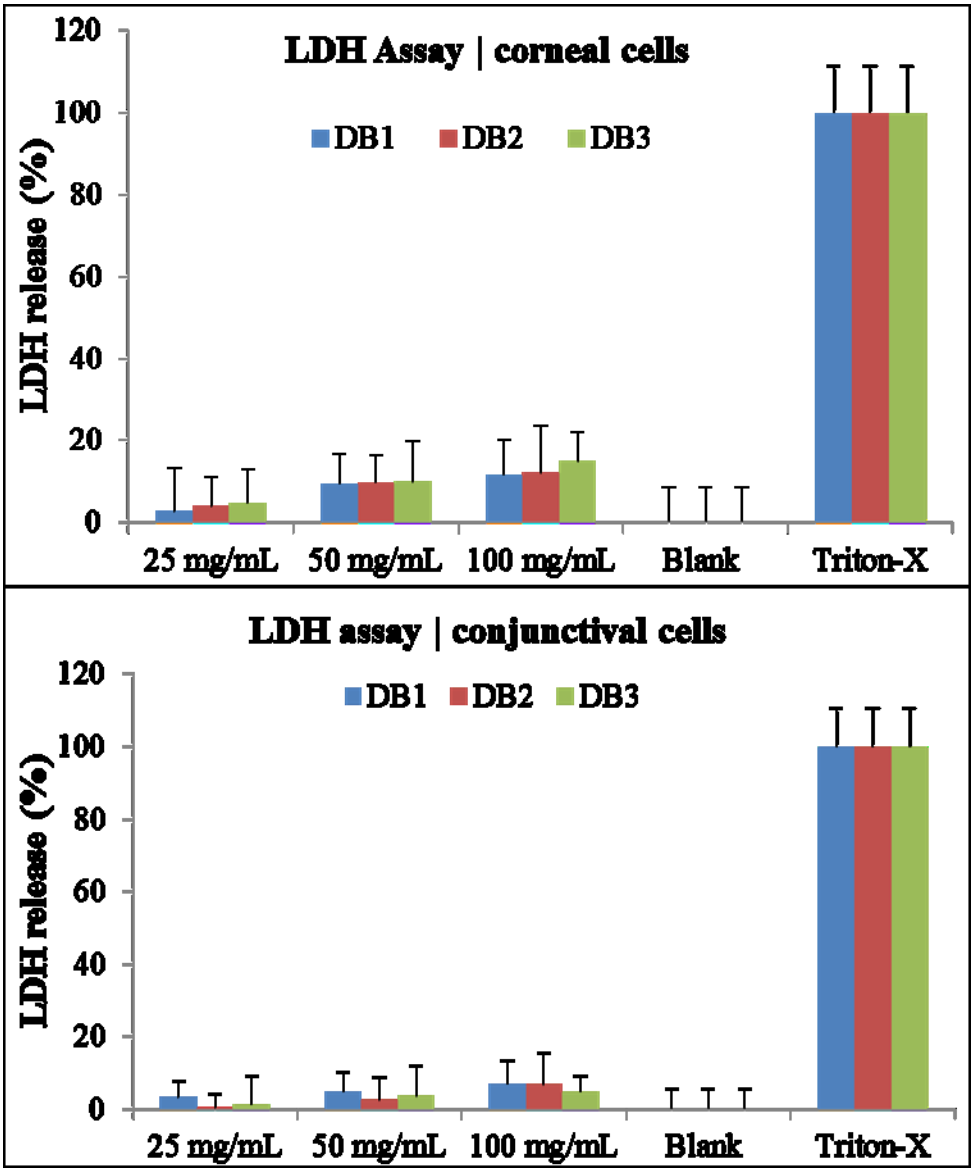

Figure 3-5 Cytotoxicity study by LDH assay in conjunctival ad corneal epithelial cells. Blank (medium alone) is negative control. Triton-X is positive control.

CHAPTER 4

4. PREPARATION AND OPTIMIZATION OF DEX-LOADED NANOMICELLES OF MEAN SIZE 30 NM USING DB2 POLYMERS[84]

4.1. Methods

4.1.1. Film-hydration method for nanomicelle preparation (Exploratory model, Method-1)

DEX-loaded nanomicelles (DEXM) were prepared by film hydration method. The calculated amount of polymer and DEX were accurately weighed out and dissolved in acetone/chloroform mixture (1:1). Organic solvents were evaporated under vacuum in desiccator for 24 h to generate films. Films were then added with 1 mL of DDI (65 ºC) and vortexed for 3 min. Nanomicellar solutions were syringe filtered (0.22 μm) to separate undissolved DEX and subsequently analyzed for DEX content by reverse phase HPLC.

4.1.2. Modified film-hydration method for nanomicelle preparation (Optimization model, Method-2)

Method-1 was modified based on the results obtained from exploratory model to obtained higher drug dissolution in nanomicelle core. The modified method is as follows. Briefly, drug and polymer films were obtained as described in method-1. The films were then heated at 65 ºC for 15 min to allow melting of the semi-crystalline polymer. The melted films were added with 1 mL DDI water (37 ºC) and vortexed for ~45 sec. The solutions were allowed to cool down to RT and filtered through 0.22 μm syringe filters. Clear micellar solutions were analyzed for DEX solubility by reverse phase HPLC.

4.1.3. Solubility determination (HPLC)

Reverse phase HPLC method described earlier was used with necessary modifications [88]. Shimadzu LC pump (Waters, Milford, MA) equipped with a UV detector (SPD-20AV,

Shimadzu) was employed for the HPLC analysis. The mobile phase consisted of 65% tetrabutylammonium hydrogen sulfate (TBAHS) buffer and 35% ACN on a reverse phase C18 column (Phenomenex C18 Kinetex® column 100 × 4.6 mm, 5 µm) as a stationary phase. Mobile phase flow rate was set at 0.4 mL/min. UV detector was set at 254 nm for quantifying DEX.

4.1.4. Exploratory model (Experiment design-1 (ED-1))

In order to understand the factors and interactions influencing DEX solubilization in nanomicelles, a 2-factor 3-level response surface design (RSD) was employed. The factors under investigation were polymer amount (X1) and dexamethasone amount (X2) for their effects on DEX solubility (Y) in nanomicelles. The experimental design was generated with statistical design software SAS 9.02. The RSD-small composite Hartley method was utilized for the aforementioned independent variables and dependent variables (Table 4-1). The primary reason for selecting this design is the least number of runs as compared to other designs. The design had 9 runs in total, including 3 center points. DEX-loaded micelles were prepared by film-hydration method (Method-1).

Statistical Analysis: Influence of two factors (Polymer (X1) and DEX (X2) amount) on one dependent variable was studied in exploratory model. Hence, a statistical model with interactive and polynomial terms was used to evaluate their influence on the response variable (Y) (Equation 4.1).

$$Y = b_0+b_1X1+b_2X2+b_3X1X2+b_4X1X1+b_5X2X2 \quad \ldots (4.1)$$

Where, Y is response variable (DEX solubility, mg/mL); b_0 represents the intercept; b_1, b_2, b_3, b_4, b_5 represents the regression coefficients for factor and interactions. X1 (Polymer amount in mg) and X2 (DEX amount in mg) are individual effects. X1X1 and X2X2 are

polynomial terms of individual effects, which represent the polymer-polymer and drug-drug interactions, respectively. X1X2 is the interaction term representing drug-polymer interaction.

Results from this design were analyzed with one-way analysis of variance (ANOVA). F-test was carried out at $\alpha = 0.05$ to determine significance of regression relationship between response variable (Y) and a set of independent variables. Significant factors and interactions were identified by t-test at 95% significance level. R^2 and adjusted R^2 were also calculated for the regression model. The model was validated by checking model assumptions and lack of fit test. Statistical analysis was performed with SAS 9.02 and JMP 9.0.

4.1.5. Optimization model (Experimental design-2 (ED-2))

The primary goal of ED-2 was to predict optimal DEX:polymer ratios providing DEX solubility of ≥1 mg/mL. Hence, ED-2 could also be referred to as predictive model. We were also interested in delineating the effect of melting (Micelle preparation method-2) on DEX solubility. RSD-small composite Hartley method described earlier was employed to achieve these goals (Table 4-1). Based on experiments with method-1, we considered that DEX solubility of 1 mg/mL would be a significant increase. Hence, DEX solubility of 1 mg/mL was set as optimal/target value. Statistical treatment described in earlier section was applied to this design as well. In addition, a reduced model was generated by removing insignificant effects. The reduced model was utilized to predict the DEX:polymer ratio providing optimal DEX solubility and validated by checking model assumptions, lack of fit test and checkpoint analysis.

Table 4-1 Details of response surface design.

Design Description: Small Composite Hartley Method				
Number of factors	2			
Number of runs	9			
Factors	**Unit**	**Low (-1)**	**Medium (0)**	**High (+1)**
Polymer (X1)	mg	10	30	50
Dexamethasone (X2)	mg	1	3	5
Response variable	**Unit**			
Dexamethasone Solubility (Y)	mg/mL			

4.1.6. Micelle size, polydispersity and surface morphology

Mean micelle size and polydispersity index (PDI) were determined with Zeta Sizer (Zetasizer Nano ZS, Malvern Instruments Ltd, Worcestershire, UK) at RT. A 500-750 μL of solution was used without any dilution. Morphology of nanomicelles was examined by transmission electron microscopy (TEM) (Philis CM12 STEM). About 50 μL of micellar solution was placed on a carbon-coated copper grid. The excess of solution was removed by Kimwipe. Samples were negatively stained by phosphotungstic acid and completely dried before taking TEM images.

4.1.7. Powder X-ray diffraction (XRD)

XRD analysis was performed for DEX, polymer, dried DEX-polymer film and freeze-dried DEXM formulation. A Rigaku MiniFlex powder automated X-ray diffractometer (Rigaku, The Woodland, Texas, USA) was utilized for the analysis at RT. Cu Kα radiation (λ = 1.5418 Å) at 30 kv and 15mA was utilized. The diffraction angle covered from 2Θ 4.0° to 45.0°, and a step of 0.05° with 3 sec/step were applied. The diffraction patterns were processed using Jade 8 (Materials Data, Inc., Livermore, CA).

4.1.8. ^{1}H-NMR spectroscopy of nanomicelles

To perform ^{1}H-NMR spectroscopy, polymeric and DEX combination was dissolved in d6-DMSO. Blank or DEXM were prepared in D_2O for NMR analysis. Spectra were recorded with Varian-400 NMR instrument. NMR data was processed using VNMRJ or ACD labs software.

4.1.9. In vitro release

The release mechanism for DEX from nanomicelles was determined by *in vitro* release study in simulated tear fluid (STF compositions: 2 g $NaHCO_3$, 6.7 g NaCl, 0.08 g $CaCl_2 \cdot 2H_2O$, and deionized water was added up to 1 L, tween-80 (0.5% w/w)) [55] with a dialysis method [89]. The optimal formulation obtained from the ED-2 was prepared and characterized for initial drug content. A five-hundred μL of micellar solution was added in a dialysis bag (MWCO 2000 Da). The bag was tied at both ends and immersed in 10 mL of STF containing tween-80 (0.5% w/w) at 37 ^{o}C. The release medium was replaced with fresh STF at predetermined time points. Amount of DEX released was quantified by a reverse phase HPLC method. Release study was performed in triplicates. The results were plotted as mean±SD. The release data was fitted for zero order, first order, Higuchi and Korsmeyer-Peppas model to determine the kinetics of DEX release.

4.2. Results and discussion

4.2.1. Exploratory model (Experimental design-1)

Preliminary experiments to prepare DEXM with film hydration method did not result in appreciable increase in solubility. Hence, a response surface methodology (Small Composite Hartley Design) was employed to understand the influence of drug-polymer interactions on drug solubility in micelle core and identify the factors/interactions responsible for poor DEX loading in nanomicelles. The design runs (coded and uncoded runs) and corresponding DEX solubility are presented in Table 4-2.

Table 4-2 Design runs and solubility of dexamethasone for ED-1 (Micelle preparation method 1).

Run #	Coded design		Uncoded design		Solubility Y (mg/mL)
	Polymer X1	Dexamethasone X2	Polymer X1 (mg)	Dexamethasone X2 (mg)	
1	-1	-1	10	1	0.26
2	1	1	50	5	0.37
3	-1.19	0	6.2	3	0.18
4	1.19	0	53.8	3	0.24
5	0	-1.19	30	0.6	0.20
6	0	1.19	30	5.4	0.30
7	0	0	30	3	0.27
8	0	0	30	3	0.27
9	0	0	30	3	0.33

Solubility of DEX ranged from 0.18 to 0.37 mg/mL. Among all the runs, the highest solubility of DEX was observed for run#2 (0.37 mg/mL), where both drug and polymer were at their highest levels (+1). Statistical treatment explained earlier was applied to analyze the data. Second order least square equation for the master model is given by equation 4.2.

$$Y = 0.28+0.0217*X1+0.0382*X2+0.1052*X1X2-0.0494*X1X1-0.02083*X2X2 \quad \ldots (4.2)$$

Master model:

Table 4-3 summarizes analysis of variance (ANOVA), lack of fit and correlation coefficient for the master model. The master model was found to be significant ($p = 0.0155$), indicating solubility of DEX (Y) was considerably dependent on the set of X variables. The correlation coefficient (R^2) for the regression model was 0.9720. It means that the model explains 97.2% of variation in DEX solubility. Lack of fit p-value of 0.5953 also suggested that the master model was significant and could predicting DEX solubility.

Estimated coefficients for each term (factors and interactions) with associated p-values are represented in Table 4-4. The estimated coefficients with $p < 0.05$ were considered to be significant. Significant terms from the model were amount of DEX (X2, $p = 0.0156$), DEX-polymer interaction (X1X2, $p = 0.0069$) and polymer-polymer interaction (X1X1, $p = 0.0157$) as indicated by pareto chart (Figure 4-1). X1X1 had negative influence, while X1X2 and X2 had positive effect on DEX solubility. X2X2 also had negative effect on DEX solubility but the interaction was not significant ($p = 0.1236$). Reduced model was not generated since the aim of the exploratory model was to delineate the influence of the set of X variables on DEX solubility.

Table 4-3 Summary statistics for master model (ED -1).

Summary of Fit					
RSquare	0.9720				
RSquare Adj	0.9253				
Analysis of Variance					
Source	DF	Sum of Squares	Mean Square	F Ratio	Prob > F
Model	5	0.0249	0.0050	20.8257	0.0155
Error	3	0.0007	0.0002		
C. Total	8	0.0256			
Lack Of Fit					
Source	DF	Sum of Squares	Mean Square	F Ratio	Prob > F
Lack Of Fit	1	0.0001	0.0001	0.3917	0.5953
Pure Error	2	0.0006	0.0003		
Total Error	3	0.0007			

Table 4-4 Parameter estimates for master model (ED-1).

Term	Estimate	Std Error	t Ratio	Prob>|t|
Intercept	0.2800	0.0089	31.36	<.0001
X1(10,50)	0.0217	0.0077	2.81	0.0671
X2(1,5)	0.0382	0.0077	4.98	0.0156
X1*X2	0.1053	0.0158	6.66	0.0069
X1*X1	-0.0494	0.0100	-4.96	0.0157
X2*X2	-0.0208	0.0098	-2.12	0.1236

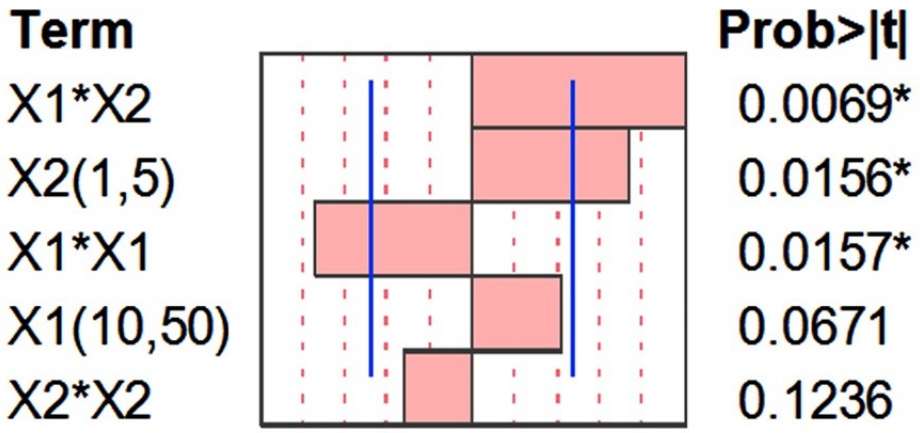

Figure 4-1 Pareto chart for master model (ED-1). * next to p-value represents significant term.

The response surface curve provides a diagrammatical representation of DEX solubility as a function of polymer and DEX amounts (Figure 4-2). The response surface was found to be non-planar. Interestingly, increasing the polymer amount had variable effects on DEX solubility depending on the amount of DEX. For example, at a high level of DEX (+1 or 5 mg), raising the polymer amount had positive influence on solubility of DEX, as anticipated. The increase in DEX solubility could be attributed to enhanced DEX-polymer interaction (X1X2), which was the most significant term according to master model ($p = 0.0069$). Nonetheless, solubility increase was not linear; such nonlinearity could be attributed to X1X1 interaction in the dried film, which may lower DEX solubility. On contrary, increasing the polymer amount at low DEX level (-1 or 1 mg) resulted in decrease in solubility. Moreover, the decline in solubility was steeper and non-linear which may be explained by X1X1 interaction. At low level of DEX, X1X1 would be dominant interaction compared to X1X2 that may explain the steeper decline in DEX solubility with increase in polymer amount.

To characterize the physical form of DEX and polymer, the dried polymer-DEX film was studied by XRD. Polymer:DEX film was prepared at a ratio X1:X2::30:5. XRD showed presence of characteristic peaks of PCL ($2\theta = 21.9$) and mPEG ($2\theta = 19.2$ and 23.8) in the dried film (Figure 2C), suggesting that the X1X1 interaction represents crystallization of the polymer upon evaporation of organic solvent. Small peaks corresponding to DEX were also present ($2\theta = 14$, 15.6 and 17) in the dried film, indicative of slight crystallization and X2X2 interaction. From exploratory model, it can be concluded that solubility of DEX in micellar core is governed by polymer-DEX interaction (X1X2).

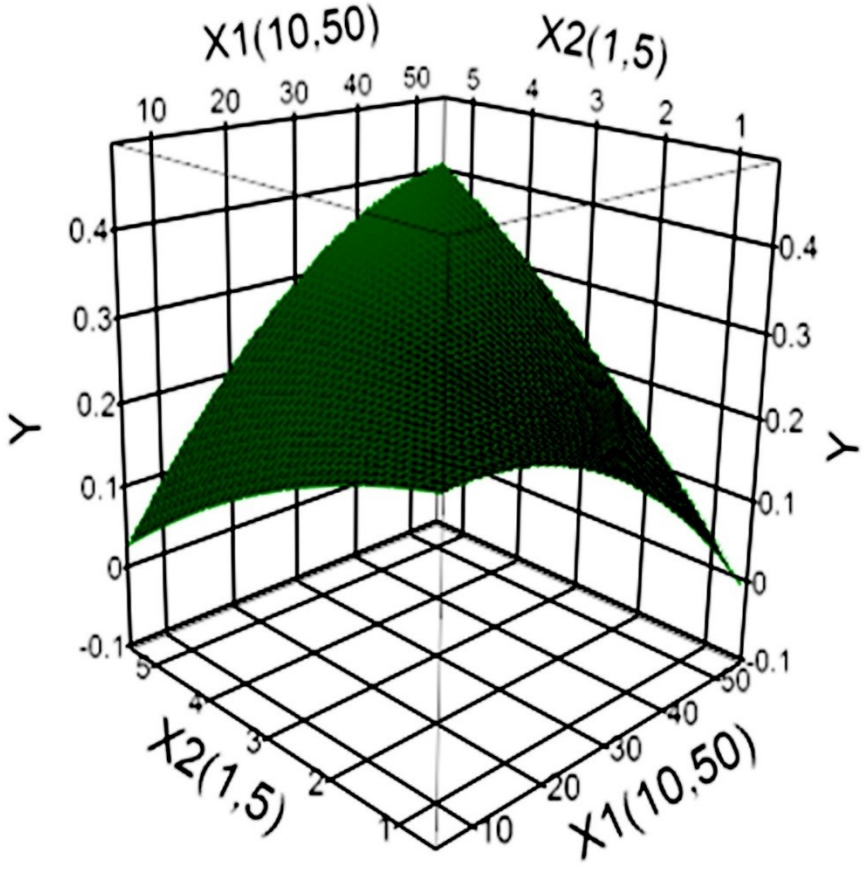

Figure 4-2 Response surface for master model (ED-1). DEX solubility (Y) is plotted as a function of polymer (X1) and DEX (X2) amounts between -1 and 1.

We can also infer that polymer-polymer interaction (X1X1) occurs during solvent evaporation leading to significantly lower DEX entrapment. In order to improve DEX solubility, we need to overcome X1X1 interactions. In this case, X1X1 interaction represents the crystallization of polymer. We hypothesize that heating the dried polymer-DEX film above the melting point of polymer (t_m = 60-62 ^oC) may overcome X1X1 interaction (nanomicelle preparation method-2). Lowering X1X1 interaction may allow free polymer to interact with DEX thus maximizing DEX entrapment in micelle core.

4.2.2. Optimization model (Experimental design-2)

Based on our hypothesis, in order to overcome X1X1 interaction, we modified the nanomicelle preparation method-1. A response surface design as explained earlier for exploratory model was generated for independent variables polymer amount (X1) and DEX amount (X2); and response variable DEX solubility (Y). DEXM were prepared by modified film-hydration method (method-2). Table 4-5 summarizes design runs (uncoded design), DEX solubility for each run, micelle size and polydispersity index (PDI). Highest solubility of 1.36 mg/mL was obtained for design run#4.

Master model:

Quadratic equation for the master model is given by equation 4.3,

$$Y = 0.733+0.436*X1+0.045*X2+0.011*X1X2+0.037*X1X1-0.066*X2X2 \quad \ldots (4.3)$$

Statistical parameters for the master model including parameter estimates, ANOVA for the master model and lack of fit analysis are summarized in Table 4-6. The master model was found to be significant, based on model p-value (p = 0.0128), lack of fit p-value (p = 0.0901) and adjusted R^2 of 0.9345. The parameter estimates for master model are shown in Table 4-7.

Table 4-5 Summary of uncoded design and corresponding solubility, micelle size and PDI for ED-2 (Micelle preparation method 2).

RUN	Polymer X1 (mg)	Dexamethasone X2 (mg)	Solubility Y (mg/mL)	Size (nm)	PDI
1	10	1	0.30	26.44	0.094
2	50	5	1.13	27.32	0.125
3	6.2	3	0.21	27.99	0.070
4	53.8	3	1.36	28.01	0.135
5	30	0.6	0.53	28.38	0.100
6	30	5. 4	0.75	28.98	0.225
7	30	3	0.68	27.79	0.076
8	30	3	0.75	27.99	0.122
9	30	3	0.77	27.17	0.106

Table 4-6 Summary statistics of master model (ED-2).

Summary of Fit					
RSquare	0.9754				
RSquare Adj	0.9345				
Analysis of Variance					
Source	DF	Sum of Squares	Mean Square	F Ratio	Prob > F
Model	5	1.0303	0.2061	23.8266	0.0128
Error	3	0.0259	0.0086		
C. Total	8	1.0562			
Lack Of Fit					
Source	DF	Sum of Squares	Mean Square	F Ratio	Prob > F
Lack Of Fit	1	0.0215	0.0215	9.6167	0.0901
Pure Error	2	0.0045	0.0022		
Total Error	3	0.0259			

Table 4-7 Parameter estimates for master model (ED-2).

Term	Estimate	Std Error	t Ratio	Prob>|t|
Intercept	0.7333	0.0537	13.66	0.0008
X1(10,50)	0.4364	0.0465	9.38	0.0026
X2(1,5)	0.0453	0.0465	0.98	0.4014
X1*X2	0.0111	0.0956	0.12	0.9147
X1*X1	0.0365	0.0600	0.61	0.5858
X2*X2	-0.0660	0.0600	-1.1	0.3519

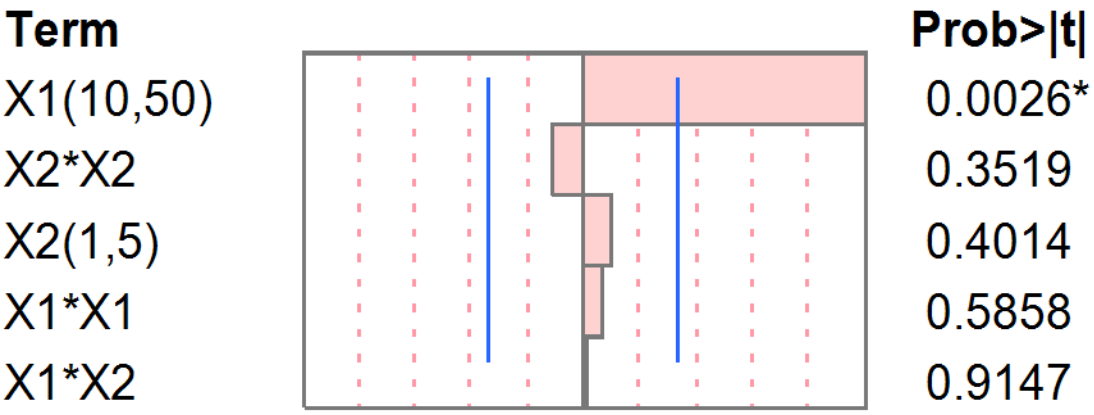

Figure 4-3 Pareto Chart for master model (ED-2). * next to p-value represents significant term.

According to pareto chart, only statistically significant factor was polymer amount (X1, p = 0.0026), unlike method-1 where polymer amount did not have any significant effect on DEX solubility (Figure 4-3). High DEX solubility may be attributed to melting of polymer in the film that allowed polymer to overcome X1X1 interaction, as we hypothesized. No influence of X1X1 interaction on drug solubility (p = 0.5858) was observed with modified film-hydration method. XRD analysis of dried DEX-polymer film was conducted after heating the films to delineate the effect of heating on physical form of polymer. DEX-polymer film was prepared at 30:5::X1:X2 ratio. The peaks for mPEG-PCL were present despite heating the film at 65 ^{o}C (Figure 4-4d). These results could be explained by the fact that XRD patterns were recorded at RT. Gradual cooling of DEX-polymer film to RT could result in recrystallization of polymer. It also worth noting that heating the film did not have any effect on physical form of DEX, as predicted.

Reduced model:

A reduced or predictive model was generated by removing the non-significant terms with p>0.05 from the master model. Hence, terms X1X2 and X1X1 were removed. XRD analysis indicated crystallization of DEX in polymer-DEX film (after heating) representing X2X2 interaction (Figure 2c and 2d). In addition, removing the X2X2 interaction did not improve the model p-value, lack of fit p-value or adjusted R^2 (Data not shown). Hence, term X2X2 was not removed from the master model. Summary statistic for the reduced model is presented in Table 4-8. The predictive model was compared with master model for p-values of the model, p-value of lack of fit and adjusted R^2. The reduced model had p-value of 0.0003, lack fit p-value of 0.2056 and adjusted R^2 of 0.9524, indicating that the reduced model was superior in predicting DEX solubility (Y). The parameter estimates for the reduced model are shown in Table 4-9. Pareto chart for the reduced model is depicted in Figure 4-5.

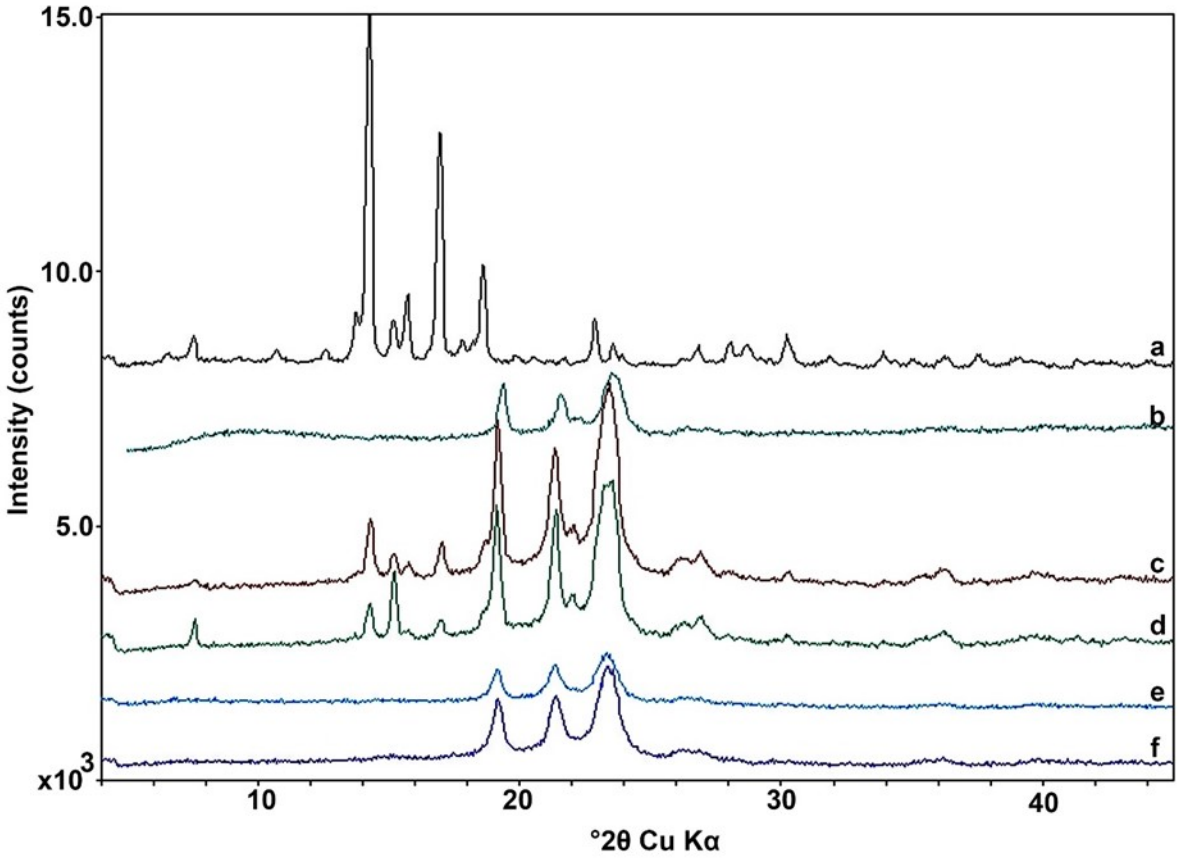

Figure 4-4 X-ray diffraction pattern for (a) Dexamethasone, (b) DB2 (PCL-mPEG) polymer, (c) Polymer:DEX film before heating (Polymer:DEX::30:5), (d) Polymer:DEX film after heating (Polymer:DEX::30:5), (e) Freeze dried Blank micelles (f) Freeze dried DEXM (0.1% w/v DEX).

Table 4-8 Summary statistics of reduced model for ED-2.

Summary of Fit					
RSquare	0.9703				
RSquare Adj	0.9524				
Analysis of Variance					
Source	DF	Sum of Squares	Mean Square	F Ratio	Prob > F
Model	3	1.0248	0.3416	54.388	0.0003
Error	5	0.0314	0.0063		
C. Total	8	1.0562			
Lack Of Fit					
Source	DF	Sum of Squares	Mean Square	F Ratio	Prob > F
Lack Of Fit	3	0.0269	0.0090	4.0205	0.2056
Pure Error	2	0.0045	0.0022		
Total Error	5	0.0314			

Table 4-9 Parameter estimates for reduced model (ED-2).

Term	Estimate	Std Error	t Ratio	Prob>|t|
Intercept	0.757	0.0350	21.6	<.0001
X1(10,50)	0.436	0.0396	11.0	0.0001
X2(1,5)	0.045	0.0396	1.14	0.3044
X2*X2	-0.069	0.0429	-1.61	0.1673

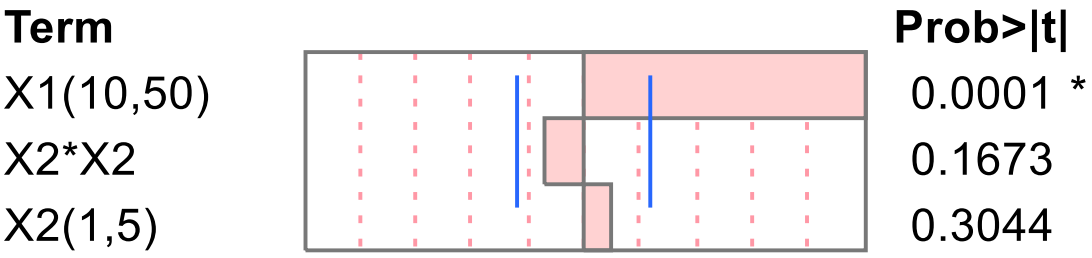

Figure 4-5 Pareto chart for reduced model (ED-2). * next to p-value represents significant term.

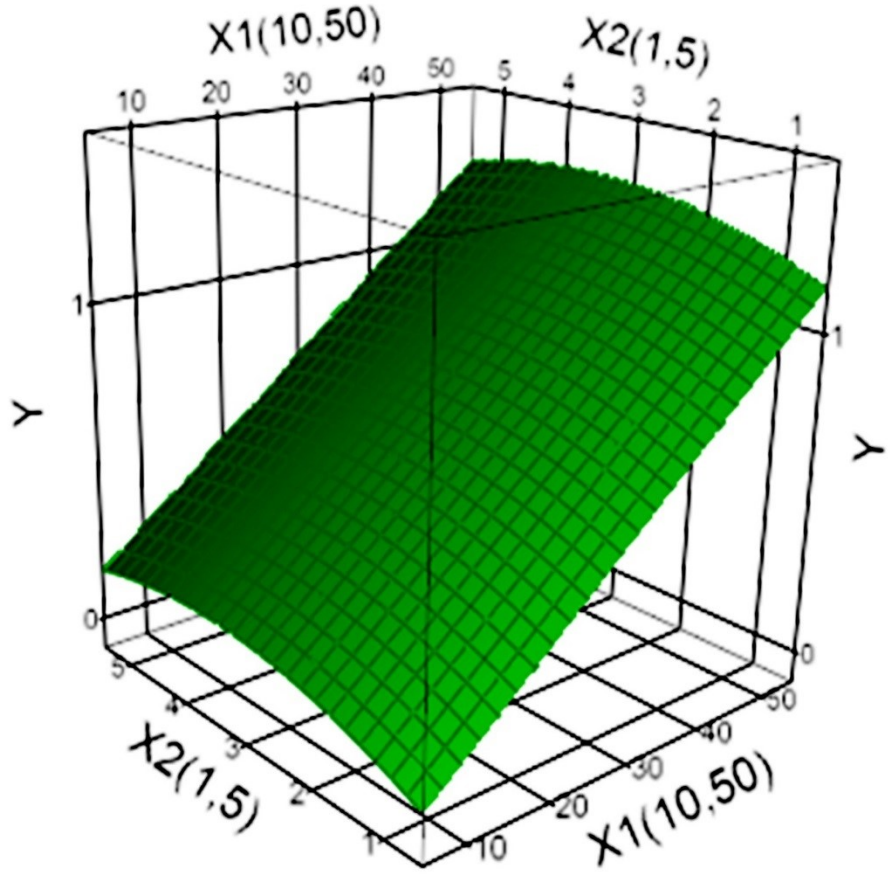

Figure 4-6 Response surface of predictive model for ED-2. DEX solubility (Y) is plotted as a function of polymer (X1) and DEX (X2) amounts between -1 and 1.

Again the only significant term influencing DEX solubility was X1 ($p = 0.0001$). Interactions between DEX molecules (X2X2) was not significant ($p = 0.1673$) as per model and, as expected, and had negative effect on DEX solubility with method-2. Similar observation was noted for method-1 (Exploratory model) suggesting that the melting has no influence on DEX crystallization. The prediction expression for reduced model is represented by equation 4.4,

$$Y = 0.757+0.436*X1+0.045*X2-0.069*X2X2 \quad \ldots (4.4)$$

Response surface showing the change in solubility of DEX as a function of DEX and polymer amounts is illustrated in Figure 4-6. Unlike exploratory model, we were able to overcome negative effect of X1X1 on DEX solubility with the modified method. Hence, solubility of DEX increased linearly with increasing polymer amount at all the DEX levels. Nonetheless, solubility increase was not linear with increasing DEX amount due to X2X2 interaction. It is worth noting that despite the ratio for the DEX:polymer is same in runs 1, 2 and 7, the amount of polymer and DEX are different (Table 4-5). These different amounts resulted in variable solubility of DEX depending on the strength of DEX*DEX, polymer*DEX and Polymer*Polymer interactions in the film upon drying. Hence, we see different solubility for DEX at same DEX:polymer ratios. Furthermore, upon overcoming X1X1 interaction in optimized method 2, a significant enhancement in solubility of DEX was observed (Table 4-2 and Table 4-5) for same amount of DEX and polymers. For example, solubility of DEX was 0.37 mg/mL and 1.13 mg/mL at 50 mg polymer and 5 mg DEX with method 1 and 2, respectively (Run#2 in Table 4-2 and Table 4-5).

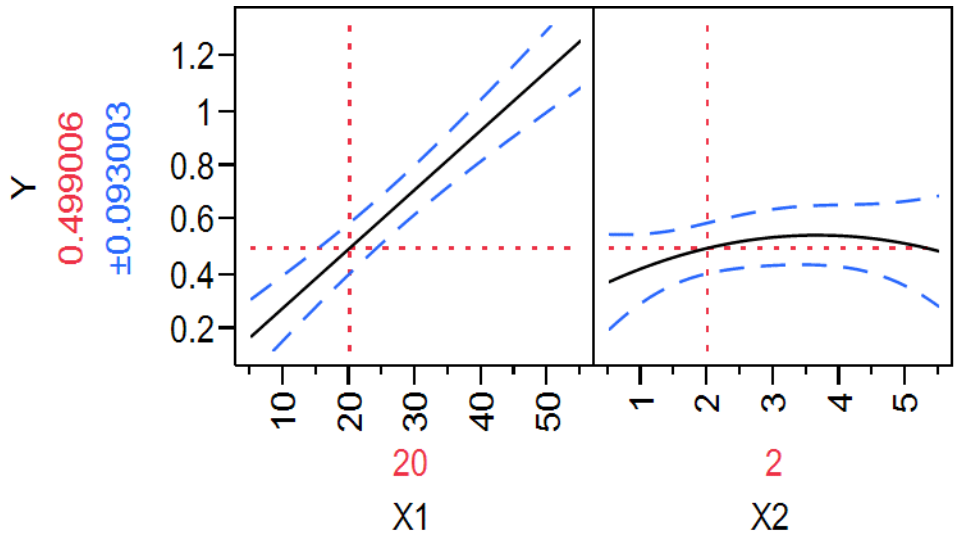

Figure 4-7 Prediction profile of reduced model depicting solubility (Y) as function of polymer (X1) and DEX (X2) amounts.

Table 4-10 Checkpoint analysis for reduced model (ED-2).

X1:X2 ratio (n = 3)	**Predicted solubility (mg/mL)**	**Experimental solubility (mg/mL)**	**Two-tailed P-value**	**% Standard error**
20:2	0.499 ± 0.093	0.588 ± 0.038	0.367	5.8%
50:3.5	1.201 ± 0.127	1.146 ± 0.166	0.672	1.2%

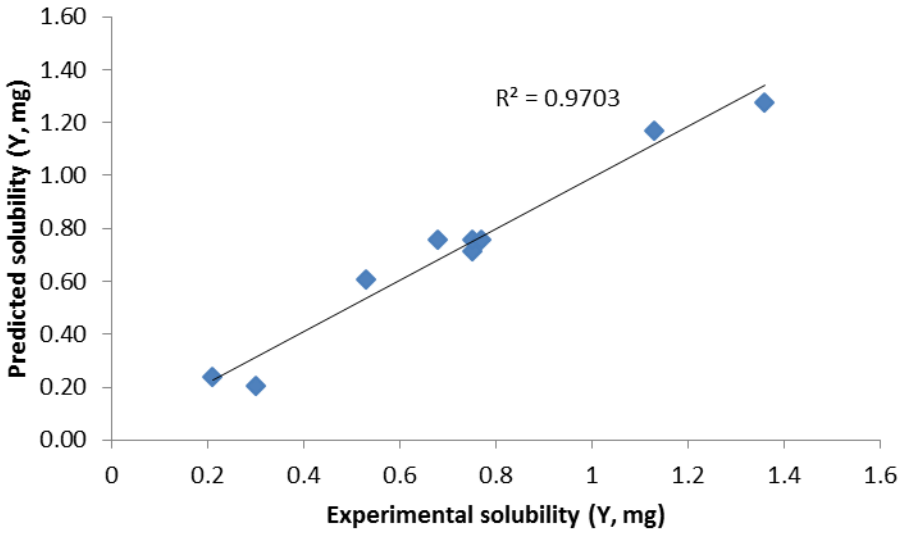

Figure 4-8 Experimental solubility verses predicted solubility for predictive model for ED-2. R2 of 0.97 suggests that DEX solubility predicted by reduced model are very close to experimental values.

The prediction profile was generated to determine the optimal point with the highest desirability. The checkpoint analysis was carried out to validate the reduced model at X1:X2::20:2 ratio. Ratio X1:X2::20:2 was selected for checkpoint analysis, as it was not a part of design runs suggested by the statistical software (SAS 9.02). No statistically significant difference was observed between experimental and predicted DEX solubility ($p>0.05$) (Figure 4-7 and Table 4-10). The model was also validated by plotting predicted verses actual solubility (Figure 4-8). The relationship was found to be linear with R^2 of 0.97 indicating predicted solubility by model is close to experimental one. Based on checkpoint analysis and experimental verses predicted solubility, it was concluded that the reduced model could accurately predict DEX solubility. Using prediction profile for reduced model, optimal X1:X2 ratio to obtain DEX solubility ≥1mg/mL was obtained.

4.2.3. Micelle size and morphology

Nanomicelle size and distribution were determined by dynamic light scattering method for all the runs in ED-2. The results are presented in Table 4-5. The size ranged from 26 to 28 nm with unimodal distribution irrespective of DEX solubility. The PDI for all the runs were below 0.23 indicating narrow size distribution. Size distribution showing mean size and PDI for design runs #2 is illustrated in Figure 4-9a. The average size was 27.32 nm with PDI of 0.125. It is expected that micelle size would increase with increase in DEX solubility from 0.21 mg/mL to 1.36 mg/mL. However, it is worth noting that even with this increase in solubility, drug loading did not vary appreciably. Hence, we did not observe an appreciable increase in nanomicelle size or polydispersity with increase in solubility.

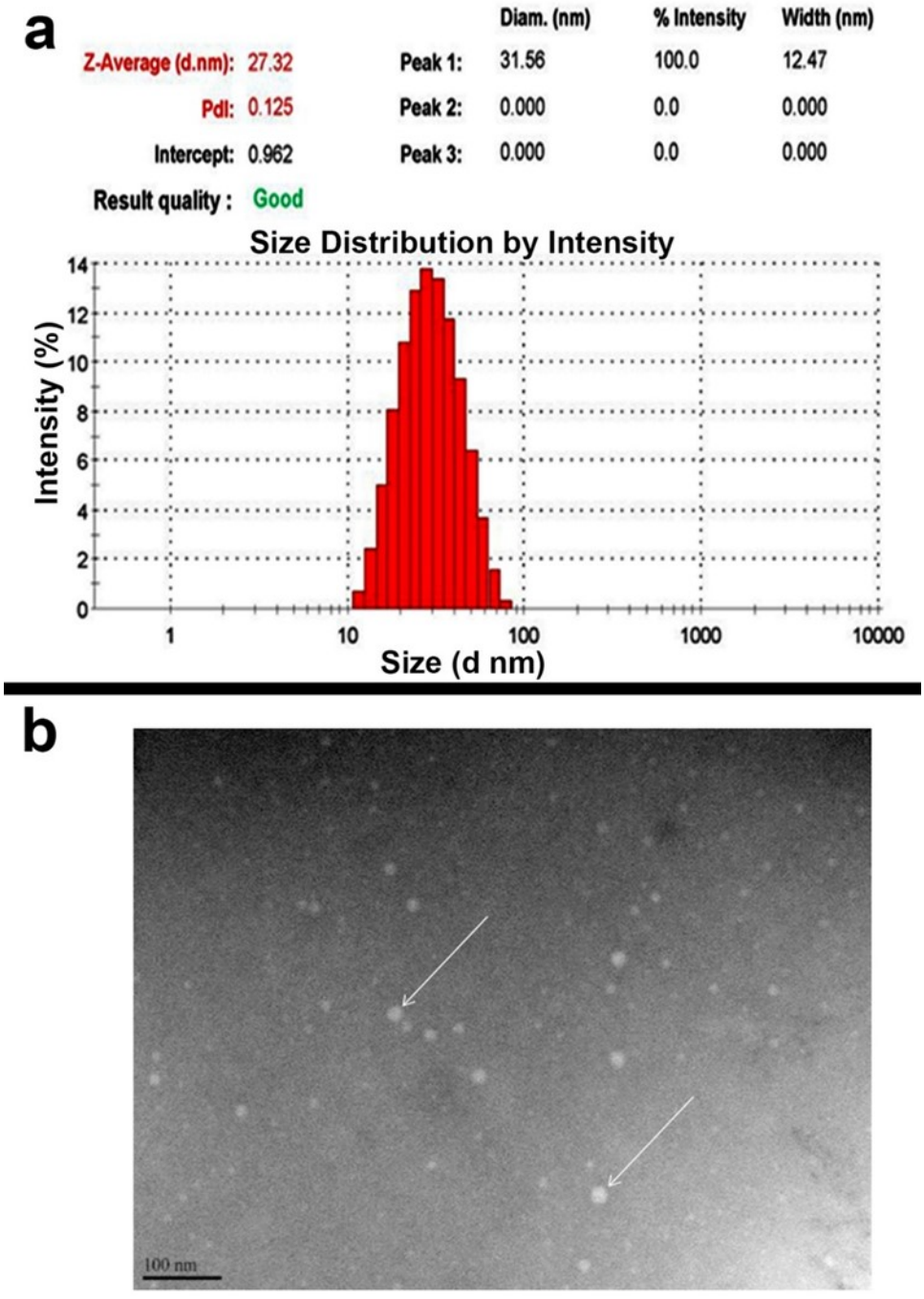

Figure 4-9 (a) Micelles size distribution for DEXM for design run #2 of ED-2. (b) Transmission electron micrograph for DEXM. Nanomicelles appear as a white spot on dark background as indicated by arrows.

The morphology of nanomicelle was studied by TEM (Figure 4-9b). TEM micrograph of nanomicelles indicated that the nanomicelles were spherical in shape.

4.2.4. ^{1}H-NMR spectroscopy of blank micelles and DEXM

Process of micelle formation and DEX encapsulation in micelle core were studied with proton NMR spectroscopy. ^{1}H-NMR for blank PCL-mPEG micelles was recorded in D_2O and compared with NMR spectra in $CHCl_3$. Weak ^{1}H-NMR signal from PCL and sharp signal from mPEG protons in D_2O clearly indicated micelle formation (Figure 4-10B). During micelle formation PCL block assemble to form the hydrophobic core and mPEG segment forms hydrophilic corona. Since the core of micelle lacks accessibility to solvent, movement of PCL segment in the core is limited and hence the proton NMR signal is very weak compared to signal in $CDCl_3$. In contrast, the corona forming mPEG segment is free to move in D_2O showing good ^{1}H-NMR signal intensity.

^{1}H-NMR spectroscopy was also used to ascertain the presence of DEX in nanomicelle core. ^{1}H-NMR spectra for physical mixture of DEX and polymer in d_6-DMSO, DEXM in D_2O and DEX in d_6-DMSO were recorded (Figure 4-10). The ^{1}H-NMR spectra for combination of DEX and polymer in d_6-DMSO showed all the characteristic peaks corresponding to DEX, PCL and mPEG (Figure 4-10d). ^{1}H-NMR for DEXM in D_2O also showed presence of characteristic peak for mPEG segment at 3.4-3.6 ppm and those for PCL were absent, indicating micellization. Characteristic peaks for DEX were absent due to restricted mobility inside micelle core, implying that drug was molecularly dispersed in micelle core (Figure 4-10e).

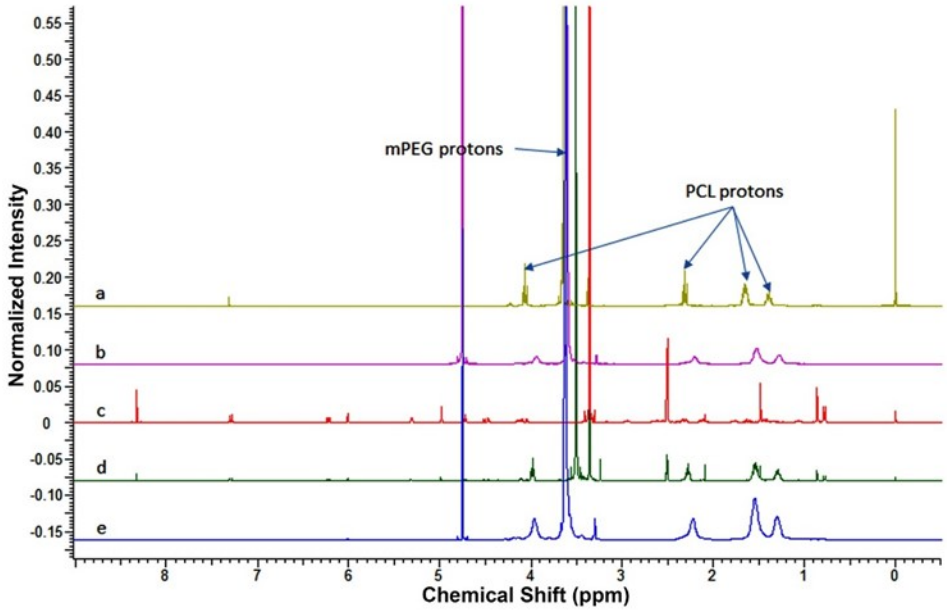

Figure 4-10 1H-NMR spectroscopies for (a) PCL-mPEG polymer in $CDCl_3$ (b) Blank PCL-mPEG micelles in D_2O (c) Dexamethasone in d_6-DMSO, (d) PCL-mPEG (50mg) and dexamethasone (1mg) in d_6-DMSO, (e) 0.1% DEXM in D_2O.

4.2.5. Powder XRD analysis of blank micelles and DEXM

Blank micelles and DEXM were also studied by XRD to seek further insight into physical state of polymer and DEX in nanomicelles. The results are presented in Figure 4-4e and 4f. XRD pattern for freeze-dried DEXM was devoid of DEX peaks indicating that the drug was molecularly dispersed in nanomicelle. Both blank micelles and DEXM showed characteristic peaks for PCL at 2θ 19° and 23°. PCL, due to its semi-crystalline nature, does not self-assemble in water to form micelles at RT. However, at temperatures close to melting point provides PCL with necessary chain mobility to self-assemble into micelles. Once the micelles are formed and system reaches RT, PCL segments in core reestablishes the polymer-polymer interactions regaining its semi-crystalline state in nanomicelle core. We expect that the semi-crystal nature of nanomicelle core would provide rigid core to the nanomicelles. Such rigid micelle core may provide resistance against sheer stress while transport of nanomicelles across the scleral pores. Rigidity has been shown to be beneficial for liposomal formulation during transport across the sclera [78].

4.2.6. Release kinetics of DEX from nanomicelles

The release study was performed in simulated tear fluid at 37 °C, under sink condition, to identify mechanism of DEX release from nanomicelles. Cumulative % DEX released verses time profile is illustrated in Figure 4-11a. DEX release from the nanomicellar system lasted for 2.5 days. About 50% DEX was released by 24 h from nanomicelles. Previously, it has been shown mPEG-PCL could sustain the release of hydrophobic agent such as honokiol (log p 5.21, Polar surface area 40.46 [90]) for up to 2 weeks [68]. However, DEX is relatively polar molecule with log p of 1.68 and large polar surface area of 94.83 [90]. This may be responsible for poor interaction with hydrophobic PCL chains resulting in relatively faster release pattern.

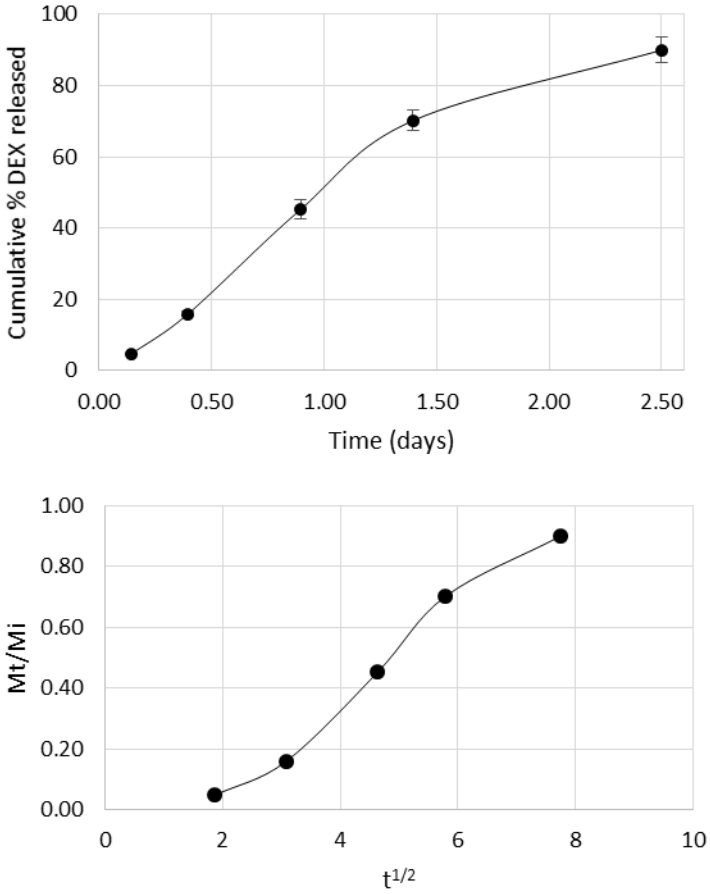

Figure 4-11 (a) Release profile of dexamethasone from nanomicelles under sink conditions at 37 ˚C (mean ± SD, n = 4). (b) Fraction of DEX released at time t (Mt/Mi) vs $t^{1/2}$ profile showing sigmoidal shape suggesting case II transport as drug release mechanism.

Release data was fitted to zero order, first order, Higuchi and Korsmeyer-Peppas model to determine the kinetics of DEX release. The best fit was found with the Korsmeyer-Peppas model with R^2 of 0.9998 compared to other models. The n value was calculated using the data points where less than 60% DEX was released. The n value was found to be 1.24 suggesting super case II transport as release mechanism. In super case II transport, drug release is controlled mainly by the polymer chain relaxation [91]. Polymer chain relaxation may result in loss of DEX-polymer interaction, which encapsulate DEX in micelle core. In addition, due to semicrystalline nature of PCL chains, upon release of DEX from micelles the polymer chain will have more freedom to align and form rigid crystalline core. Formation of rigid core upon release will also hinder the repartition of DEX back in nanomicelle core. Furthermore, volume of release medium was 10 mL with Tween-80 (0.5% w/w) which would aid solubilization released DEX. To confirm super case II release mechanism, fraction of drug release (M_t/M_i) as a function of square root of time ($t^{1/2}$) was plotted. The graph had sigmoidal shape suggesting the mechanism was indeed super case II transport (Figure 4-11b).

CHAPTER 5

5. DEVELOPMENT OF DEX-LOADED NANOMICELLES OF MEAN SIZE 60 NM USING DB3 POLYMER.

5.1. Methods

5.1.1. Modified film-hydration method of nanomicelle preparation

DEX encapsulated nanomicelles were prepared using DB3 polymer. For details on modified-film hydration methods, see section 4.1.2 for method.

5.1.2. Solubility determination (HPLC)

See section 4.1.3 for method.

5.1.3. Small composite Hartley method

See section 4.1.4 for method. The design details including number of runs, factors, levels and response variable are summarized in the Table 5-1.

5.1.4. Micelle size determination

See section 4.1.6 for method.

5.1.5. Powder XRD analysis of blank micelles and DEXM

See section 4.1.7 for method.

5.1.6. 1H-NMR spectroscopy of blank micelles and DEXM

See section 4.1.8 for method.

5.1.7. Release kinetics of DEX from nanomicelles

See section 4.1.9 for method.

Table 5-1 Details of response surface design.

Design Description: Small Composite Hartley Method				
Number of factors	2			
Number of runs	9			
Factors	**Unit**	**Low (-1)**	**Medium (0)**	**High (+1)**
Polymer (X1)	mg	10	30	50
Dexamethasone (X2)	mg	1	3	5
Response variable	**Unit**			
Dexamethasone Solubility (Y)	mg/mL			

5.2. Results and discussion

5.2.1. Optimization of DEX solubility using DoE

DEXM were prepared using the modified film-hydration method explained in chapter 4. The optimal drug:polymer ratio was identified by using DOE. The design details including number of runs, factors, levels and response variable are summarized in the Table 5-1. There were total nine runs in this RSD, which were performed in triplicates (Table 5-2). The design runs and corresponding DEX solubility and size of nanomicelle are presented in Table 5-2. DEX solubility ranged from 0.32 mg/mL (Run#3) to 1.43 mg/mL (Run#4). Highest solubility of 1.43 mg/mL was observed for combination of 53.8 mg polymer and 3 mg of DEX. The design runs were subjected to statistical treatment explained in chapter 4.

Master model: Summary of fit including analysis of variance (ANOVA), lack of fit and correlation coefficient for the master model are summarized in Table 5-3. The master model was not found to be significant ($p = 0.0738$). The correlation coefficient (R^2) for the regression model was 0.9181 indicating that the model explains 91.8% of variation in DEX solubility. Lack of fit p-value was more than 0.05 ($p = 0.146$) suggesting that the master model was significant and can predict DEX solubility.

The parameter estimates for master model are shown in Table 5-4. According to Pareto chart, only statistically significant factor was polymer amount (X1, $p = 0.0227$) (Figure 5-1), which is very similar to DEXM formulated with DB2. No influence of X1X1 interaction on drug solubility ($p = 0.8830$) was observed with modified film-hydration method. Quadratic equation for the master model is given by equation 5.1.

$$Y = 0.899+0.382X1+0.104X2+0.126X1X2-0.018X1X1-0.219X2*X2 \quad \ldots(5.1)$$

Table 5-2 Summary of uncoded design and corresponding solubility, micelle size and PDI.

Run#	Polymer (mg)	DEX (mg)	Solubility (mg/mL)	Micelle size (nm)	PDI
1	10	1	0.42	49.61	0.13
2	50	5	1.16	63.72	0.30
3	6.2	3	0.32	52.00	0.18
4	53.8	3	1.43	55.45	0.21
5	30	0.6	0.36	56.56	0.22
6	30	5.4	0.81	56.07	0.21
7	30	3	0.78	55.66	0.22
8	30	3	1.01	54.55	0.20
9	30	3	0.91	53.89	0.17

Table 5-3 Summary statistics of master model.

Summary of Fit					
RSquare	0.9181				
RSquare Adj	0.7815				
Analysis of Variance					
Source	DF	Sum of Squares	Mean Square	F Ratio	Prob > F
Model	5	1.051	0.210	6.723	0.074
Error	3	0.094	0.031		
C. Total	8	1.145			
Lack Of Fit					
Source	DF	Sum of Squares	Mean Square	F Ratio	Prob > F
Lack Of Fit	1	0.068	0.068	5.388	0.146
Pure Error	2	0.025	0.013		
Total Error	3	0.094			

Table 5-4 Parameter estimates for master model.

Term	Estimate	Std Error	t Ratio	Prob>|t|
Intercept	0.899	0.102	8.81	0.0031
X1(10,50)	0.383	0.088	4.33	0.0227
X2(1,5)	0.105	0.088	1.18	0.3220
X1*X2	0.126	0.182	0.69	0.5375
X1*X1	-0.018	0.114	-0.16	0.8830
X2*X2	-0.220	0.114	-1.93	0.1498

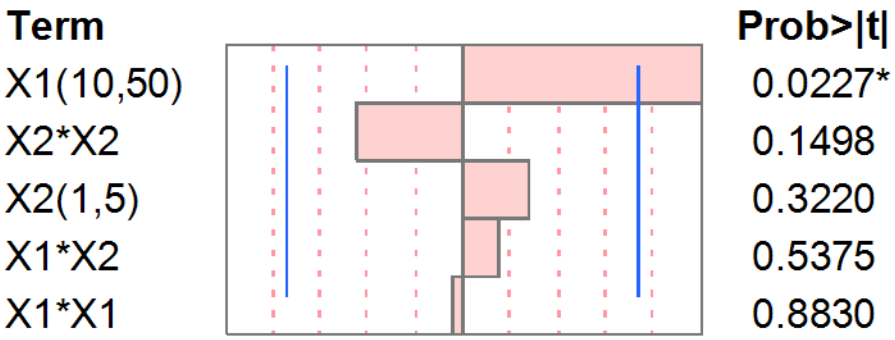

Figure 5-1 Pareto chart for master model. * next to p-value represents significant term.

Table 5-5 Summary statistics of reduced model.

Summary of Fit					
RSquare	0.903				
RSquare Adj	0.845				
Analysis of Variance (ANOVA)					
Source	DF	Sum of Squares	Mean Square	F Ratio	Prob > F
Model	3	1.034	0.345	15.577	0.0057
Error	5	0.111	0.022		
C. Total	8	1.145			
Lack Of Fit					
Source	DF	Sum of Squares	Mean Square	F Ratio	Prob > F
Lack Of Fit	3	0.085	0.028	2.238	0.324
Pure Error	2	0.025	0.013		
Total Error	5	0.111			

Table 5-6 Parameter estimates for reduced model.

Term	Estimate	Std Error	t Ratio	Prob>|t|
Intercept	0.897	0.066	13.6	<.0001
X1(10,50)	0.383	0.074	5.15	0.0036
X2(1,5)	0.105	0.074	1.41	0.2187
X2*X2	-0.182	0.081	-2.26	0.0731

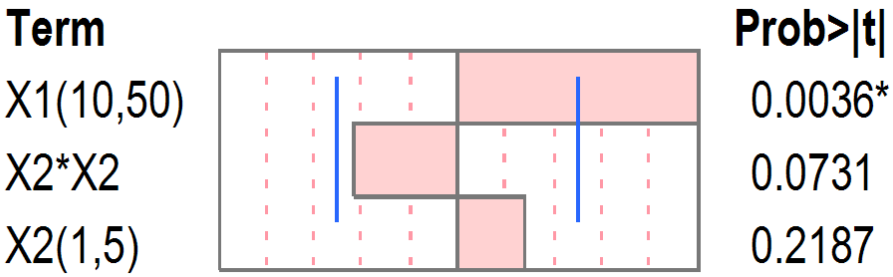

Figure 5-2 Pareto chart for reduced model. * next to p-value represents significant term.

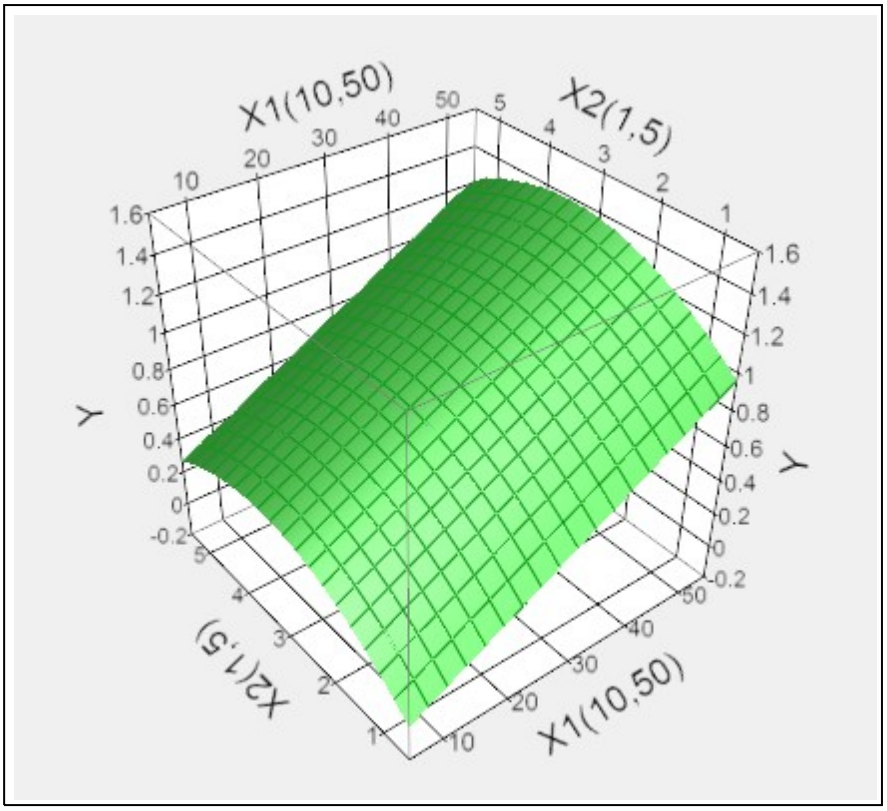

Figure 5-3 Response surface of predictive model. DEX solubility (Y) is plotted as a function of polymer (X1) and DEX (X2) amounts between -1 and 1.

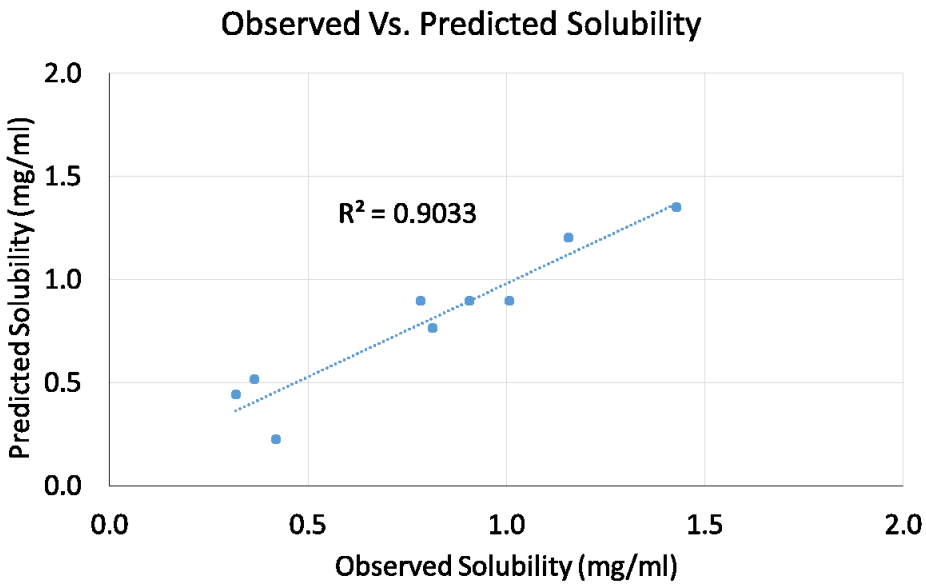

Figure 5-4 Experimental solubility verses predicted solubility for predictive model for ED-2. R2 of 0.90 suggests that DEX solubility predicted by reduced model are very close to experimental values.

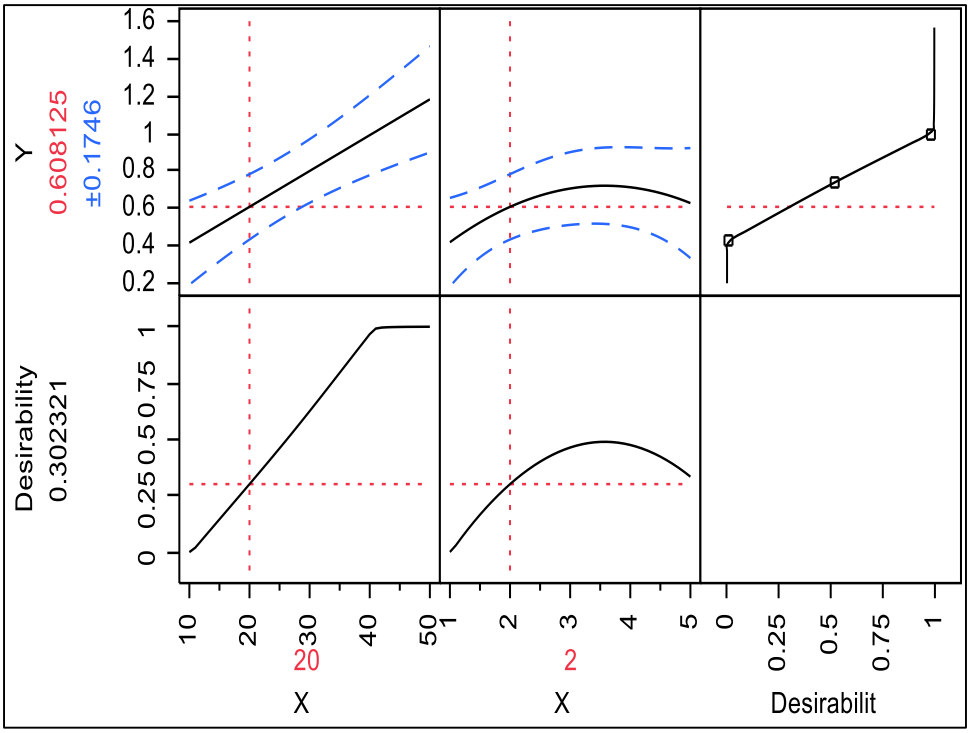

Figure 5-5 Prediction profile of reduced model depicting solubility (Y) as function of polymer (X1) and DEX (X2) amounts.

Table 5-7 Checkpoint analysis for reduced model.

X1:X2 ratio (n = 3)	**Predicted solubility (mg/mL)**	**Experimental solubility (mg/mL)**	**Two-tailed P-value**	**% Standard error**
20:2	0.608 ± 0.175	0.573 ± 0.062	0.760	3.5%

To characterize the physical form of DEX and polymer, the dried polymer-DEX film was studied by XRD. Polymer:DEX film was prepared at a ratio X1:X2::30:5. XRD showed presence of characteristic peaks of PCL (2θ = 21.9) and mPEG (2θ = 19.2 and 23.8) in the dried film (Figure 5-7c), suggesting that the X1X1 interaction represents crystallization of the polymer upon evaporation of organic solvent. Small peaks corresponding to DEX were also present (2θ = 14, 15.6 and 17) in the dried film, indicative of slight crystallization and X2X2 interaction. XRD analysis of dried DEX-polymer film was conducted after heating the films to delineate the effect of heating on physical form of polymer. The peaks for mPEG and PCL were present following heating of film at 65 ^{o}C (Figure 5-7c and Figure 5-7d). These results could be explained by the fact that XRD patterns were recorded at RT. Gradual cooling of DEX-polymer film to RT could result in recrystallization of polymer. It also worth noting that heating the film did not have any effect on physical form of DEX, as predicted (Figure 5-7d).

Reduced model:

A reduced or predictive model was generated by removing the non-significant terms with $p>0.05$ from the master model. Hence, terms X1X2 ($p = 0.5375$) and X1X1 ($p = 0.8830$) were removed. XRD analysis indicated crystallization of DEX in polymer-DEX film (after heating) representing X2X2 interaction (Figure 5-7c-d). Hence, term X2X2 was included in predictive model. Summary statistic for the reduced model is presented in Table 5-5. The predictive model was compared with master model for p-values of the model, p-value of lack of fit and adjusted R^2. The reduced model had p-value of 0.0057, lack fit p-value of 0.324 and adjusted R^2 of 0.845, indicating that the reduced model was superior in predicting DEX solubility (Y). The parameter estimates for the reduced model are shown in Table 5-6. Pareto chart for the reduced model is depicted in Figure 5-2. Again the only significant term influencing DEX solubility was X1 (p =

0.0036). Interactions between DEX molecules (X2X2) was not significant (p = 0.0731) as per model and had negative effect on DEX solubility with method-2. The prediction expression for reduced model is represented by equation 5.1.

$$Y = 0.897+0.383X1+0.105X2-0.182X2*X2 \quad \ldots(5.2)$$

Response surface showing the change in solubility of DEX as a function of DEX and polymer amounts is illustrated in Figure 5-3. Solubility of DEX increased linearly with increasing polymer amount at all the DEX levels. Nonetheless, solubility increase was not linear with increasing DEX amount due to X2X2 interaction. The prediction profile was generated to determine the optimal point with the highest desirability.

The checkpoint analysis was carried out to validate the reduced model at X1:X2::20:2 ratio (Figure 5-5). Ratio X1:X2::20:2 was selected for checkpoint analysis, as it was not a part of design runs suggested by the statistical software (SAS 9.02). No statistically significant difference was observed between experimental and predicted DEX solubility (p = 0.7604) (Table 5-7). The model was also validated by plotting predicted verses actual solubility (Figure 5-4). The relationship was found to be linear with R^2 of 0.90 indicating predicted solubility by model is close to experimental one. Based on checkpoint analysis and experimental verses predicted solubility, it can be concluded that the reduced model can accurately predict DEX solubility. Using prediction profile for reduced model, optimal X1:X2 ratio to obtain DEX solubility ≥1mg/mL was obtained.

5.2.2. Micelle size determination

Nanomicelle size and distribution were determined by dynamic light scattering method for all the runs (Table 5-2). The size ranged from 50 to 64 nm with unimodal distribution irrespective of DEX solubility.

			Diam. (nm)	% Intensity	Width (nm)
Z-Average (d.nm):	58.10	Peak 1:	77.80	98.9	46.03
PdI:	0.249	Peak 2:	4432	1.1	908.0
Intercept:	0.941	Peak 3:	0.000	0.0	0.000
Result quality :	Good				

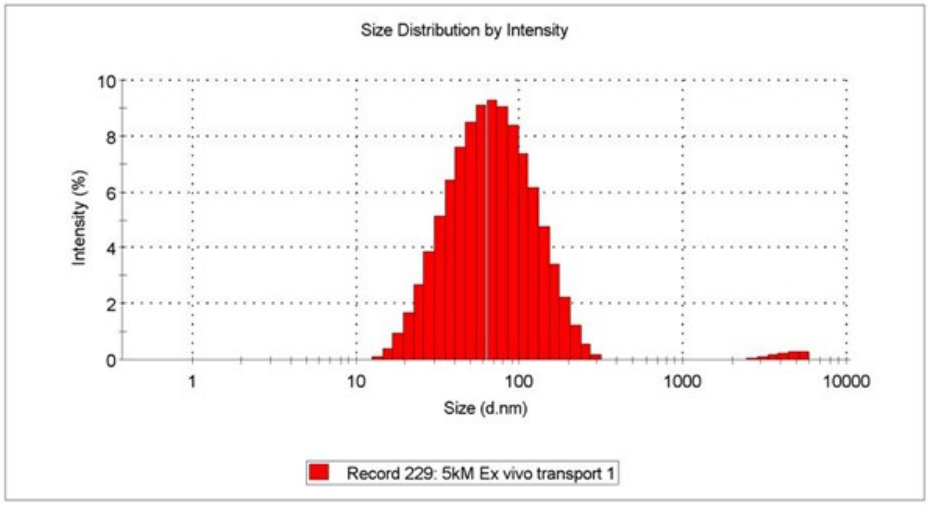

Figure 5-6 Micelle size distribution for DEXM prepared using DB3 polymer.

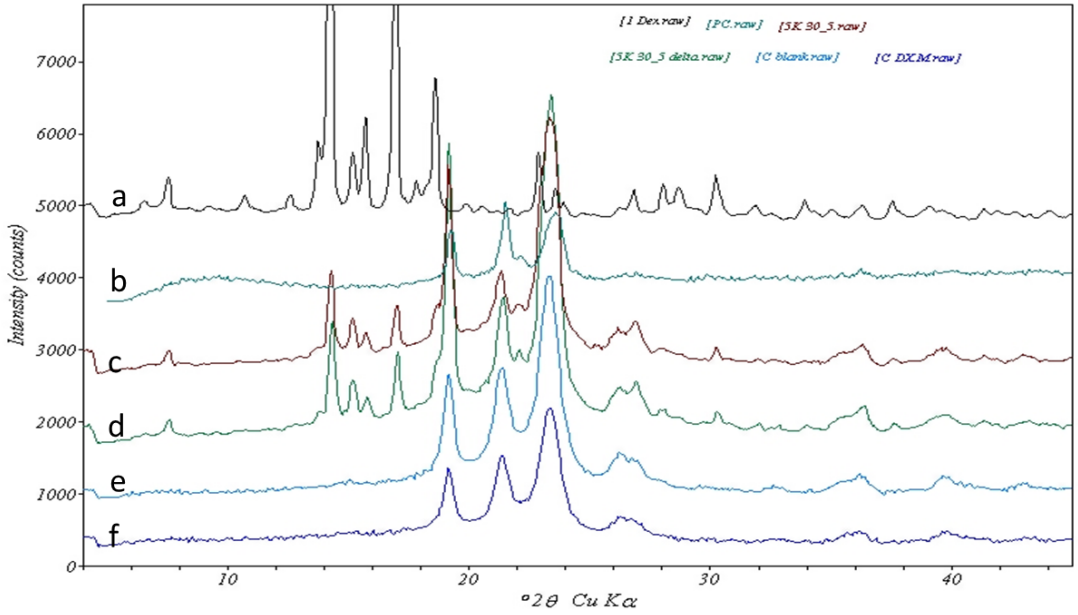

Figure 5-7 X-ray diffraction pattern for (a) Dexamethasone, (b) PCL-mPEG polymer, (c) Polymer:DEX film before heating (Polymer:DEX::30:5), (d) Polymer:DEX film after heating (Polymer:DEX::30:5), (e) Freeze dried Blank micelles (f) Freeze dried DEXM (0.1% w/v DEX).

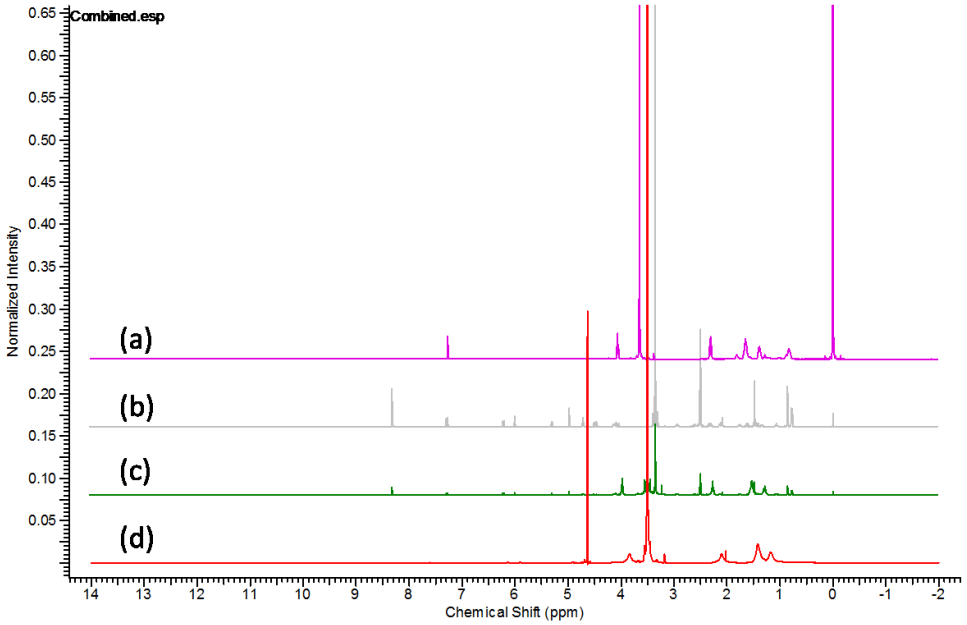

Figure 5-8 ^{1}H-NMR spectrums for (a) PCL-mPEG polymer in $CDCl_3$ (b) Dexamethasone in d_6-DMSO, (c) PCL-mPEG (50mg) and dexamethasone (1mg) in d_6-DMSO, (d) 0.1% DEXM in D_2O.

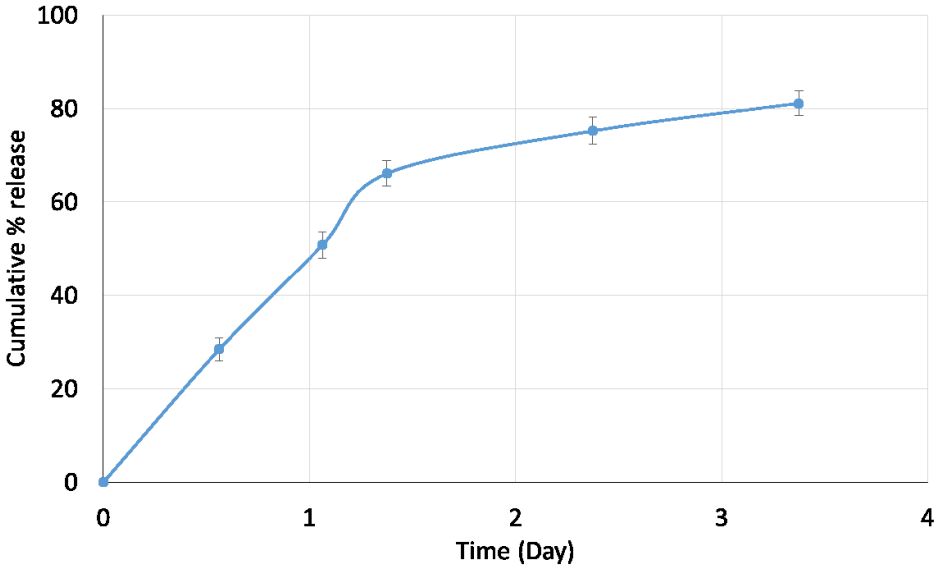

Figure 5-9 Release profile of dexamethasone from nanomicelles under sink conditions at 37 ˚C (mean ±SD, n = 4).

The PDI for all the runs were below 0.22 indicating narrow size distribution. Size distribution showing mean size and PDI for DEXM is illustrated in Figure 5-6. The average size was 58.1 nm with PDI of 0.25. It is expected that micelle size would increase with increase in DEX solubility. However, even with this increase in solubility, drug loading did not vary appreciably. Hence, we did not observe an appreciable increase in nanomicelle size or polydispersity with increase in solubility. The control over nanomicelle size was achieved by controlling the molecular weight of PCL and PEG segments of diblock polymer.

5.2.3. ^{1}H-NMR spectroscopy of Blank micelles and DEXM

^{1}H-NMR spectroscopy was used to ascertain the presence of DEX in nanomicelle core. ^{1}H-NMR spectra for physical mixture of DEX and polymer in d_6-DMSO, DEXM in D_2O and DEX in d_6-DMSO were recorded (Figure 5-8). The ^{1}H-NMR spectra for combination of DEX and polymer in d_6-DMSO showed all the characteristic peaks corresponding to DEX, PCL and mPEG (Figure 5-8c). ^{1}H-NMR for DEXM in D_2O also showed presence of characteristic peak for mPEG segment at 3.4-3.6 ppm and those for PCL were absent, indicating micellization. During micelle formation PCL block assemble to form the hydrophobic core and mPEG segment forms hydrophilic corona. Since the core of micelle lacks accessibility to solvent, movement of PCL segment in the core is limited and hence the proton NMR signal is very weak compared to signal in DMSO. In contrast, the corona forming mPEG segment is free to move in D_2O showing good ^{1}H-NMR signal intensity. Characteristic peaks for DEX were absent due to restricted mobility inside micelle core, implying that drug was molecularly dispersed in micelle core (Figure 5-8e).

5.2.4. Powder XRD analysis of blank micelles and DEXM

Blank micelles and DEXM were also studied by XRD to seek further insight into physical state of polymer and DEX in nanomicelles. The results are presented in Figure 5-7e and Figure 5-7f. XRD pattern for freeze-dried DEXM was devoid of DEX peaks indicating that the drug was molecularly dispersed in nanomicelle. Both blank micelles and DEXM showed characteristic peaks of PCL ($2\theta = 21.9$) and mPEG ($2\theta = 19.2$ and 23.8). PCL, due to its semi-crystalline nature, does not self-assemble in water to form micelles at RT. However, at temperatures close to melting point provides PCL with necessary chain mobility to self-assemble into micelles. Once the micelles are formed and system reaches RT, PCL segments in core reestablishes the polymer-polymer interactions regaining its semi-crystalline state in nanomicelle core. We expect that the semi-crystal nature of nanomicelle core would provide rigid core to the nanomicelles. Such rigid micelle core may provide resistance against sheer stress while transport of nanomicelles across the scleral pores. Rigidity has been shown to be beneficial for liposomal formulation during transport across the sclera [78]. Similar results were observed for DEXM prepared using DB2 polymer.

5.2.5. Release kinetics of DEX

The release study was performed in simulated tear fluid at 37 °C, under sink condition, to identify mechanism of DEX release from nanomicelles. Cumulative % DEX released verses time profile is illustrated in Figure 5-9. DEX release from the nanomicellar system lasted for >3 days. About 50% DEX was released by day one from nanomicelles. Very similar results were observed for low molecular weight DB2 polymer.

Release data was fitted to zero order, first order, Higuchi and Korsmeyer-Peppas model to determine the kinetics of DEX release. The best fit was found with the Korsmeyer-Peppas

model with R^2 of 0.9993 compared to other models. The n value was found to be 0.92. Value of diffusion exponent (n) >0.89 suggests that mechanism of release was super case II transport. In super case II transport, drug release is controlled mainly by the polymer chain relaxation [91]. The polymer chain relaxation may result in loss of DEX-polymer interaction, which facilitates DEX encapsulation in micelle core. In addition, due to semicrystalline nature of PCL chains, upon release of DEX from micelles the polymer chain will have more freedom to align and form rigid crystalline core. Formation of rigid core upon release will also hinder the repartition of DEX back in nanomicelle core.

CHAPTER 6

6. DEVELOPMENT OF DEX-LOADED NANOMICELLES OF MEAN SIZE 10 NM USING DB1 POLYMER.

6.1. Methods

6.1.1. Modified film-hydration method of nanomicelle preparation

DEX encapsulated nanomicelles were prepared using DB1 following modified-film hydration method described in section 4.1.2.

6.1.2. Solubility determination (HPLC)

See section 4.1.3 for method.

6.1.3. Small composite Hartley method

See section 4.1.4 for method. The design details including number of runs, factors, levels and response variable are summarized in the Table 6-1.

6.1.4. Micelle size determination

See section 4.1.6 for method.

6.1.5. Powder XRD analysis of blank micelles and DEXM

See section 4.1.7 for method.

6.1.6. ^{1}H-NMR spectroscopy of blank micelles and DEXM

See section 4.1.8 for method.

6.1.7. Release kinetics of DEX from nanomicelles

See section 4.1.9 for method.

Table 6-1 Details of response surface design.

Design Description: Small Composite Hartley Method				
Number of factors	2			
Number of runs	9			
Factors	**Unit**	**Low (-1)**	**Medium (0)**	**High (+1)**
Polymer (X1)	mg	30	55	80
Dexamethasone (X2)	mg	2	3.5	5
Response variable	**Unit**			
Dexamethasone Solubility (Y)	mg/mL			

6.2. Results and discussion

6.2.1. Preparation of DEXM

DEXM using DB1 polymer were prepared using the modified film-hydration method explained in chapter 4. The optimal drug:polymer ratio was identified by using Small composite-Hartley method. The design details including number of runs, factors, levels and response variable are summarized in the Table 6-1. There were total nine runs in this RSD, which were performed in triplicates (Table 6-2). The design runs and corresponding DEX solubility and size of nanomicelle are presented in Table 6-2. DEX solubility ranged from 0.6 mg/mL (Run#3) to 2.3 mg/mL (Run#2). Highest solubility of 2.3 mg/mL was observed for combination of 80 mg polymer and 5 mg of DEX. The design runs were subjected to statistical treatment explained in chapter 4.

Master model:

Summary of fit including analysis of variance (ANOVA), lack of fit and correlation coefficient for the master model are summarized in Table 6-3. The master model was found to be significant ($p = 0.0009$), suggesting that solubility of DEX (Y) was dependent on the set of X variables. The correlation coefficient (R^2) for the regression model was 0.9959 indicating that the model explains 99.59% of variation in DEX solubility. Lack of fit p-value was more than 0.05 ($p = 0.3897$) suggesting that the master model was significant and can predict DEX solubility. The parameter estimates for master model are shown in Table 6-4. According to Pareto chart, statistically significant terms were polymer amount (X1, $p = 0.0002$), X1X1 interaction ($p = 0.0046$), DEX*DEX interaction (X2X2, $p = 0.0047$) and polymer*DEX interaction (X1X2, $p = 0.0055$) (Figure 6-1).

Table 6-2 Summary of uncoded design and corresponding solubility, micelle size and PDI.

Run#	Polymer (mg)	DEX (mg)	Solubility (mg/mL)	Micelle size (nm)	PDI
1	30	2	1.0	10	0.112
2	80	5	2.3	9.6	0.102
3	25.3	3.5	0.6	9.9	0.106
4	84.7	3.5	2.1	9.5	0.094
5	55	1.7	1.3	9.6	0.091
6	55	5.3	1.5	9.8	0.080
7	55	3.5	1.7	9.8	0.080
8	55	3.5	1.7	9.7	0.073
9	55	3.5	1.8	9.8	0.074

Table 6-3 Summary statistics of master model.

Summary of fit					
RSquare	0.9959				
RSquare Adj	0.9891				
Analysis of Variance (ANOVA)					
Source	DF	Sum of Squares	Mean Square	F Ratio	Prob > F
Model	5	2.182995	0.436599	146.4546	0.0009
Error	3	0.008943	0.002981		
C. Total	8	2.191938			
Lack Of Fit					
Source	DF	Sum of Squares	Mean Square	F Ratio	Prob > F
Lack Of Fit	1	0.003331	0.003331	1.1868	0.3897
Pure Error	2	0.005613	0.002806		
Total Error	3	0.008943			

Table 6-4 Parameter estimates for master model.

Term	Estimate	Std Error	t Ratio	Prob>|t|
Intercept	1.750	0.0315	55.53	<.0001
X1 (30,80)	0.601	0.0273	22.02	0.0002
X2(2,5)	0.065	0.0273	2.38	0.0972
X1*X2	0.405	0.0561	7.21	0.0055
X1*X1	-0.271	0.0352	-7.69	0.0046
X2*X2	-0.269	0.0352	-7.64	0.0047

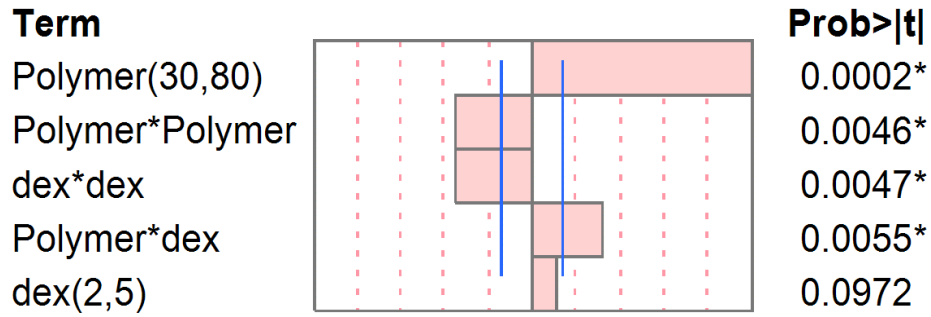

Figure 6-1 Pareto chart for master model. * next to p-value represents significant term.

Terms with positive influence on DEX solubility were X1 and X1X2 interaction suggesting low molecular DB1 polymer had better interaction with DEX resulting in higher solubility. On the other hand, X1X1 and X2X2 interactions lead to decrease in solubility. We subjected Polymer-DEX film, blank nanomicelles and DEXM to PXRD to understand to nature of X1X1 and X2X2 interactions.

DB1 polymer was completely devoid of characteristic peaks of PCL (2θ = 21.9) and mPEG (2θ = 19.2 and 23.8) suggesting that the low molecular weight mPEG-PCL polymer is amorphous in nature (Figure 6-2b). Polymer:DEX film was prepared at a ratio X1:X2::30:5. XRD showed complete absence of characteristic peaks of PCL (2θ = 21.9) and mPEG (2θ = 19.2 and 23.8) in the dried film (Figure 6-2c), suggesting that the X1X1 interaction does not represent crystallization of the polymer in case of DB1. Peaks corresponding to DEX were also very small (2θ = 14, 15.6 and 17) in the dried film, indicative of slight crystallization and X2X2 interaction. XRD analysis of dried DEX-polymer film was conducted after heating the films to delineate the effect of heating on physical form of polymer. The peaks for mPEG-PCL were also absent following heating of film at 65 ^{o}C (Figure 6-2c and Figure 6-2d). Unknown sharp peaks were noted at 2θ = 7.2 and 15 which did not correspond to DEX or polymer.

Master model by itself served as predictive model as all factors and interactions were significant. The prediction expression for reduced model is represented by equation 6.1.

$$Y = 1.750 + 0.601*X1 + 0.065*X2 + 0.405*X1X2 - 0.271*X1X1 - 0.269*X2X2 \quad \ldots(6.1)$$

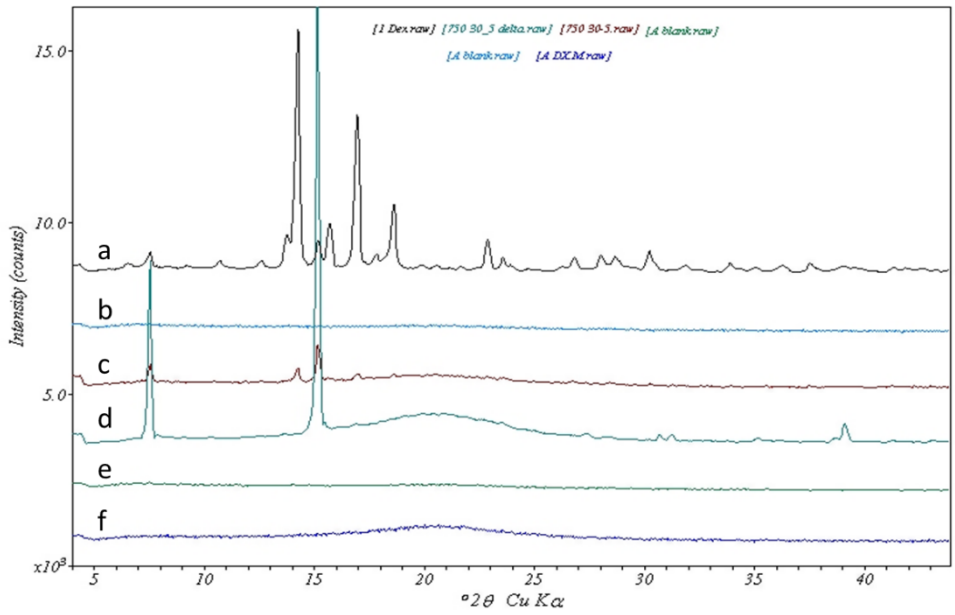

Figure 6-2 X-ray diffraction pattern for (a) Dexamethasone, (b) PCL-mPEG polymer, (c) Polymer:DEX film before heating (Polymer:DEX::30:5), (d) Polymer:DEX film after heating (Polymer:DEX::30:5), (e) Freeze dried Blank micelles (f) Freeze dried DEXM (0.1% w/v DEX).

Response surface showing the change in solubility of DEX as a function of DEX and polymer amount is illustrated in Figure 6-3. In this case, solubility of DEX did not increase linearly with increasing polymer amount at all the DEX levels. The non-linearity can be attributed the X1X1 and X2X2 interactions. The prediction profile was generated to determine the optimal point with the highest desirability (Figure 6-4). The checkpoint analysis was carried out to validate the reduced model at X1:X2::80:4 ratio. Ratio X1:X2::80:4 was selected for checkpoint analysis, as it was not a part of design runs suggested by the statistical software (SAS 9.02). No statistically significant difference was observed between experimental and predicted DEX solubility ($p = 0.8852$) (Table 6-5).

The model was also validated by plotting predicted verses actual solubility (Figure 6-5). The relationship was found to be linear with R^2 of 0.9959 indicating predicted solubility by model is close to experimental one. Based on checkpoint analysis and experimental verses predicted solubility, it can be concluded that the reduced model can accurately predict DEX solubility. Using prediction profile for reduced model, optimal X1:X2 ratio to obtain DEX solubility ≥1mg/mL was obtained.

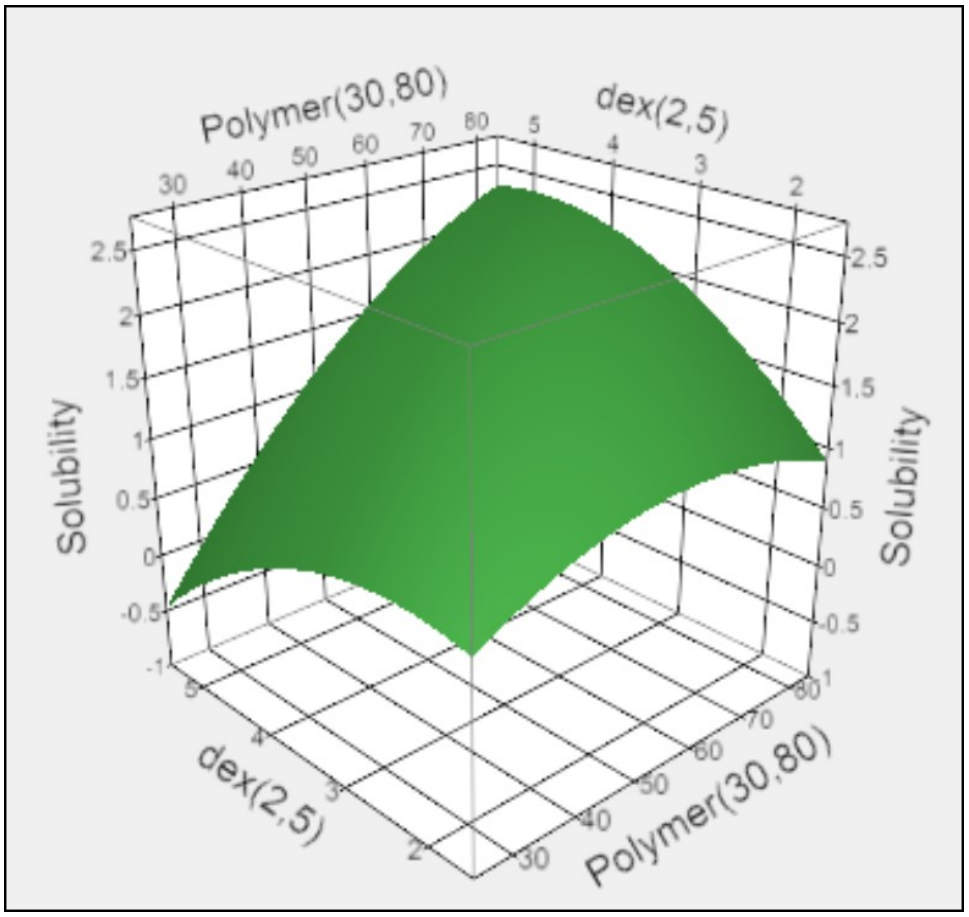

Figure 6-3 Response surface of predictive model. DEX solubility (Y) is plotted as a function of polymer (X1) and DEX (X2) amounts between -1 and 1.

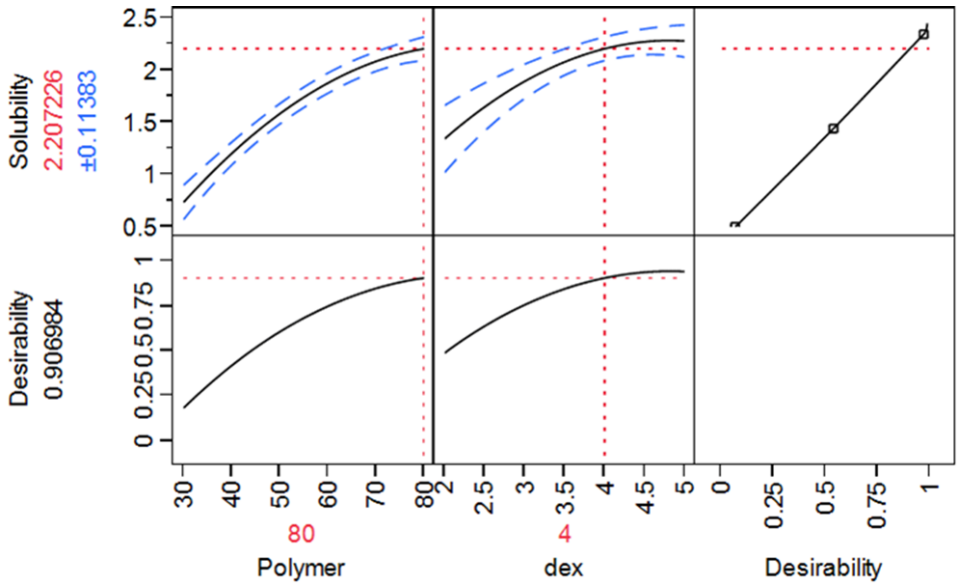

Figure 6-4 Prediction profile of reduced model depicting solubility (Y) as function of polymer (X1) and DEX (X2) amounts.

Table 6-5 Checkpoint analysis for master model.

Polymer:DEX amount (mg) (n = 3)	**Predicted solubility (mg/mL)**	**Experimental solubility (mg/mL)**	**Two-tailed P-value**	**% Standard error**
80:4	2.2 ± 0.093	2.2 ± 0.114	0.8852	1.33

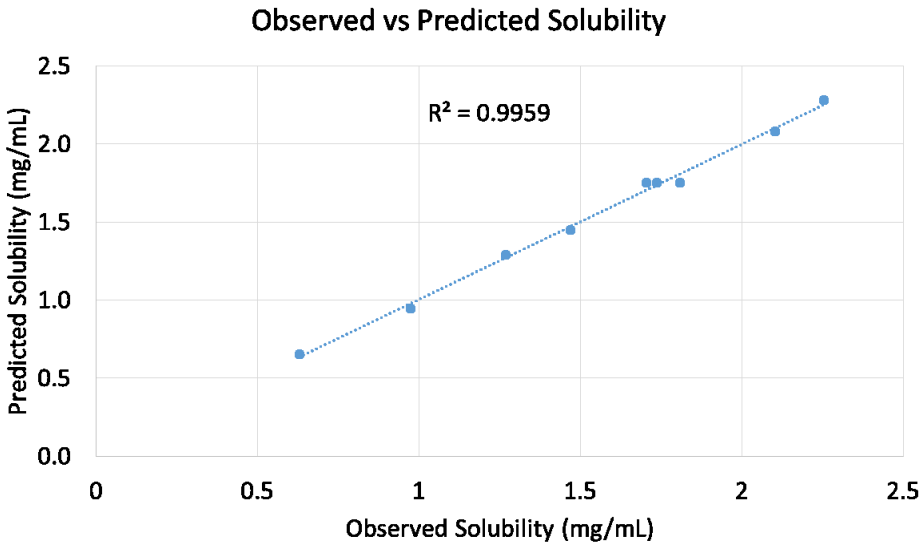

Figure 6-5 Experimental solubility verses predicted solubility for predictive model for ED-2. R2 of 0.9959 suggests that DEX solubility predicted by reduced model are very close to experimental values.

6.2.2. Micelle size and morphology

Nanomicelle size and distribution were determined by dynamic light scattering method for all the runs (Table 6-2). The size ranged from 9.8-10 nm with unimodal distribution irrespective of DEX solubility. The PDI for all the runs were below 0.11 indicating very narrow size distribution. A DSL analysis showing average size and PDI for DEXM is illustrated in Figure 6-6a. The average size was 9.5 nm with PDI of 0.11. The control over nanomicelle size was achieved by controlling the molecular weight of PCL and PEG segments of diblock polymer. The morphology of optimal nanomicelle was studied by TEM (Figure 6-6b). TEM micrograph of nanomicelles indicated that the nanomicelles were spherical in shape and the size of nanomicelles is consistence with DLS analysis.

6.2.3. PXRD of blank nanomicelles and DEXM

Blank micelles and DEXM were also studied by XRD to seek further insight into physical state of polymer and DEX in nanomicelles. The results are presented in Figure 6-2e and Figure 6-2f. XRD pattern for freeze-dried DEXM was devoid of DEX peaks indicating that the drug was molecularly dispersed in nanomicelle. Both blank micelles and DEXM did not show characteristic peaks for PCL. Unlike DB2 and DB3 polymers, DB1 is low molecular weight polymer with very short PCL and PEG chain length. This short chain length may be a reason for absence if characteristic peaks associated with PCL and PEG.

6.2.4. ^{1}H-NMR spectroscopy of blank micelles and DEXM

^{1}H-NMR spectroscopy was used to ascertain the presence of DEX in nanomicelle core. ^{1}H-NMR spectra for physical mixture of DEX and polymer in d_6-DMSO, DEXM in D_2O and DEX in d_6-DMSO were recorded (Figure 6-7).

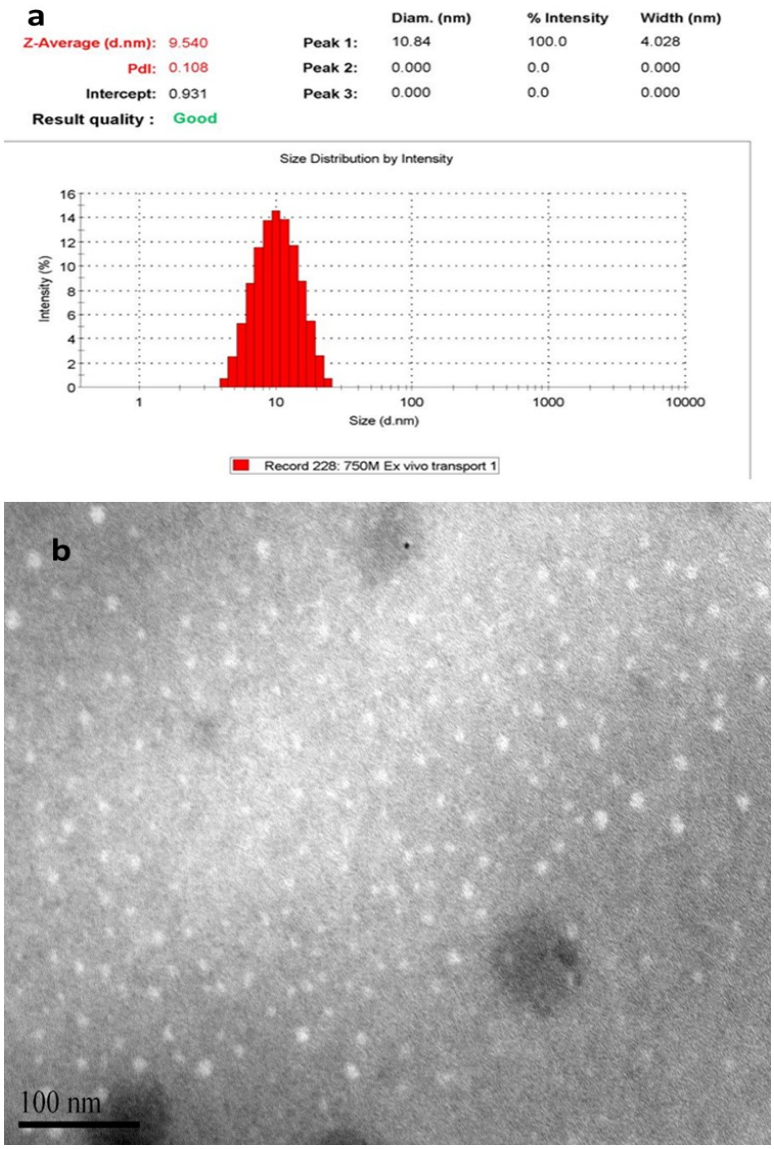

Figure 6-6 (a) Micelles size distribution for DEXM. (b) Transmission electron micrograph for DEXM. Nanomicelles appear as a white spot on dark background as indicated by arrows.

The ^{1}H-NMR spectra for combination of DEX and polymer in d_6-DMSO showed all the characteristic peaks corresponding to DEX, PCL and mPEG (Figure 6-7c). ^{1}H-NMR for DEXM in D_2O also showed presence of characteristic peak for mPEG segment at 3.4-3.6 ppm and those for PCL were absent, indicating micellization. During micelle formation PCL block assemble to form the hydrophobic core and mPEG segment forms hydrophilic corona. Since the core of micelle lacks accessibility to solvent, movement of PCL segment in the core is limited and hence the proton NMR signal is very weak compared to signal in DMSO. In contrast, the corona forming mPEG segment is free to move in D_2O showing good ^{1}H-NMR signal intensity. Characteristic peaks for DEX were also absent due to restricted mobility inside micelle core, implying that drug was molecularly dispersed in micelle core (Figure 6-7d).

6.2.5. Release kinetics of DEX release from DEXM

The release study was performed in simulated tear fluid at 37 °C, under sink condition, to identify mechanism of DEX release from nanomicelles. Cumulative % DEX released verses time profile is illustrated in Figure 6-8. DEX release from the nanomicellar system lasted for 3.5 days. More than 50% DEX was released by day one from nanomicelles. Overall release pattern was similar to that observed for high molecular weight DB3 and DB2 nanomicelles. Release data was fitted to zero order, first order, Higuchi and Korsmeyer-Peppas model to determine the kinetics of DEX release. The best fit was found with the Korsmeyer-Peppas model with R^2 of 0.9862 compared to other models. The n value was found to be 0.63. Value of diffusion exponent $0.45 < n < 0.89$ suggests that mechanism of release was anomalous transport. In this case, drug release is controlled both diffusion of drug and erosion of polymer.

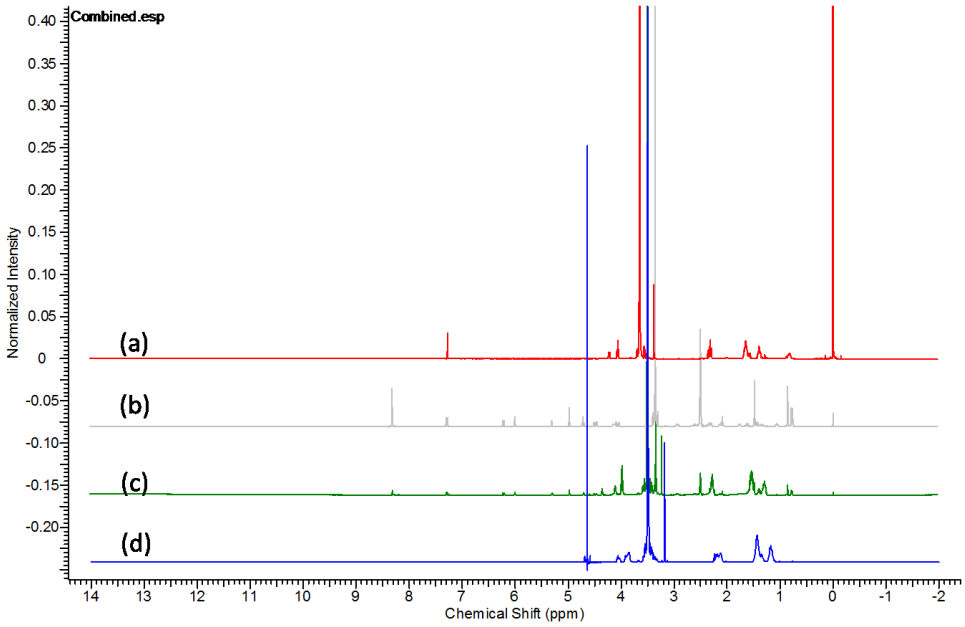

Figure 6-7 ^{1}H-NMR spectrums for (a) PCL-mPEG polymer in $CDCl_3$ (b) dexamethasone in d_6-DMSO, (c) PCL-mPEG (50mg) and dexamethasone (1mg) in d_6-DMSO, (d) 0.1% DEXM in D_2O.

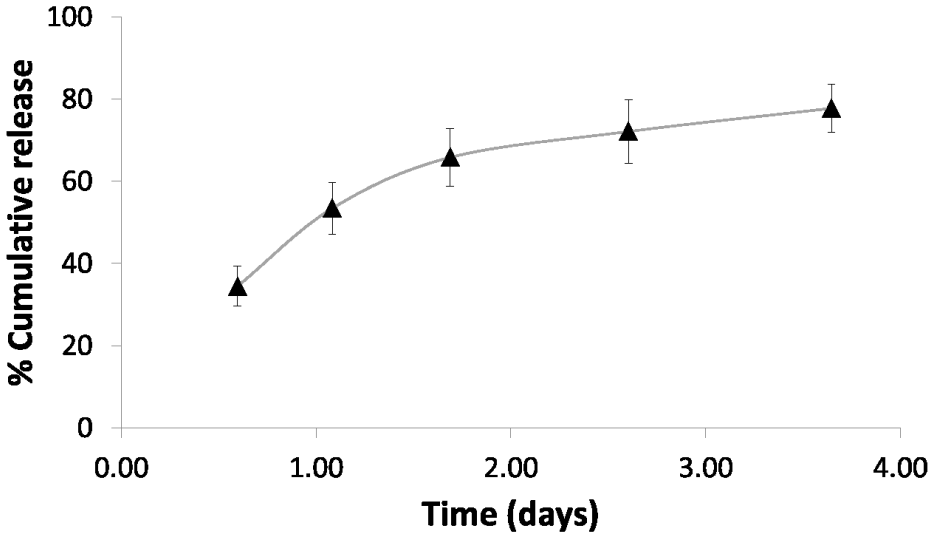

Figure 6-8 Release profile of dexamethasone from nanomicelles under sink conditions at 37 ˚C (mean ±SD, n = 4).

CHAPTER 7

7. EFFECT OF NANOMICELLE SIZE ON PERMEABILITY.

7.1. Methods

7.1.1. In vitro permeability across HCEC cells

Transwell diffusion chamber system was utilized for determining *in vitro* permeability of DEX from DEXM across conjunctival cells following a published protocol. Cells were seeded at a density of 25,000 per well in 12-well collagen-coated Transwell® permeable inserts (Costar®) and grown until confluency by changing medium every alternate day. Prior to a transport experiment, cell monolayers grown on the Transwell® inserts were rinsed with DPBS (pH 7.4) and incubated at 37 °C for 10 min for twice for both apical (AP) and basolateral (BL) sides. Transport was initiated by adding 400 µL of DEX suspension or DEXM (in DPBS, pH 7.4) to the donor chamber (AP side) of cells. DPBS pH 7.4 was added in receiver chamber (BL side). Transport experiment was conducted for 3 h. Samples (100 µL) were collected from the receiver chamber at predetermined time intervals of 30, 60, 90, 120, 150, and 180 min and fresh DPBS pH 7.4 was replaced to maintain sink conditions in receiver chamber. The samples were analyzed by LC-MS/MS analysis following a previously published method from our laboratory [92]. Permeability (P_{app}) of DEX was calculated using equation 7.1.

$$P_{app} = M/A*C_d \qquad \ldots (7.1)$$

Where, M represents the slope obtained from plot of cumulative amount of drug permeated verses time, A denotes surface area of membrane exposed to drug and C_d is the drug concentration in donor chamber at t = 0.

Transport study was conducted in quadruplicate for all test and control sets. A statistical significance between permeability of DEX suspension and DEXM at $p<0.05$ was considered to be significant.

7.1.2. Ex vivo permeability across excised rabbit sclera

Tissue Preparation: Adult New Zealand male rabbits weighing between 2 and 2.5 kg were obtained from Harlan laboratory. All animal handling procedures were approved by the Institutional Animal Care and Use Committee (IACUC) of University of Missouri-Kansas City (UMKC, Kansas City, MO). Rabbits were anesthetized with I.M. administration of ketamine HCl (35 mg/kg) and xylazine (5 mg/kg). The animals under deep anesthesia were euthanized by an overdose of sodium pentobarbital (100 mg/kg) administered through marginal ear vein. Eyes were removed carefully and the posterior segment was separated by cutting along the limbus. The sclera was separated from retina and choroid and was placed in a petri dish containing Dulbecco's phosphate-buffered saline (pH 7.4).

In order to carry out permeability studies, the excised tissue was mounted on a Franz-type vertical diffusion cell (PermeGear Inc., Hellertown, PA) with episcleral side facing the donor chamber. The receptor chamber was filled with isotonic phosphate buffer saline (IPBS; pH 7.4). DEX suspension or DEXM formulation was added to the donor chamber to begin transport study. At a regular time interval 200 µL of sample was withdrawn from receptor chamber and replaced with an equal volume of fresh IPBS buffer. Experiments were carried under sink conditions, for 3 h at 37 ^{o}C (n = 4). The samples were analyzed by LC-MS/MS following a method published previously from our laboratory[92]. Permeability (P_{app}) of was calculated according to equation 7.1.

7.1.3. Analysis of DEX in buffer samples by LC/MS–MS

LC-MS/MS method described earlier from our lab [92] was utilized with a few modifications for quantitating DEX in buffer samples from *ex vivo* transport studies. Ninety-microliter aliquots of buffer samples were spiked with 20 ng of prednisolone (IS) and vortexed for 15 s. The analytes were then extracted with 900 µL of ice cold TBME and vortexed for 3.5 min. Samples were centrifuged at 10,000 rpm for 7 min to separate the aqueous and organic layers. Seven hundred and fifty µL of the organic layer was collected and dried in vacuum. Dried sample was reconstituted in 100 µL of mobile phase (ACN:Water::40:60, 0.1% formic acid). Ten microliter of reconstituted sample was injected onto the LC/MS–MS for analysis. LC/MS-MS QTrap® API-3200 mass spectrometer, equipped with Shimadzu quaternary pump, vacuum degasser and autosampler (Shimadzu Scientific Instruments, Columbia, MD, USA) was employed to analyze samples from *ex vivo* studies.

LC separation was performed on an XTerra® MS C18 column 50 mm × 4.6 mm, 5.0 µm (Waters, Milford, MA). The mobile phase consisted of 40% ACN and 60% water with 0.1% formic acid, pumped at a flow rate of 0.25 mL/min. Multiple reactions monitoring (MRM) mode was utilized to detect the compounds of interest. The mass spectrometer was operated in the positive ion mode for detection. The precursor to product ions (Q1 → Q3) for DEX and IS during quantitative optimization were (m/z) 393.20→355.30 and 361.30→147.20, respectively. The operational parameters for the tandem mass spectrum for each analyte were obtained after running them in quantitative optimization mode. The turbo ion spray setting and collision gas pressure were optimized (IS voltage: ±5500 V, temperature: 350 °C, nebulizer gas: 40 psi, curtain gas: 30 psi). The lower limit of quantification was found to be 31.25 ng/mL for DEX.

7.2. Results and discussion

7.2.1. In vitro transport across conjunctival cells

We examined DEX transport across conjunctival cells (*in vitro*) and excised rabbit sclera (*ex vivo*) as we hypothesize that the nanomicelles size may influence permeability of encapsulated drug. Figure 7-1a illustrates cumulative percentage DEX transported across conjunctival cells from nanomicelles and suspension (control). The permeability of DEX from suspension was 0.69×10^{-6} cm/sec (Figure 7-1b). Permeability with all DEXM were significantly higher; about 2-fold, compared to control (ANOVA $p<0.0001$). However, there was no significant difference between permeability among nanomicelles of various sizes (ANOVA, $p = 0.3461$). These results clearly suggest that the nanomicelles can increase DEX permeability across the conjunctival cells. In addition, there was no influence of nanomicelles size on permeability.

7.2.2. Transscleral permeability of DEX

The sclera acts as a static barrier for transport of drug/nanocarriers towards back of the eye following topical administration. Hence, transport of DEX across the excised rabbit sclera was carried out for the nanomicelles and compared with DEX suspension (0.1% w/v). Cumulative %DEX verses time profile for DEXM and DEX suspension are illustrated in Figure 7-2a. Figure 7-2b depicts permeability for DEX suspension and DEXM. Permeabilities were compared using ANOVA (more than two groups) and t-test (two groups). P-value less than 0.05 were considered significant. P_{app} for DEX suspension was 1.19×10^{-6} cm/sec. A statistically significant increase in P_{app} was observed with DEXM of all three sizes (Figure 7-2b, ANOVA $p<0.0001$).

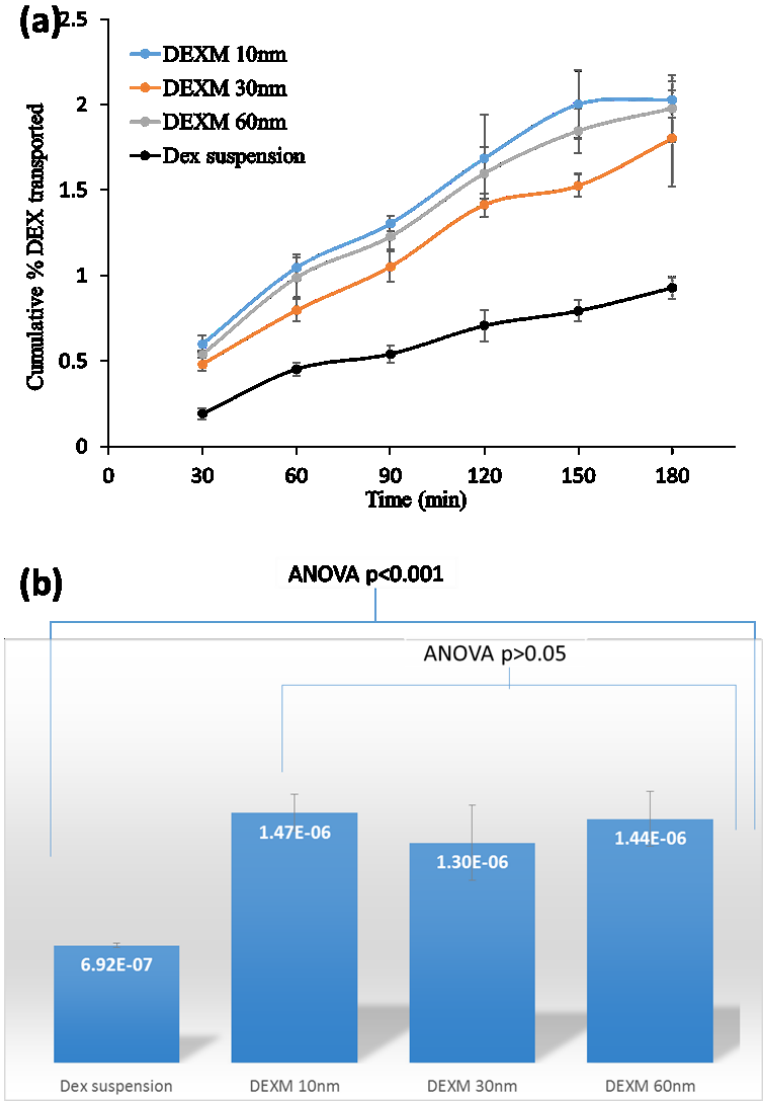

Figure 7-1 (a) Cumulative % DEX transported across conjunctival cells verses time profile for dexamethasone suspension (Control) and DEXM. (b) Apparent permeabilities of DEX with DEXM and DEX suspension. (Data represented as mean ±SD, n=3).

In addition, P_{app} of DEX across the sclera also increased with decrease in micelle size (ANOVA, $p<0.0001$) as we hypothesized. Permeability of DEX from 60nm DEXM was minimal and very close to control, statistically significant nonetheless (t-test, $p = 0.029$). In addition, there was a lag time and DEX was below detection at 30 min time points for 60 nm DEXM compared to other DEXM and control. This could be attributed to higher size of nanomicelles that permeates slowly compared to smaller size DEXM or soluble DEX from suspension. Interestingly, no significant difference in P_{app} of DEX was observed for DEXM of 10 nm and 30 nm (t-test $p = 0.094$).

The increase in permeability with nanomicelles could be attributed to transport through the aqueous scleral pores [32]. Based on these results, it can be concluded that the nanomicelles of mean size 30nm or less may improve bioavailability of drugs in the uveal track following topical administration. In addition, the conjunctival-scleral route could be of more importance compared to the corneal route in order to achieve higher intraocular levels. Trans-scleral route may be favored due to high surface are and absence of tight junctions like in the cornea. Moreover, nanomicelles typically have hydrophilic surface, which may limit its permeability across hydrophobic corneal tissue. Nanomicelles exhibited significantly high permeability for transport across the conjunctival cell line and sclera. Based on these preliminary experiments, we could suggest that there is a high possibility of achieving elevated drug levels in the intraocular tissues (uveal track) via conjunctival-scleral route. In addition, the *in vitro* release of DEX from nanomicelles was relatively slower and lasted for more than three days. Thus, the frequency of topical administrations may also be reduced increasing patient compliance.

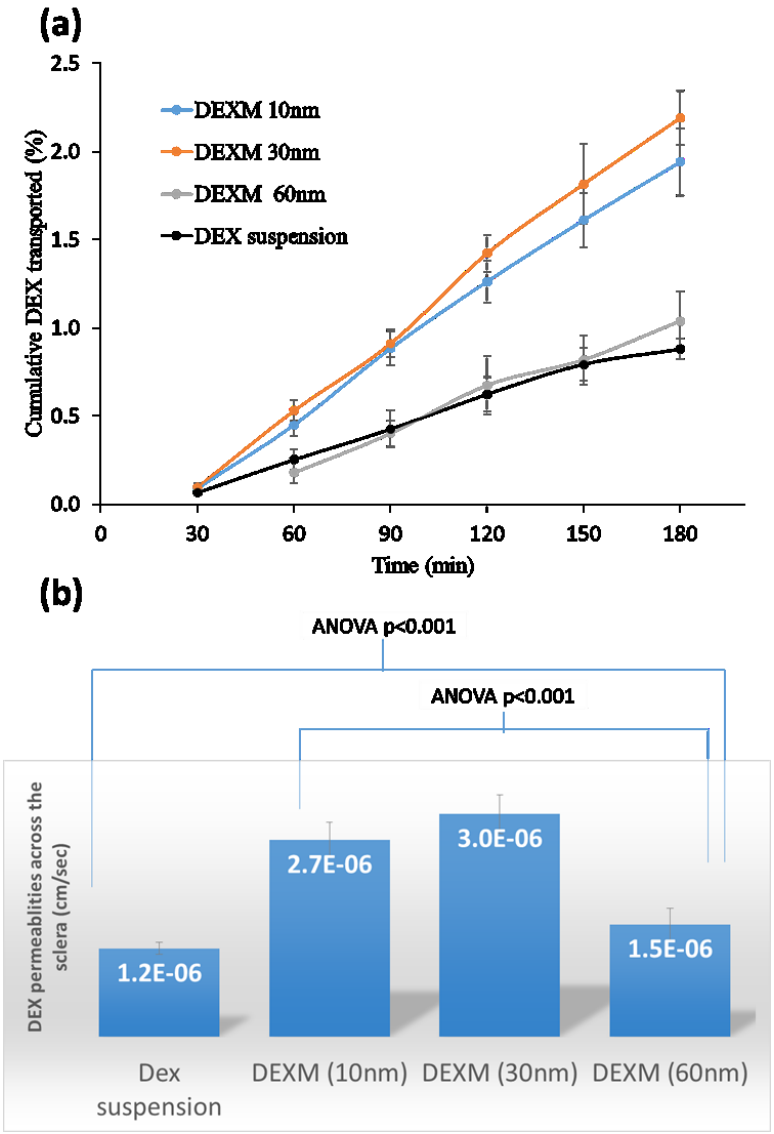

Figure 7-2 (a) Cumulative % DEX transported across the excised rabbit sclera verses time profile for dexamethasone suspension (Control) and DEXM. (b) Apparent permeabilities of DEX from DEXM and DEX suspension. (Data represented as mean ±SD, n=3).

CHAPTER 8

8. SUMMARY AND RECOMMENDATIONS.

8.1. Summary

Nanocarriers have been exploited for a long time for enhanced ocular drug delivery as they offer a number of advantages over conventional formulations. Nanocarriers such as nanoparticles, liposome and nanomicelles have been examined for anterior and posterior segment delivery. Nanomicelles, however, have gained a significant attention as ODD vehicle in the past decade.

Drug delivery to the intraocular tissues such as uveal track following topical administration is highly challenging task due to structure of the eye, which forms formidable barriers to drug delivery. However, a surfactant mixed micelle formulations from our laboratory have shown a significant potential in delivering variety of drugs to the intraocular tissues. In addition, liposomal formulations have also been shown to be effective in delivery hydrophobic molecules to the intraocular tissues. For these formulations, trans-scleral pathway may more significant than trans-corneal route to deliver drugs to the intraocular tissues. Therefore, it is important to delineate the influence of nanocarrier size on trans-scleral transport of encapsulated drugs.

In order to achieve this goal, we synthesized mPEG-PCL di-block copolymers. Di-block polymers were characterized for its structure, molecular weight, polydispersity. All polymers possessed acceptable polydispersity. Biocompatibility of these newly synthesized polymers by *in vitro* cell cytotoxicity in ocular cell lines indicated that the polymers are safe for ODD. Control over nanomicelles size is very crucial factor in this study. Control over nanomicelle size was achieved by simple molecular weight control of polymers, which will ultimately constitute

micelles. Nanomicelles of various sizes including 10nm, 30nm and 60nm. DEX was utilized as model agent, which is also clinically used to treat ocular inflammation such as uveitis.

DEX has a very poor aqueous solubility (~90-100 μg/mL). Nanomicelle is an ideal system to improve aqueous solubility of DEX by dissolving it in the hydrophobic micelle core. Film-hydration method (Method-1) was utilized to dissolve DEX in nanomicelle core as this is method is very simple and can be scaled up at industrial level relative to solvent-extraction methods. However, this method did not result in very high solubility of DEX in nanomicelles prepared using DB2 polymer. Therefore, an exploratory model was employed to identify the factors or interactions influencing the DEX solubilization in nanomicelles. A 3-level response surface design was utilized as this design has a center points which allows determine the curvature effect in the response variable due to second order interactions such as polymer*polymer (X1X1) and DEX*DEX (X2X2) interactions in our case. Exploratory model suggested that the X1X1 was major interaction resulting in poor DEX solubilization. The nature of X1X1 interaction was found to be crystallization of polymer, which was confirmed by PXRD analysis of dried polymer-DEX film.

Based on the results from exploratory model, it was clear that we have to overcome the crystallization of polymer during solvent evaporation, which may favor interaction between drug and polymer leading to higher solubility. This was achieved by simple heating of the polymer-DEX film at melting temperature of the PCL polymer (Modified film-hydration method). Reconstitution of this melted film in water lead to micelle formation and higher solubility of DEX (0.1 wt%) in nanomicelle core. Similar increase in aqueous solubility was observed for DB1 and DB3 polymers with modified film-hydration method. PXRD studies with DB2 and DB3 polymers indicated that these polymers have relatively similar behaviors in terms of

physical state in the dried polymer-DEX film before and after heating. Low molecular weight DB1 was amorphous compared to DB2 and DB3. A very high DEX solubility with DB1 was achieved which could be attributed to its amorphous nature which may resulted in better polymer-DEX (X1X2) interactions during solvent evaporation compared to crystalline DB2 and DB3 polymers. DEX was molecularly dispersed in all nanomicelles prepared with all DB polymers as suggested by PXRD analysis of freeze-dried DEXM and proton-NMR of DEXM. Kinetic of DEX release from DEXM was studied by performing *in vitro* release studies in STF. Total release duration ranged from 2-3 days for all DEXM. Thus, these nanomicelles may also minimize the frequency of topical administration due to long-term release.

In vitro permeability of DEX with all DEXM were significantly higher; about 2-fold higher compared to control (DEX suspension). Nanomicelles increased DEX permeability across the conjunctival cells. However, there was no significant influence of nanomicelles size on permeability across the conjunctival cells. The sclera acts as a static barrier for transport of drug/nanocarriers towards back of the eye following topical administration. Hence, transport of DEX across the excised rabbit sclera was carried out for the all nanomicelles and compared with DEX suspension. Permeabilities of DEX from 10nm and 30nm nanomicelles were significantly high compared to control and 60nm nanomicelles clearly suggesting an influence of nanomicelles size on permeability. Interestingly, no significant difference in Papp of DEX was observed for DEXM of 10 nm and 30 nm. Based on these results it can be concluded that the nanomicelles of mean size 30nm or less may improve bioavailability of drugs in the uveal track following topical administration.

8.2. Recommendations

Trans-scleral pathway could be targeted using nanocarriers such as nanomicelles. Conjunctiva-scleral route may be favored due to high surface are and absence of tight junctions like in the cornea. Moreover, nanomicelles typically have hydrophilic surface that may limit its permeability across hydrophobic corneal tissue. Therefore, the trans-scleral route could be of more importance compared to the corneal route in order to achieve higher intraocular levels following topical administration.

We have here shown that the size of nanocarrier is a significant parameter that influences permeability across porous tissue like sclera. Based on these results, a nano-formulation can be designed to achieve higher drug levels in intraocular tissues following topical administration. This may be a potential explanation for enhanced retinal drug levels from mixed micelles formulation in rabbits. Nevertheless, further *in vivo* studies may be required. Other parameters such as surface charge, hydrophobicity, hydrophobicity may also influence permeation. These factors may require further studies. Stability of nanocarrier, especially for nanomicelles and liposome is important parameter during transport of nanocarrier across the sclera and conjunctiva. Nanocarriers such as nanoparticles may be better option due to their rigid structure and sustained release behaviors. In contrary, nanomicelles represent more fluid character and faster degradation. The fluid nature of nanomicelles especially ones made from low molecular DB1 (amorphous) polymer may fall apart under sheer stress while transport across the sclera. This may result in premature release of drug and it may precipitate depending on its aqueous solubility. In such case, high molecular weight DB2 polymers may be a suitable candidate. Nanomicelles core rigidity may also be enhanced by cross-linking the core forming polymer block. However, the cross-linked construct should be biodegradable.

PART II: STRATEGIES TO MINIMIZE OCTREOTIDE ACYLATION DURING SUSTAINED RELEASE FROM BIODEGRADABLE POLYMERS.

CHAPTER 1

1. LITERATURE REVIEW: SUSTAINED PROTEIN AND PEPTIDE DELIVERY[93].

1.1. Challenges in protein and peptide delivery

Proteins are large biomolecules with complex tertiary (3°) and quaternary (4°) structures. These macromolecules participate in a number of biological pathways and have diverse functionalities such as enzymes, hormones, interferons and antibodies. The complex 3° and 4° structures impart important properties including selectivity, specificity and high potency. Abundance in various biological functions, specificity and potency are most important parameters. Newer targets are being discovered at a rapid rate due to advanced understanding of pathology such as cancer and autoimmune diseases. Precise number of proteins expressed in the human body is not known yet. But various reports suggest that there are at least 84,000 to 200,000 different proteins in the human body [94]. Protein-protein interaction plays a key role in most biological pathways. It may be targeted by designing agonist or antagonist peptides and proteins [95]. Advancement in high throughput (HTS) technology such as hot-spot determination has also catalyzed development of novel biotherapeutics [95a, 96]. Therapeutic protein and peptide development and production have reached advanced stages owing to innovations in manufacturing technology [97], process control [98], and protein characterization [99]. Additionally, protein biotherapeutics have shown to be very efficacious and specific, such as antibodies. However, we are yet to take full advantage of these potent biotherapeutics despite the fast-paced advancements in protein therapeutics R&D and production. U.S. biopharmaceutical industry is one of most innovative and research intensive enterprise as noted by Congressional Budget Office [100]. As per recent market survey pharmaceutical/biotech industry invested nearly a $50 billion every year from 2011 to 2013 in R&D of new medicines and most of it was spent for

biopharmaceutical R&D [101]. As a result, there are more than 907 biotherapeutics in various phases of clinical trials. Of these biotherapeutics, majority are protein biotherapeutics including 338 monoclonal antibodies, 93 recombinant proteins, 20 interferons and 250 vaccines for various conditions such as cancer, autoimmune diseases and infectious diseases[94a].

Proteins and peptides pose a number of delivery related challenges due to a myriad of factors. Some of them are large size, hydrophilicity, poor permeability across biological membranes (such as GI tract), susceptibility to enzymatic degradation, complex structure and immunogenicity [102]. Large molecular size and hydrophilicity hinder permeation across biological barriers such as GI mucosa leading to poor absorption following oral administration. Extreme gastric pH and digestive enzymes degrade these biologics prior to oral absorption. Following GI absorption, the first pass metabolism eliminates a significant fraction of absorbed biomolecules. Hence, delivery of biologics via most favored - oral route - is highly challenging. Hence, a large portion of approved and investigational protein molecules is administered via parenteral routes (IV, IM or SC). Proteins and peptides also suffer from a number of physical, chemical and biological instability due to their complex secondary, tertiary and quaternary structures. Any alteration in "active" confirmation may lead to loss of activity and irreversible aggregation of proteins. Vulnerability towards enzymatic degradation under *in vivo* condition results into short half-lives even with parenteral administration. Many biologics are intended for chronic ailments such as bevacizumab for age-related macular degeneration. Short half-lives of proteins require frequent parenteral administrations to maintain therapeutic levels. However, frequent parenteral administrations are not patient compliant. In addition, frequent administrations may not be well tolerated. For example, frequent intravitreal injections have been shown to be associated with many complications including cataract, retinal hemorrhage and detachment [103].

Invasive and non-invasive routes have been investigated with various formulations to deliver biologics. As mentioned earlier, most frequently used invasive routes are IV, IM and SC. Non-invasive routes include oral, rectal, transdermal and inhalation. Of these, the most preferred noninvasive route is per-oral administration, which is also the "Holy Grail" of protein delivery. It is highly challenging among the noninvasive routes due to the limitations discussed earlier. Major approaches used for oral protein delivery include use of absorption enhancers such as surfactants, enzyme inhibitors, polymer–inhibitor conjugates, mucoadhesive particles, thiolated polymers, nanoparticles, microparticles and emulsion based formulations[77d, 104]. Nevertheless, all these approaches suffer from certain drawbacks and side effects. For example, cost of effective enzyme inhibitors, adverse effects due to frequent oral administrations in chronic diseases, poor stability of formulations such as liposomes in GI track, poor loading efficiency of protein in particles owing to hydrophilicity, polydispersed size distribution and particle aggregation [104c]. Similar limitations are also associated with non-invasive routes of delivery[105]. Moreover, it is challenging to achieve controlled protein delivery for extended duration via 'patient compliant' non-invasive routes. A potential reason for the failure of treatment strategy in chronic diseases may be lack of adherence to a given treatment regimen by patient. Therefore, frequent administration is not a recommended strategy for chronic ailments. As per an estimate by WHO, only 50% of patients suffering from chronic diseases stick to the treatment regime in developed countries [106]. In developing countries, adherence to prolonged therapy is even lower [106]. Therefore, proteins are suitable candidate for sustained release formulations. Advantages of sustained delivery formulation include better adherence to chronic therapy, *in vivo* stability, local delivery, fewer side effects, reduction in dose and dosing frequency, and improved patient compliance. Furthermore, parenteral routes, although not very patient compliant, may be a

simpler answer to limitations and drawbacks associated with non-invasive administrations. Extended duration of delivery with lower frequency of administration may improve patient compliance significantly.

Ideal protein delivery formulation should be able to provide controlled release to maintain therapeutic levels for an extended duration and ensure stability of encapsulated protein. Components of delivery system must be biodegradable and/or biocompatible, non-immunogenic, non-toxic and preferably FDA approved for human use. If the formulation is intended via parenteral route, it should be possible to inject it through a narrow gauge needle to minimize pain. In addition, in a few cases, it is impractical to use higher gauge needles. For example, in case of intravitreal injections, a 27G to 30G needle is recommended to avoid damage to intraocular tissues. Volume of injection should also be considered carefully depending on the route of administration. Structure and activity should not be altered during the preparation of delivery system and biologics must be in active conformation following *in vivo* release. In particulate and hydrogel based systems, initial burst release is a serious concern. In the case of particle-based systems, burst release is due to high surface adsorption of biologics. Higher initial burst release may shorten total duration of release and result in dose-dependent adverse effects. Therefore, the formulation must be optimized to achieve minimal burst release. Above all these factors, method of formulation preparation should be scalable, robust and reproducible. Statistical methods such as quality-by-design, design of experiments [107] and in-process quality control methods such as six-sigma may be able to aid development of high quality product with robust and reproducible method of manufacturing [98, 108].

1.2. Microparticles as sustained delivery formulation

Controlled release of protein from parenteral formulation can be achieved by a matrix-type delivery system. Microsphere formulation holds distinct advantages and has gained popularity in recent years[109]. More than 200 studies have been published per year pertaining to biodegradable microsphere formulations for peptide and protein delivery. Advantage of employing microspheres formulation for delivery of proteins is that it offers stability for molecules, which are rapidly degraded or eliminated *in vivo*. Encapsulation in microsphere prevents contact of protein from cells or enzymes such as proteases/esterases in surrounding tissues, until it has been released from microsphere. Microsphere formulation can be easily delivered to the target sites via IV, IM or oral route. Owing to the recent advancements in polymer science and synthesis technology, development of controlled release microsphere formulations has gained immense popularity. The polymers should not produce harmful side effects or toxic degradation products, and neither should it alter any pharmacological properties of the active ingredient. It should also be non-toxic, non-irritant and biocompatible if not biodegradable[110].

Formulation of microspheres from biodegradable polymer is initiated by selecting an appropriate encapsulation method in order to achieve desired/ideal controlled release. Particle size and polydispersity is another important aspect as it directly influences syringeability, which is one of the important requirement for an ideal microsphere system. During microsphere formulation process, there should be no alteration in biological activity of encapsulated protein. Methods in which exposure of protein/peptide in strong denaturing solvent are not employed [111].

Spray drying method has also been employed in formulating microspheres. Volatile organic solvents such as dichloromethane or acetone are used to dissolve biodegradable polymer.

Then the drug is dispersed into the polymer solution in solid form by high-speed homogenization. Volatile organic solvent is then evaporated yielding microspheres of 1 to 100 mm size range. Proteins such as recombinant human erythropoietin were encapsulated in microsphere using spray drying method in nitrogen atmosphere[112]. Release of active ingredient from microspheres occurs via different mechanisms such as diffusion, polymer degradation, or combination of them[113].

Chronic ulcerations of the skin have been reported due to the deficiency of prolidase enzyme. This enzyme is involved in the later stages of protein catabolism. To overcome this problem, PLGA microspheres encapsulating prolidase were formulated by w/o/w multiple emulsion technique. Results obtained from *ex vivo* studies demonstrated that microencapsulation imparted stability to protein inside the polymer matrix leading to release of active enzyme from the formulation. This technique can be employed for enzyme replacement therapy[114].

Similarly, another formulation of PLGA microspheres has been prepared with β-lacto globulin (BLG). Newborns are prone to allergies related to milk proteins, which can be prohibited by prompting oral tolerance to these proteins. PLGA microspheres encapsulating a major allergenic protein, BLG, were formulated by w/o/w double emulsion technique. Controlled release of proteins and higher encapsulation efficiency were reported after introduction of tween 20 in the formulation. Improved encapsulation efficiency and controlled release resulted in the reduction of dose required for specific anti-BLG IgE response following oral administration [115].

A microsphere formulation encapsulated with Interferon α (IFN α) and comprising of calcium alginate core surrounded by PELA (poly D, L-lactide-poly ethylene glycol) was prepared by w/o/w multiple emulsion technique. Coated microspheres impart stability to IFN α in the PELA matrix. These microspheres also demonstrated enhanced encapsulation efficiency

and retention of biological activity as compared to microspheres produced by conventional method[110]. In another study, PLGA microspheres encapsulated with salmon calcitonin exhibited 5-9 days release following S.C. injection in rats [116]. Blends of poly(ethylene glycol) (PEG) with poly(lactic acid) (PLA) homopolymer and PLGA copolymer were utilized to prepare insulin-loaded microspheres by w/o/w multiple emulsion technique. The resulting microspheres exhibited high entrapment efficiency and provided controlled release of insulin for 28 days[117]. In another study, ZnO-PLGA microspheres containing insulin demonstrated rapid and long-lasting suppression of glucose levels for 9 days following subcutaneous administration in rats[118]. Table 1-1 summarizes the clinically approved sustained-release microparticle formulations.

Table 1-1 Clinically approved sustained-release microparticle formulations.

Trade name	**Drug**	**Indications**	**Delivery System**	**Length of release**	**Approval year**
Lupron Depot® (TAP)	Leuprolide	Prostate cancer, endometriosis	Injectable PLGA microparticles (intramuscular injection)	1-, 3- and 4- month formulations	1989
Sandostatin® LAR® (Novartis)	Octreotide	Acromegaly	Injectable PLGA microparticles (intramuscular injection)	1-month	1998
Somatuline® LA (Ipsen)	Lantreotide	Acromegaly	Injectable PLGA microparticles (intramuscular injection)	10-14 days	1998
Nutropin Depot® (Alkermes/ Genentech)	Human growth hormone (hGH)	Growth hormone deficiency	Injectable PLGA microparticles (subcutaneous injection)	1-month	1999
Trelstar Depot® (Debiopharm)	Triptorelin	Prostate cancer	Injectable PLGA microparticles (intramuscular injection)	1- and 3-month formulations	2000
Risperdal® Consta® (Alkermes/Janssen)	Risperidone	Schizophrenia	Injectable PLGA microparticles (intramuscular injection)	2 weeks	2003

1.3. Nanoparticles-in-gel composite systems

A considerable attention has been paid to sustained delivery of protein therapeutics via encapsulating in nano/micro particles. Nano/micro particles provide a stable environment for peptide/protein against catalytic enzymes, allowing improved biological half-lives. However, protein-loaded particulate drug delivery systems exhibited major disadvantage of burst effect (dose dumping) which may result in severe dose related toxicity. Nanoparticle-in-gel composite systems has been investigated to minimize the burst release of proteins and provide localized delivery[119].

Posterior segment ocular diseases such as wet age-related macular degeneration (wet-AMD), diabetic retinopathy, and diabetic macular edema are sight-threatening disorders mainly observed in elderly patients. Many protein therapeutics such as bevacizumab, ranibizumab and aflibercept are repeatedly injected (intravitreally) for the treatment of above-mentioned ocular diseases. Repeated intravitreal injections lead to many complications like endophthalmitis, retinal detachment and retinal hemorrhage, and more importantly patient noncompliance. Recently, Mitra et al. have described protein encapsulation in pentablock (PB) polymer nanoparticles dispersed in PB thermosensitive gel for the sustained delivery of proteins following intravitreal delivery [120]. PB copolymers exhibited excellent biocompatibility with negligible toxicity. A composite formulation (protein-encapsulated PB NPs dispersed in PB thermosensitive gel) exhibited nearly zero order release with no burst effect. Recently, we have discussed the applicability of a PB polymeric nanoparticles and nanoparticles-in-gel composite formulation for the sustained delivery of proteins in the treatment of posterior segment ocular diseases [119b, 121]. Results demonstrated that model proteins (bovine serum albumin, IgG and bevacizumab)-loaded PB composite formulations exhibited nearly zero order release up to 45-60

days. Burst effect in nanoparticles is observed due to immediate release of surface adsorbed proteins. However, when the NPs are dispersed in thermosensitive gel matrix, an additional diffusion layer provided by gelling polymer hinders the release of surface adsorbed drug resulting in elimination of burst effect. In addition, biological activity of the protein molecules was confirmed by *in vitro* experiments.

Administration of vascular endothelial growth factor (VEGF) in appropriate dose may prove as a promising treatment for the deficient bladder reconstruction therapy. However, short half-lives and high instability due to deamidation, diketopiperazine formation and oxidation of proteins (VEGF) resulted in disappointing clinical trials. Due to high instability, large dose of protein is required which often attributed to sever side effects such as progression of malignant vascular tumors[122]. In order to achieve sustained release with minimum burst release of VEGF, Geng et al. prepared VEGF-encapsulated PLGA nanoparticles and dispersed them in Pluronic-F127 thermosensitive polymer solutions[123]. VEGF-NPs exhibited up to ~40% of burst release within the first two days which is significantly reduced to ~15% with the formulation of VEGF-NPs dispersed in thermosensitive gel [123]. Controlled delivery of VEGF from a biocompatible delivery system may eliminate the requirement of repeated dosing and possible dose related toxicity. Promising preliminary results observed with the composite delivery system in the treatment of chronic diseases may prove to be cost effective highly patient compliant therapy.

CHAPTER 2

2. STATEMENT OF PROBLEM, HYPOTHESIS AND OBJECTIVES

2.1. Statement of problem

Proteins and peptides based biotherapeutics are currently being introduced rapidly into the clinical trials for treatment of a number of diseases. These biologics suffer from a myriad of delivery related constrains such as poor bioavailability, permeability across biological membranes and *in vivo* stability. Short *in vivo* half-life leads to frequent multiple parenteral administrations, which lowers patient compliment. Sustained delivery of biologics may address these issues and improve their potential as therapeutics. Among the approaches investigated for sustained delivery of biologics, nano- and microparticles are in the forefront and clinically available for various ailments [93], such as Sandostatin LAR® depot containing octreotide.

Octreotide is a semisynthetic cyclic octapeptide, a somatostatin analogue, indicated for acromegaly (

Figure 2-1a)[124]. It is also recommended for symptomatic relief by suppressing severe diarrhea and flushing episodes associated with metastatic carcinoid tumors[124-125]. Half-life of this peptide following S.C. and I.M. administrations is short, about 100 min [126]. It is marketed as solution for subcutaneous injection (lactate buffer, pH 4.2) and as a depot form for intramuscular administration. PLGA-glucose star polymer microparticles (MPs) (size ~40 μm) provide delivery over a period of 4 weeks. PLGA has been widely investigated for the delivery of bioactive peptide and proteins [93]. However, it may not be the best polymer for delivering peptide and protein biologics due to acylation of biologics during release[127]. It has been well documented that chemical stability of octreotide is compromised due to acylation during the release[127a]. Less than 20% of native octreotide was released from Sandostatin LAR® depot during *in vitro* release[127a].

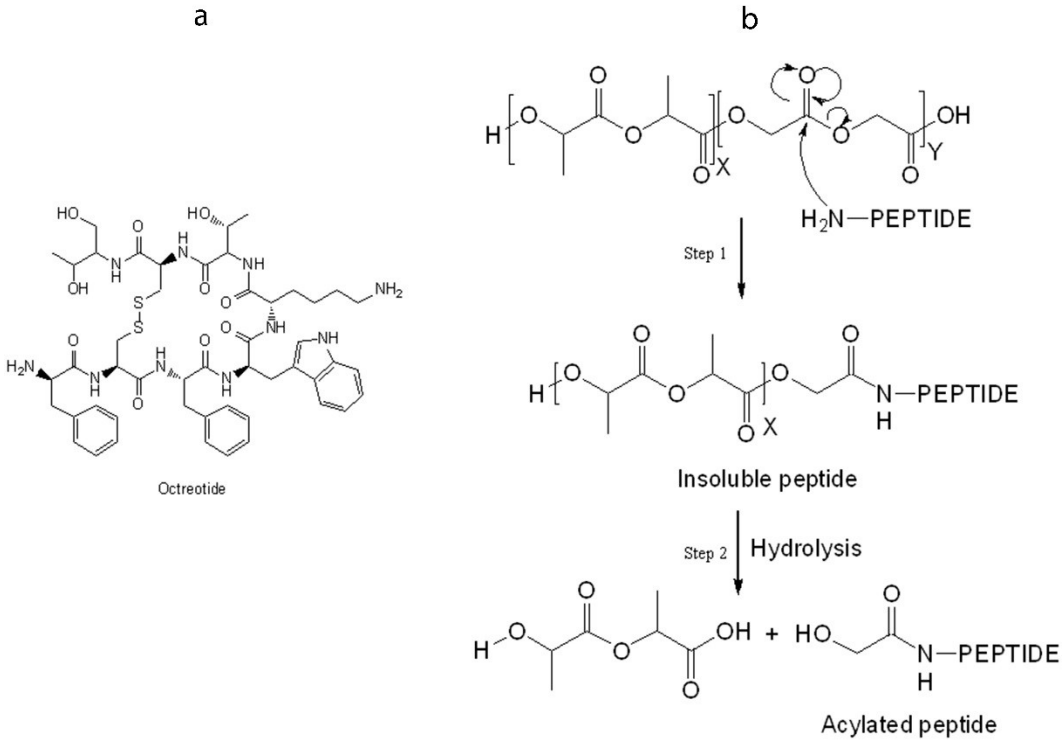

Figure 2-1 (a) Structure of octreotide. (b) Nucleophilic carbonyl-substitution mechanism of peptide acylation in PLGA microparticles. Nucleophilic attack of amine from peptide on partial positive carbon of degraded PLGA fragment results into formation of insoluble adduct (step 1). Alcohol (-OH) and thiol (-SH) groups may also act as nucleophile. Hydrolysis of polymer side chain in insoluble peptide adduct results in release of soluble acylated peptide (step 2).

Nearly 60% octreotide was released as acylated adduct over period of 3 months[127a]. Chemical derivatization of octreotide is because of reaction of peptide with degraded PLGA oligomers inside the MP core. Structure of octreotide and mechanism of peptide acylation is illustrated in

Figure 2-1. Preliminary data indicates that nucleophilic attack of amine from peptide on partial positive carbonyl carbon is responsible for chemical derivatization of peptide during release. Thiol (-SH) and alcohol (-OH) groups have also been reported to act as nucleophiles. The mechanism of acylation reaction is nucleophilic carbonyl substitution. Similar phenomenon has been reported for other protein and peptides such as bovine serum albumin, human atrial natriuretic peptide, human parathyroid hormone, leuprolide, insulin and salmon calcitonin[127b, 128]. Acylation of peptide also leads to formation of water insoluble adducts resulting in incomplete release of peptide from MPs (

Figure 2-1b, step 1) [127c]. As a result, 15% of octreotide was not released, which may be attributed to formation of water insoluble adducts[127a].

Several strategies have been undertaken to minimize peptide acylation with limited success. Some of them are polymer modifications and encapsulation of divalent cations[127a, 128b, 128d, 129]. Thus, there is an unmet need to develop an extended release formulation, which can deliver peptides in active form.

2.2. Strategies and objectives

There are two primary objectives of this research (1) extended delivery of octreotide (2) minimize peptide acylation during release. We aim to examine two strategies to minimize or prevent acylation of peptide during extended release from biodegradable polymers.

Strategy 1: Effect of various polymer compositions on octreotide acylation will be tested. Effect of polycaprolactone (PCL), polylactic acid (PLA) and polyglycolic acid (PGA) will be examined. Effect of PLA and PGA on peptide acylation is well established. However, no information is available on effect of PCL on peptide acylation. We hypothesize that modification of the composition of polymer blocks may minimize acylation and sustained release. MPs of triblock polymer (PCL_{10k}-PEG_{2k}-PCL_{10k}) and pentablock co-polymers (PLA_{3k}-PCL_{7k}-PEG_{2k}-PCL_{7k}-PLA_{3k} and PGA_{3k}-PCL_{7k}-PEG_{2k}-PCL_{7k}-PGA_{3k}) will be developed for extended delivery of octreotide. Further, to sustain the release and minimize the possibility of burst effect[130], MPs will be suspended in thermo-responsive gel solution. Special emphasis was placed on acylation of octreotide during release from caprolactone, glycolide and lactide based polymeric MPs.

Strategy 2: In the second strategy, we will test potential of reversible hydrophobic ion-paring complexation in minimizing acylation of octreotide from polylactide-co-glycolide polymers. Amine of peptide is the most reactive nucleophile resulting in peptide acylation. In this strategy, the anime functional group will be masked using an ion-pairing agent. The complex is hypothesized to be stable at lower pH inside the microparticle core and will dissociate at physiological condition to release free native peptide, based on previous studies from our laboratory. HIP complex of octreotide will be encapsulated in MPs of PLGA polymer. PLGA (50/50) will be utilized to examine potential of HIP complex in minimizing peptide acylation, as it is known to cause acylation of peptides and proteins.

Based on these strategies, specific aims of this proposal are as follows.

1. Synthesis and characterization of triblock polymer (TB = PCL_{10k}-PEG_{2k}-PCL_{10k}). Polymer will be characterized for molecular weight, purity, structure and physical property. Pentablock co-

polymers for nanoparticle preparation (PB = PLA_{3k}-PCL_{7k}-PEG_{2k}-PCL_{7k}-PLA_{3k} and PGA_{3k}-PCL_{7k}-PEG_{2k}-PCL_{7k}-PGA_{3k}) and thermosensitive gel (PLA_{250}-PCL_{1250}-PEG_{1500}-PCL_{1250}-PLA_{250} and PCL_{1000}-PEG_{1000}-PCL_{1000}) were synthesized and characterized earlier.

2. Preparation of MPs encapsulating octreotide using above-mentioned TB and PB polymers. Characterize MPs for size, peptide loading and *in vitro* release. Concentration of release native and acylated peptide will be determined by HPLC assay.
3. Preparation of hydrophobic ion-pairing complex of octreotide with dextran sulfate and sodium dodecyl sulfate. Characterize the effects of ion-pairing agent to octreotide on complexation efficiency and mechanism of dissociation.
4. Encapsulate HIP-complexed octreotide in MPs using PLGA polymers. Characterize MPs for size, peptide loading and *in vitro* release. Concentration of release native and acylated peptide will be determined by HPLC assay.

CHAPTER 3

3. EXTENDED RELEASE FORMULATION OF OCTREOTIDE: SIMULTANEOUS DIFFUSION AND ACYLATION OF PEPTIDE.

3.1. Materials

Octreotide acetate (PubChem CID: 383414) was procured from ChinaPeptides Co., Ltd (Shanghai, China). D,L-lactide (PubChem CID: 65432), glycolide (PubChem CID: 7272), caprolactone (PubChem CID: 10401), stannous octoate, Poly(ethylene glycol) (Mw 2000 g/mol) and polyvinyl alcohol were obtained from Sigma Aldrich (St Louis, MO). All other solvents/chemicals were of analytical reagent grade.

3.2. Methods

3.2.1. Preparation of triblock and pentablock co-polymers

TB (PCL_{10k}-PEG_{2k}-PCL_{10k}) co-polymer was synthesized by ring-opening bulk copolymerization following a published protocol from our laboratory [131]. Subscript represents molecular weight of polymer segment. PEG (Mw 2000 g/mol) with both hydroxyl end was vacuum-dried for 4 h, which acted as initiator to polymerize ε-caprolactone using stannous octoate (0.5 wt %) as catalyst. The reaction was carried out in a closed vessel under nitrogen, at 130 °C for 36 h. The resultant polymer was purified by cold ether precipitation. Purified polymer was vacuum-dried followed by freeze-drying to remove any residual solvent and moisture. Structure and molecular weight of TB copolymers were confirmed by ^{1}H-NMR and gel permeation chromatography (GPC). Pentablock (PB) co-polymers for nanoparticle preparation (PBA = PLA_{3k}-PCL_{7k}-PEG_{2k}-PCL_{7k}-PLA_{3k} and PBB = PGA_{3k}-PCL_{7k}-PEG_{2k}-PCL_{7k}-PGA_{3k}) and thermosensitive gel (PLA_{250}-PCL_{1250}-PEG_{1500}-PCL_{1250}-PLA_{250} and PCL_{1000}-PEG_{1000}-PCL_{1000}) were synthesized and characterized earlier[131-132].

3.2.2. Preparation of octreotide encapsulated microparticles

Octreotide-loaded MPs were prepared using TB, PBA or PBB polymer by methanol-oil/water solvent evaporation method. Briefly, methanol phase (Me) consisted of 5 mg octreotide dissolved in 50 µL of methanol containing triethyl amine (TEA) (mole ratio Octreotide:TEA::1:2.5). Polymer (TB or PB) was dissolved in dichloromethane (DCM) (100 mg in 500 µL DCM) constituting oil (O) phase. The methanolic phase containing octreotide was mixed with polymer solution aided by probe sonication for 30 sec at 2 output to make Me-O phase. This Me-O phase was slowly added to the water phase (650 µL, 1% PVA with 5% NaCl) under constant stirring to form a Me-O/W_1 emulsion. Emulsion was further diluted with 3 mL of 1% PVA (5% NaCl) (W_2) and stirred for 3 h under hood to remove organic solvent. The MPs were separated by centrifugation at 15,000 RPM for 10 min. Particles were washed three times with DDI water. MPs were freeze-dried using mannitol (2% w/v) as a cryoprotectant and stored at -20˚C until further use. Ghost MPs were prepared following the same method except no octreotide was added during preparation.

3.2.3. Drug loading (%) and entrapment efficiency (%)

Amount of octreotide in MPs was measured by UV spectroscopy. A known amount of freeze-dried MPs (5 mg, n = 3) were dissolved in 200 µL DMSO. UV absorbance was measured at 280 nm. Ghost MPs served as blank. Entrapment efficiency (%EE) and Drug loading (%DL) were calculated by following equations 1 and 2, respectively.

%EE = (Amount of octreotide in MPs/Total amount of octreotide)*100 … (3.1)

%DL = (Amount of octreotide in MPs /Total weight of MPs)*100 … (3.2)

3.2.4. Powder X-ray diffraction (PXRD)

Physical state of polymers was investigated by PXRD analysis. MiniFlex automated X-ray diffractometer (Rigaku, The Woodlands, Texas) with Ni-filtered Cu-kα radiation (30 kV and 15 mA) was employed to study diffraction patterns at room temperature.

3.2.5. Scanning electron microscopy

SEM analysis was performed to analyze particle morphology (size and shape). Briefly, freeze-dried MPs were applied to carbon film positioned on an aluminum stub. Surface of particles on carbon film was coated with Au-Pd under centrifugation followed by sample analysis in Phenom Pro desktop scanning electron microscope.

3.2.6. Release study

Freeze-dried MPs were subjected to *in vitro* release study in PBS buffer (137 mM NaCl, 2.7 mM KCl, 10 mM Na_2HPO_4, 1.8 KH_2PO_4; pH 7.4) at 37 °C. Predetermined amount of MPs were suspended in 400 µL of thermosensitive gel solution (20 wt%) maintained at 4°C to prevent accidental gelation. TBMPs were suspended in triblock gel (PCL_{1000}-PEG_{1000}-PCL_{1000}) solution. PBAMPs and PBBMPs were suspended in PB gel (PLA_{250}-PCL_{1250}-PEG_{1500}-PCL_{1250}-PLA_{250}) solution. Preparation and characterization of these gelling polymers has been published earlier[132-133]. Composition of MPs and gel are depicted in Table 3-1. Resulting MPs in gel suspension was incubated at 37 °C for 2 min followed by slow addition of 800 µL of PBS (pH 7.4), preincubated at 37 °C. At predefined time intervals, 700 µL of clear supernatant was collected and replaced with fresh PBS. Release samples were evaluated for amount of native and chemically modified octreotide using UFLC assay. The experiments were carried out in quadruplets and plotted as cumulative octreotide released (%) relative to %EE verses time. Ghost MPs were kept as control.

Table 3-1 Compositions of MPs-in-gel formulation for release study.

Octreotide-encapsulated MPs	**Thermoresponsive Gel composition[132]**
TBMPs	PCL_{1000}-PEG_{1000}-PCL_{1000}
PBAMPs	PLA_{250}-PCL_{1250}-PEG_{1500}-PCL_{1250}-PLA_{250}
PBBMPs	PLA_{250}-PCL_{1250}-PEG_{1500}-PCL_{1250}-PLA_{250}

3.2.7. Ultra-fast liquid chromatography (UFLC) assay

Native and acylated octreotide concentration in released media was quantified by UFLC assay. A Shimadhu (Shimadzu Scientific Instruments, Columbia, MD, USA) UFLC system coupled with pumps (LC-20AT), degasser (DGU-20A3R), DAD detector (SPD-20AV) and autosampler (SIL-20AHT) was employed. Phenomenax column (Phenomenex C18 kinetex column 100X4.6 mm, 5µm) along with a guard column (Phenomenex SecuritGuard Catridges, C18, 4x2 mm) was used at total flow rate of 0.5 mL/min. A gradient elution method was employed for separation where mobile Phase A (HPCL water (Sigma) with 0.1% formic acid) at 10% and mobile phase B (ACN with 0.1% formic acid) at 90% were ran for first 2 min followed by a linear gradient to reach 100% phase B at 18 min. Concentration for octreotide standards ranged from 100 µg/mL to 3.1 µg/mL prepared in PBS. DAD detector was set at 280 nm to determine. Injection volume was 50 µL.

3.2.8. UFLC-MS analysis

UFLC-MS was performed using electrospray ionization (ESI) in positive ion mode on a QTrap® API-3200 mass spectrometer, equipped with Shimadzu quaternary pump, vacuum degasser, DAD detector and autosampler (Shimadzu Scientific Instruments, Columbia, MD, USA). Data acquisition and data processing were performed using Analyst 1.4.2 software package (Applied Biosystems, Foster City, CA, USA). LC conditions including column and gradient composition remains same as explained in the earlier UFLC assay. Injection volumes were 30 µL for all samples. UV detector was set on 280 nm and MS was set in range of 200 to 1700 amu. Total ion chromatogram was extracted for acylated peptide m/z to produced extracted ion chromatogram and compared with UV chromatogram to identify native octreotide and chemically acylated adducts.

3.3. Results and Discussion

Peptide therapeutics typically exhibit short half-lives following systemic administration due to enzymatic degradation. Many of these biologics are indicated for chronic conditions such as octreotide for acromegaly and insulin for diabetes. Hence, these biologics are suitable candidates for sustained release formulations. Biodegradable block polymers offer many advantage over random block polymers such as PLGA. One good example is tunable chemical properties such as hydrophobicity and hydrophilicity of polymer. By tuning these properties, block co-polymers can be tailored for better entrapment efficiency and controlled release.

3.3.1. Characterization of polymers

Nano- and micro-particles based biodegradable systems have been extensively studied for extended delivery of proteins and peptide. They protect entrapped biomolecules against enzymatic degradation. Nonetheless, when using biodegradable polymers, protein/peptide-polymer interaction must be carefully investigated. Degradation products of polymers must be compatible with biologics. Chemical derivatization i.e. acylation of peptides has been reported from lactide and glycolide based polymers. We hypothesized that PCL based polymer may minimize or prevent the chemical degradation of octreotide. Hence, TB polymer (PCL_{10k}-PEG_{2k}-PCL_{10k}) was designed solely based on caprolactone units to investigate the influence on chemical stability of peptide during the release without interference of lactide or glycolide units. Pentablock co-polymers PBA (PLA_{3k}-PCL_{7k}-PEG_{2k}-PCL_{7k}-PLA_{3k}) and PBB (PGA_{3k}-PCL_{7k}-PEG_{2k}-PCL_{7k}-PGA_{3k}) were synthesized to lower crystallinity of PCL blocks, which may improve loading of peptide in MPs. Block co-polymers were synthesized by well-established ring-opening polymerization method reported from our laboratory[132-133]. Weight and number average molecular weights and polydispersity indices (PDI) from NMR and GPC are presented in Table

3-2. Molecular weight calculated from 1H-NMR was close to molecular weight (Mn) calculated based on feed ratio suggesting nearly all monomer reacted to form polymer chain. Polydispersity for TB, PBA and PBB polymers were 1.59, 1.39 and 1.42, respectively.

We have previously shown that PCL possesses semicrystalline structure and the extent of crystallinity depends on the molecular weight of PCL segment and polymer composition i.e., presence of other block polymers such as PLA and PGA in case of PBA and PBB polymers, respectively [84, 131-132, 134]. We have also reported that crystallinity of polymer directly influences the release rate[131, 133]. Hence, x-ray diffraction analysis was performed to determine the physical state of newly synthesized polymers. XRD patterns are depicted in Figure 3-1. TB polymer showed presence of very sharp peaks at 2θ 21.9 and 23.8 associated with PCL and PEG segments, respectively [84]. However, incorporation of PLA blocks in triblock polymer diminished the intensity of peaks corresponding to PCL and PEG segments. Addition of PGA segment further diminished the crystallinity of PCL and PEG and the overall polymer was almost amorphous in nature. These observations corroborates with previously published study [131]. Reduction in crystallinity of PCL could be because of hydrophobic interactions between heterogeneous polymer chains (PCL/PLA and PCL/PGA) which would minimize interaction of PCL chains leading to crystallization.

Table 3-2 Proton-NMR and GPC analysis of polymers.

Code	Block co-polymer composition	Mn[a] (gm/mol)	Mn[b] (gm/mol)	Mn[c] (gm/mol)	Mw[c] (gm/mol)	PDI[c]
TB	PCL_{10k}-PEG_{2k}-PCL_{10k}	22000	21271	16781	26824	1.59
PBA	PLA_{3k}-PCL_{7k}-PEG_{2k}-PCL_{7k}-PLA_{3k}	22000	20783	17246	24024	1.39
PBB	PGA_{3k}-PCL_{7k}-PEG_{2k}-PCL_{7k}-PGA_{3k}	22000	20122	17032	24185	1.42

Mn-Number average molecular weight, Mw-Weight average molecular weight.

[a]Theoretical value, calculated according to the feed ratio.

[b]Calculated from ^{1}H-NMR results

[c]Determined by GPC analysis

3.3.2. Preparation and characterization of octreotide-loaded MPs

Octreotide was encapsulated in MPs of TB and PB polymers by methanol-oil/water emulsion solvent evaporation method. Addition of TEA converted ionized amine of octreotide to its more hydrophobic base-form and hence it preferably partitioned into oil phase improving the entrapment efficiency. Particles were characterized for entrapment efficiency (%EE) and drug loading (%DL) by simple UV method. Table 3-3represents entrapment efficiency and drug loading for TBMPs, PBAMPs and PBBMPs. Order of %EE and %DL for polymers was PBB>PBA>TB (ANOVA $p<0.05$). Higher %EE could be attributed to minimal crystallinity of PCL segment in PB copolymers (Figure 3-1). Similar results have been observed in previously published studies, where nanoparticles were prepared with TB and PB polymers[131, 133]. SEM analysis was performed to determine surface morphology of MPs (Figure 3-2). MPs prepared using Me-O/W method were spherical in shape and non-porous. MPs also were slightly polydispersed with particle size less than 100 μm based on SEM analysis (Figure 3-2).

3.3.3. Kinetics of octreotide release

Primary objectives of this research were to deliver octreotide over period of months and investigate chemical instability of peptide during release. Hence, octreotide release kinetics from TBMPs, PBAMPs and PBBMPs was investigated by *in vitro* release studies. Release studies were performed by suspending MPs in the thermosensitive gels (Table 3-1). Release samples were analyzed by UFLC assay to quantitate native and acylated octreotide. Hydrophobic octreotide adducts eluted following the elution of native octreotide. Similar results have been observed by other investigators[127a, 135].

Table 3-3 %EE and %DL for MPs prepared by emulsion solvent evaporation method.

Polymer	**%DL**	**%EE**
TB	2.02±0.25	45.3±9.4
PB-A	3.10±0.51	59.5±10.9
PB-B	4.24±0.15	82.0±3.3
Data represented as mean ± SD, n = 4.		

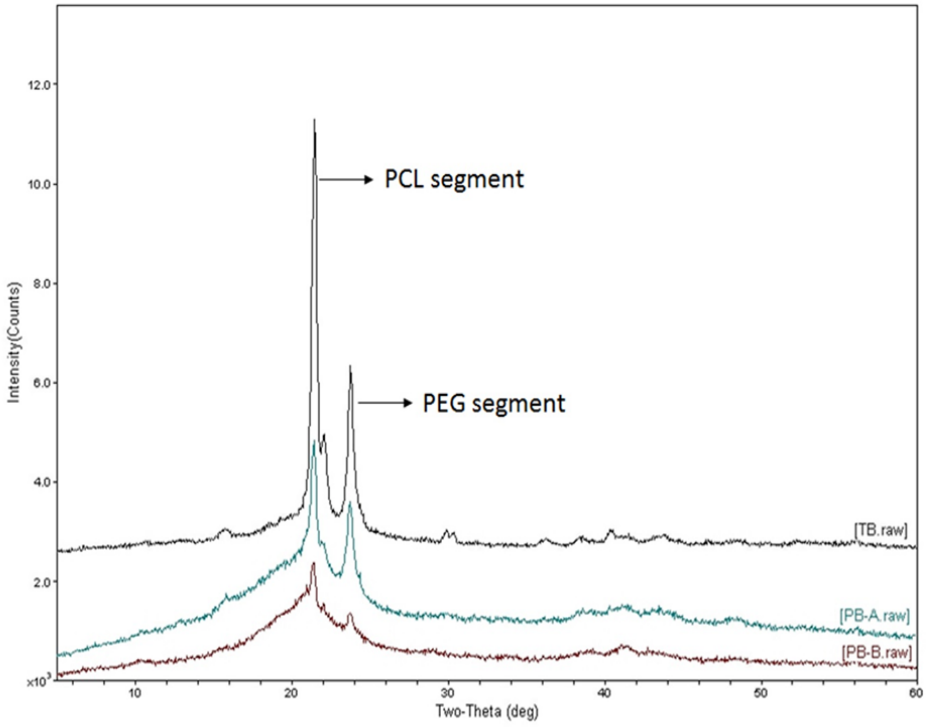

Figure 3-1 Powder X-ray diffraction patterns for TB (PCL10k-PEG2k-PCL10k), PBA (PLA3k-PCL7k-PEG2k-PCL7k-PLA3k) and PBB (PGA3k-PCL7k-PEG2k-PCL7k-PGA3k) polymers. Crystallinity of PCL segment decreased progressively in pentablock PBA and PBB polymers.

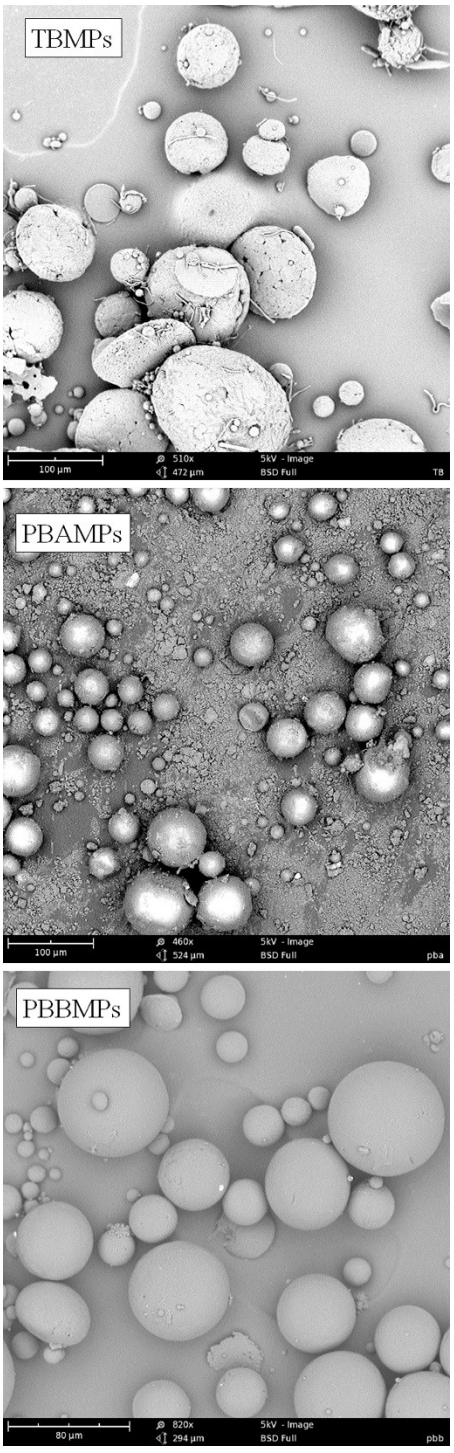

Figure 3-2 Scanning electron micrograph for TBMPs, PBAMPs and TBMPs.

Peaks in UV chromatogram were assigned to native and chemically modified octreotide using UFLC-MS analysis. The phenomenon of peptide acylation has been well studied and it is known that the process occurs during the release, within MPs core, and not while preparation or following the release in media[127a, 127c]. Octreotide possesses excellent stability at pH 7.4 at 37 °C, which is the release condition [127c]. In addition, UFLC chromatogram did not show any peak corresponding to degraded peptide, suggesting the peptide possesses excellent stability throughout release period. Further, to distinguish junk peaks from native and acylated peptides in chromatogram, corresponding ghost MPs were kept for release and sampled at same time intervals along with octreotide-loaded MPs.

Figure 3-3, Figure 3-4 and Figure 3-5 depict the release profiles of native, acylated and total octreotide from TB, PBA and PBB MPs-in-gel, respectively. A summary of cumulative octreotide release (total, native and acylated) is depicted in Table 3-4. In case of TBMPs and PBAMPs, near complete release of octreotide was achieved (Figure 3-3 and Figure 3-4). Only 53±3.2% of total octreotide was released over period of 10 months from glycolide-based PBB polymer (Figure 3-5 and Table 3-4). No substantial burst release (<10%) was observed from all MPs compositions owing to thermosensitive gel (Table 3-4), which is in accordance with previously published reports[131-132]. Burst release occurs due to quick release of surface bound drug upon hydration of particles in release media. Thermosensitive gel provides an additional diffusion barrier to the drug released from MPs and minimizes burst phase[131-132].

Table 3-4 Summary of *in vitro* release of octreotide in PBS buffer at 37 °C.

MPs polymer	**Total Octreotide released (%)**	**Native octreotide released (%)**	**[a]Acylated octreotide released (%)**	**Burst release (%)**	**[b]Acylated octreotide released (%)**	**Release duration**
TB	97.4±6.9	87.8±6.4	9.5±0.6	8.4±0.8	13±0.4%	105 Days
PBA	87.2±12.6	47.0±7.9	45.9±5.1	7.1±2.3	53±3.0%	330 Days
PBB	53.4±3.2	8.9±0.3	49.0±3.0	1.4±0.3	92±0.5%	330 Days

Data represented as mean ± SD, n = 4.
Burst release is total octreotide (%) released at 24h.
[a] calculated with respect to %EE.
[b] Calculated with respect to total octreotide released.

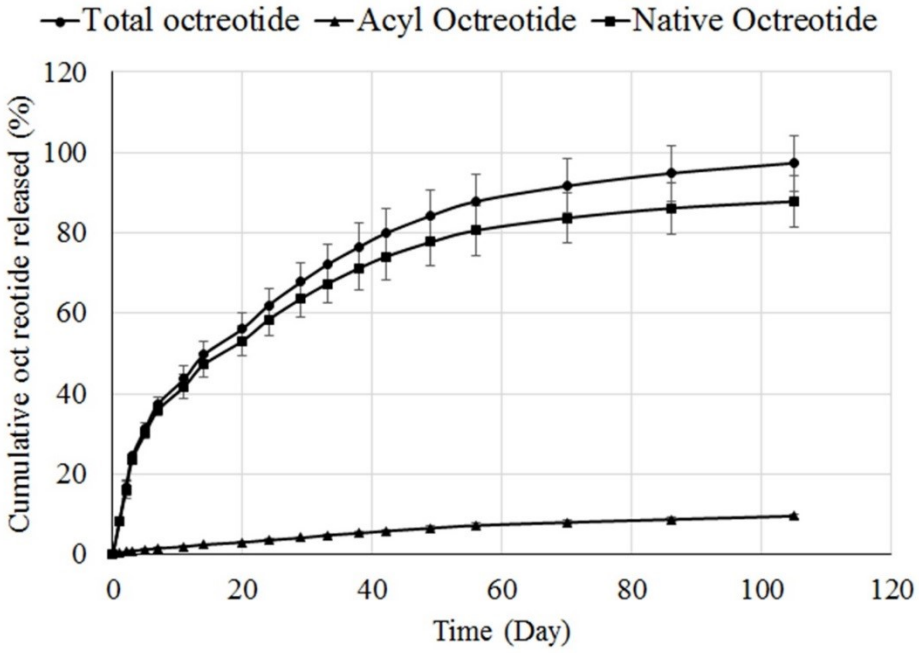

Figure 3-3 *In vitro* release of total, native and acylated octreotide from TBMPs-in-gel. Data presented as Mean ± SD, n=4.

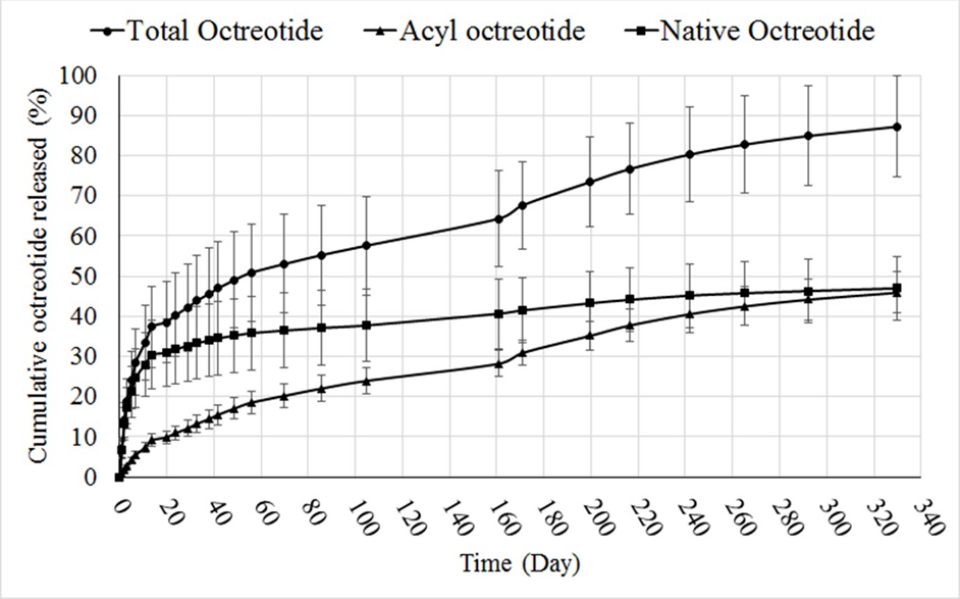

Figure 3-4 *In vitro* release of total, native and acylated octreotide from PBAMPs-in-gel. Data presented as Mean ± SD, n=4.

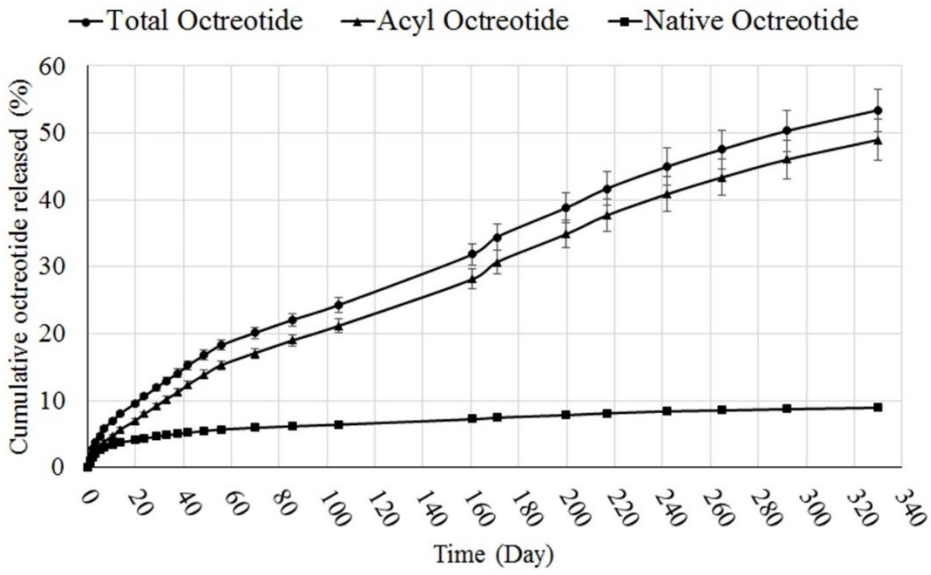

Figure 3-5 *In vitro* release of total, native and acylated octreotide from PBBMPs-in-gel. Data presented as Mean ± SD, n=4.

MPs with all polymers resulted in sustained release of peptide over a period of months. TB polymer, consisting polycaprolactone blocks, was the most efficient in preserving chemical stability of encapsulated peptide among three polymers used in this study. Only 10% of peptide was released as acylated adduct and 88% of peptide was released in its native form (Figure 3-3 and Table 3-4). In contrary, a significant fraction of peptide was acylated during the release from PBAMPs and PBBMPs. Release profile for acylated octreotide showed a steady release of acylated adducts over a long period for PBAMPs and PBBMPs (Figure 3-4 and Figure 3-5). Total 87% was released, where 46% of peptide was acylated adducts from PBAMPs over period of 10 months. PBBMPs resulted in release of total 53% peptide, where only 9% was in native form. Fraction of acylated peptide was significantly higher in case of PBBMPs, where 49% was released as derivatized peptides, which was 92% of total released peptide (Table 3-4). The propensity of protein and peptide to undergo acylation from lactide and glycolide based polymer has been reported[127b, 128]. Peptides are more prone to acylation in polymers rich in glycolide compared to lactide [127c]. Presence of methyl group close to carbonyl carbon in lactide sterically hinders nucleophilic attack[127a]. While PGA offers no steric hindrance and nucleophilic attack of peptide is relatively facile resulting in significant peptide derivatization. The order for extent of octreotide derivatization was PBBMPs>PBAMPs>TBMPs. It is worth noting that a substantial fraction of peptide was not released from PBB polymers matrix. This phenomenon can be explained by formation of water insoluble adducts upon acylation (

Figure 2-1b, step 1; Pg#148). Subsequent release of peptide is dependent on hydrolytic degradation of polymer chain (

Figure 2-1b, step 2; Pg#148).

Rate limiting factors controlling drug release from a biodegradable system may include dissolution, diffusion and/or degradation of polymer. Dissolution may not be a rate-limiting factor, as octreotide possesses excellent aqueous solubility. We have utilized a composite system consisting of microparticles embedded in hydrogel to achieve long-term delivery. The mechanism of release may further be complicated due to acylation of peptide. We theorize that the release mechanism could be diffusion and/or degradation controlled. Figure 3-6 represents hypothetical steps leading to release of native and acylated peptide from biodegradable MPs-in-gel composite system. Release of native peptide may be controlled by rate of polymer erosion and diffusion through hydrogel matrix (Figure 3-6). Release of acylated peptide may be a complicated process influenced by bulk erosion, rate of peptide acylation, polymer side-chain hydrolysis and diffusion through the hydrogel matrix (Figure 3-6). Polymer degradation may or may not contribute as rate limiting factor depending on the composition of polymer and rate of polymer degradation.

Various mechanistic and kinetic models were explored in order to determine the mechanism and order of octreotide release. Data was fitted to Higuchi, Korsmeyer-Peppas and Hixson-Crowell models to delineate the mechanism of release. Zero and first order models were utilized to determine the order of release process. Zero order rate indicates that the release rate is independent of drug concentration as opposite to first order rate where rate of release is directly proportional to the initial drug concentration. The model explaining most variability was identified by coefficient of determination (R^2) value. Table 3-5 lists calculated R^2 values and associated parameters for all models. It is evident that release of octreotide (total, native and acylated) was a first order process suggesting that release rate is dependent on concentration (Table 3-5).

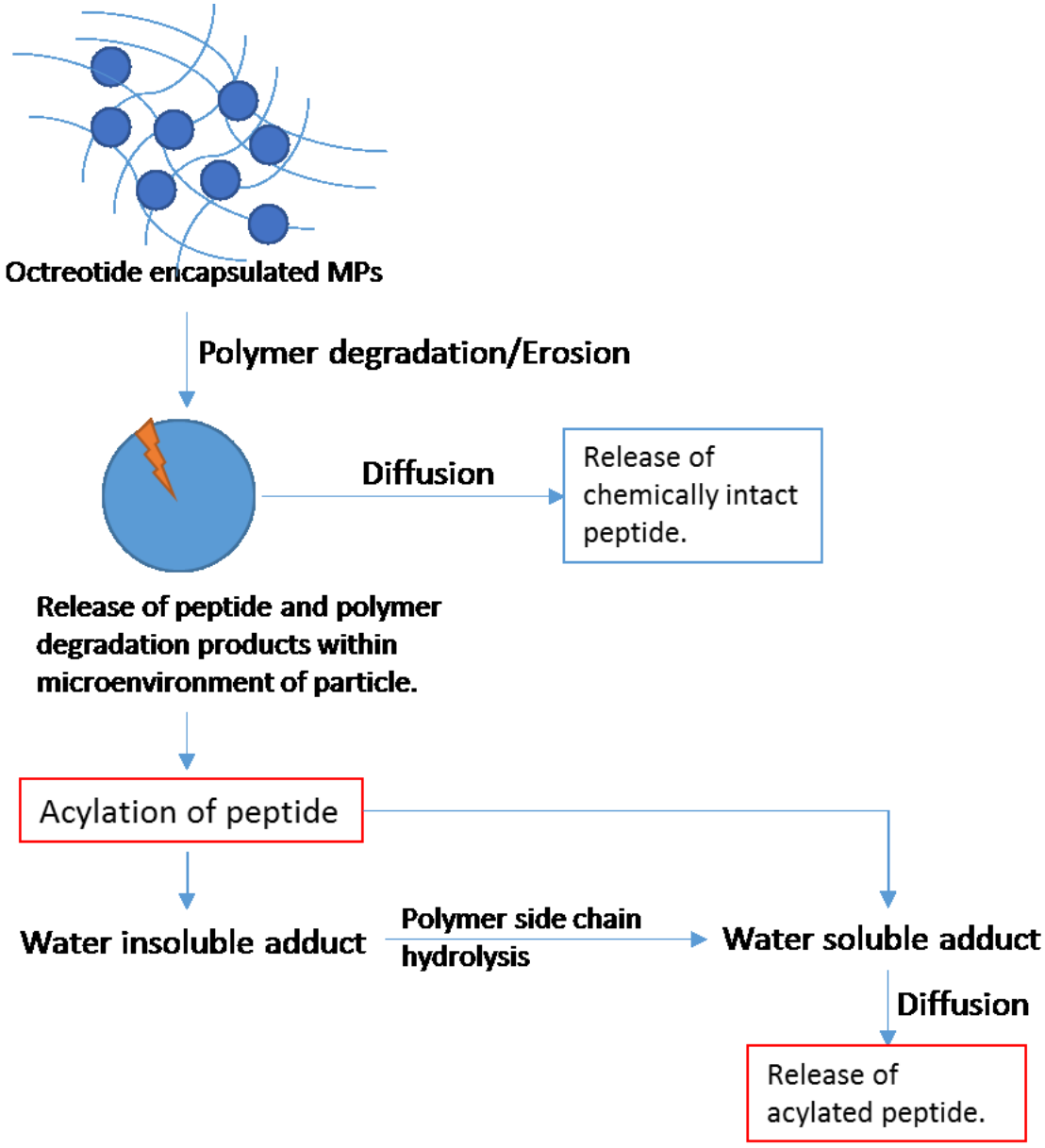

Figure 3-6 Process of native and acylated octreotide release from MPs-in-gel combination. Release of native peptide may be controlled by rate of polymer degradation and diffusion through hydrogel matrix. Release of acylated peptide may be influenced by rate of polymer degradation, rate of peptide acylation, polymer side-chain hydrolysis and diffusion through the hydrogel matrix.

Table 3-5 Summary of fit (R^2) for kinetic and mechanistic models for *in vitro* release of total, native and acylated octreotide from TB, PBA and PBB MPs-in-gel.

MPs polymer	**Octreotide**	**Kinetic and Mechanistic Models**						
		Higuchi Model	**Korsmeyer-Peppas model**		**Hixson-Crowell model**	**Zero Order**	**First order**	
		R^2	**R^2**	**n**	**R^2**	**R^2**	**R^2**	**Rate constant k (Day^{-1})**
TB	Total	0.9265	0.9559	0.6157	0.8442	0.1569	0.9975	0.3316
	native	0.8984	0.9534	0.6089	0.6325	0.0315	0.9400	0.0203
	Acylated	0.9501	0.9865	0.7700	0.8986	0.8894	0.9571	0.0009
PBA	Total	0.7886	0.9211	0.3897	0.5746	0.2120	0.9714	0.0053
	native	0.2620	0.8472	0.2469	0.7002	0.6466	0.7261	0.0012
	Acylated	0.9905	0.9817	0.6217	0.8856	0.8167	0.9777	0.0018
PBB	Total	0.9770	0.9959	0.5882	0.9474	0.8928	0.9946	0.0023
	native	0.7329	0.9688	0.3307	0.3570	0.4230	0.8372	0.0002
	Acylated	0.9406	0.9967	0.6893	0.9722	0.9406	0.9958	0.0021

Higuchi model describes Fickian release from a solid or semisolid matrix type of planar system and the drug release occurs via diffusion through porous matrix [136]. Korsmeyer-Peppas model is widely applied to distinguish between diffusion-controlled (Fickian) and anomalous (non-Fickian) release mechanisms for polymeric delivery systems [137]. The value of release exponent $n \leq 0.45$ indicates diffusion-controlled release whereas $0.45 < n < 0.89$ indicates anomalous release mechanism. The Hixson-Crowell cube root model indicates that the drug release from systems undergoing a change in surface area and diameter of particles [138].

According to R^2 values, release of total octreotide from TB and PB polymers can be explained by Korsmeyer-Peppas model (Table 3-5). Values of release exponent (n) for total octreotide release from TBMPs and PBBMPs were 0.62 and 0.59, suggesting anomalous mechanism of release involving degradation of polymer and diffusion of released peptide through the hydrogel. On contrary, n-value for total octreotide was <0.45 from PBAMPs suggesting diffusion controlled release mechanism.

The mechanism for release of native octreotide from TBMPs was non-Fickian according to Korsmeyer-Peppas model. On the other hand, release of native octreotide was diffusion-controlled for PBAMPs and PBBMPs. Release of native octreotide may be dependent on polymer degradation and diffusion of native peptide out of MPs-in-gel depot (Figure 3-6). Slower degradation of PCL polymer [133], in combination with additional diffusion barrier by hydrogel may be responsible for the non-Fickian mechanism of release from TB polymer. However, PBA and PBB polymers are nearly amorphous in comparison to TB polymers. Polymer degradation may not be a rate-limiting factor for PBA and PBB polymers due to rapid degradation of polymer. Therefore, diffusion through porous hydrogel is the only rate-limiting factors for PBA and PBB polymers.

Similarly, release mechanism for acylated octreotide from MPs of TB, PBA and PBB polymers can be explained by Korsmeyer-Peppas model. Release exponents (n) were >0.45, suggesting the mechanism of acylated peptide release was non-Fickian for all MPs. The n-values for acylated octreotide were the highest compared to total and native octreotide from all polymers. In case of PBAMPs, best fit for acylated peptide release was observed for Higuchi model (R^2 = 0.9905) suggesting diffusion-controlled release. However, Korsmeyer-Peppas model also had high R^2 value for fit (R^2 = 0.9817) with n-value of 0.62 indicating non-Fickian mechanism. We theorize that Korsmeyer-Peppas model could better explain mechanism of acylated octreotide release from PBAMPs because of possibility of additional steps involving polymer degradation. We hypothesized that the release of acylated peptide may be influenced by polymer degradation. As shown in Figure 3-6, release of acylated octreotide is a multistep process, where peptide is first released inside microenvironment of particle via polymer degradation followed by acylation. Octreotide acylation may led to formation of water insoluble adduct, which may require further hydrolysis of polymer side-chain to form water-soluble acylated adduct. Water-soluble acylated octreotide is then diffused out through porous hydrogel. Thus, influence of polymer degradation cannot be neglected and release mechanism for acylated peptide release may be anomalous as predicted by Korsmeyer-Peppas model.

3.3.4. Identification acylated octreotide adducts

The chemical instability, acylation, of peptide is a major concern with biodegradable particulate delivery systems; hence, the aim of this research was to identify polymer composition that can provide maximal chemical stability to the peptide during release. The peaks in the UFLC chromatogram were assigned to native and acylated adducts by UFLC-MS analysis. Figure 3-7, Figure 3-8 and Figure 3-9 depicts UV and MS spectrums (extracted ion chromatograms) for

TBMPs, PBAMPs and PBBMPs release samples. Native octreotide eluted at 8.5 min (UV, Figure 3-7a) and corresponding peak in MS (EIC) appears at 8.6 min (Figure 3-7b). Octreotide appeared as +1 and +2 charge states (z) resulting in species of 1019.3 m/z and 510.3 m/z. Peak at RT 9.8 min (UV, Figure 3-7a) corresponds to C-octreotide (m/z 1133.5, RT 9.99 min) as shown in chromatograms. The MS profile was also extracted for 1246.8 m/z, associated with CC-Octreotide. Two peaks at 12.1 and 12.4 min were only observed in MS chromatogram (Figure 3-7d). Low concentration of CC-octreotide may be due to low aqueous solubility. CC-octreotide following hydrolysis at CC ester linkage would result in release of C-octreotide eventually. Unlike native octreotide, masses with multiple charge states (z>1) were not observed for acylated adduct.

Similarly, release samples for PBAMPs and PBBMPs were analyzed by UFLC-MS. As expected, retention time (RT) for native octreotide remained unchanged (Figure 3-8a-b). PBA polymer consisted of PLA segment; therefore, we observed m/z 1091.5 (UV chromatogram RT 9.7 min and EIC RT 9.8 min) and 1163.2 (UV chromatogram RT 9.8 min and EIC RT 10.1 min) associated with mono and di-lactoyl adducts, respectively (Figure 3-8c-d). In case of PBBMPs, acylated adducts mono-, di- and tri-glycolide derivatives of octreotide were observed (Figure 3-9c-e). Di-glycoyl (GG-octreotide) and Tri-glycoyl (GGG-octreotide) adducts were observed at two different RT, like CC-octreotide adduct. This observation is in corroboration with published literature [135a]. It is possible for di- and tri- adducts to form with different structures and same total mass, resulting in multiple peaks due to different RT owing to different hydrophobicity. It is worth noting that the thermosensitive gel used for release studies also contained PLA segment. Interestingly, mono lactoyl adduct (m/z 1091.5) was observed in the release samples of PBBMPs

(EIC RT 9.8 min, Figure 3-9f). This observation consistent with L-octreotide elution in release samples of PBAMPs at same RT of 9.8 min (Figure 3-8c).

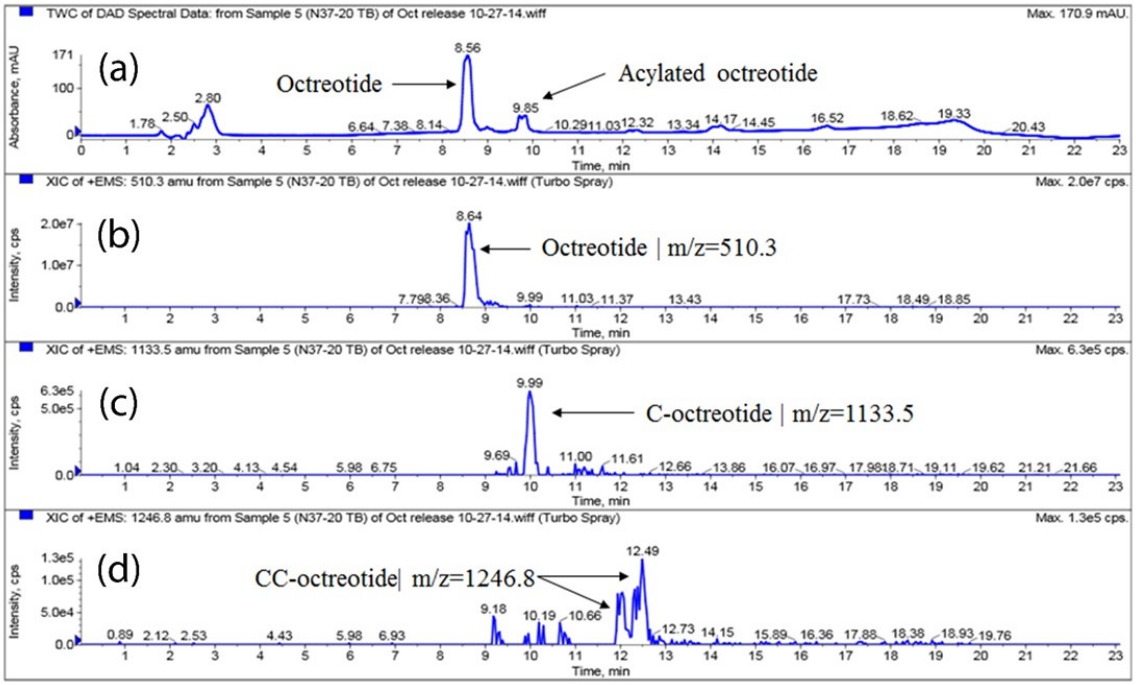

Figure 3-7 UFLC-MS spectrum of release sample (Day 105) from TBMPs-in-gel. (a) UV chromatogram. Extracted ion chromatogram (EIC) for (b) octreotide, m/z 510.3 (c) caprolactoyl-octreotide, m/z 1133.5 and (d) di-caprolactoyl-octreotide, m/z 1246.8. EIC for octreotide (m/z 510.3) shows peak at 8.64 RT which corresponds to peak at 8.56 min in UV chromatogram. Acylated adduct caprolactoyl-octreotide elutes at RT 9.85 min (UV chromatogram) and at corresponding retention time in EIC (m/z 1133.5 and RT 9.99 min). Di-caprolactoyl-octreotide adduct (m/z 1246.8) appears at two RT however no corresponding peak in UV chromatogram is observed due to possibility of low concentration.

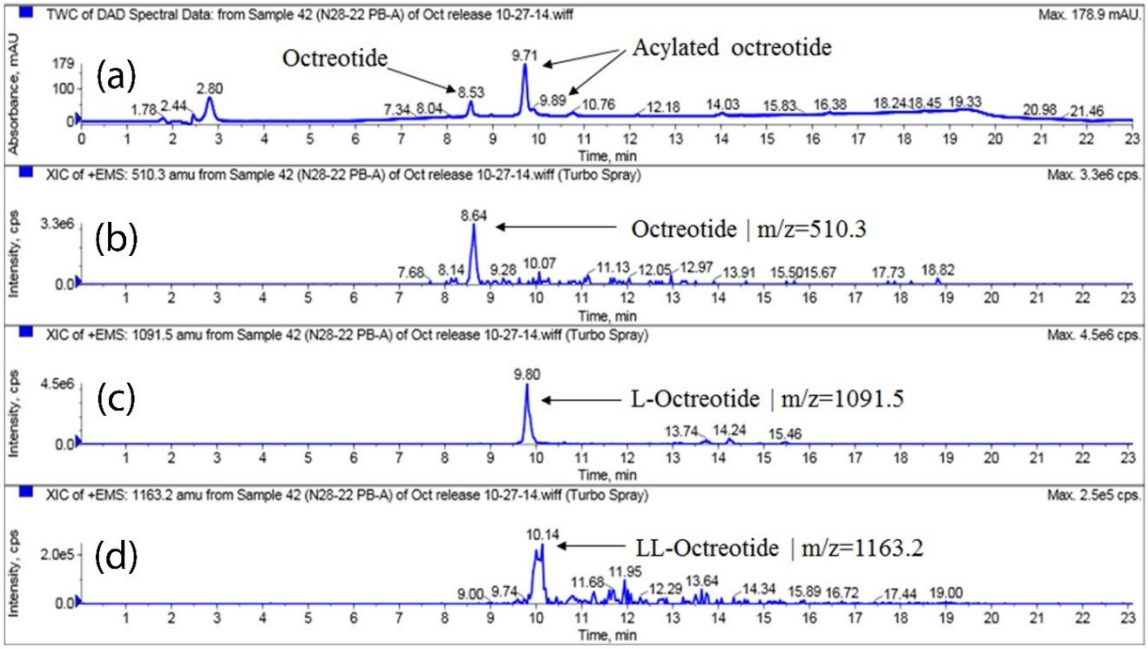

Figure 3-8 UFLC-MS spectrum of release sample (Day 171) from PBAMPs-in-gel. (a) UV chromatogram. Extracted ion chromatogram (EIC) for (b) octreotide, m/z 510.3 (c) Lactoyl-octreotide, m/z 1091.5 and (d) Di-lactoyl-octreotide, m/z 1163.2.

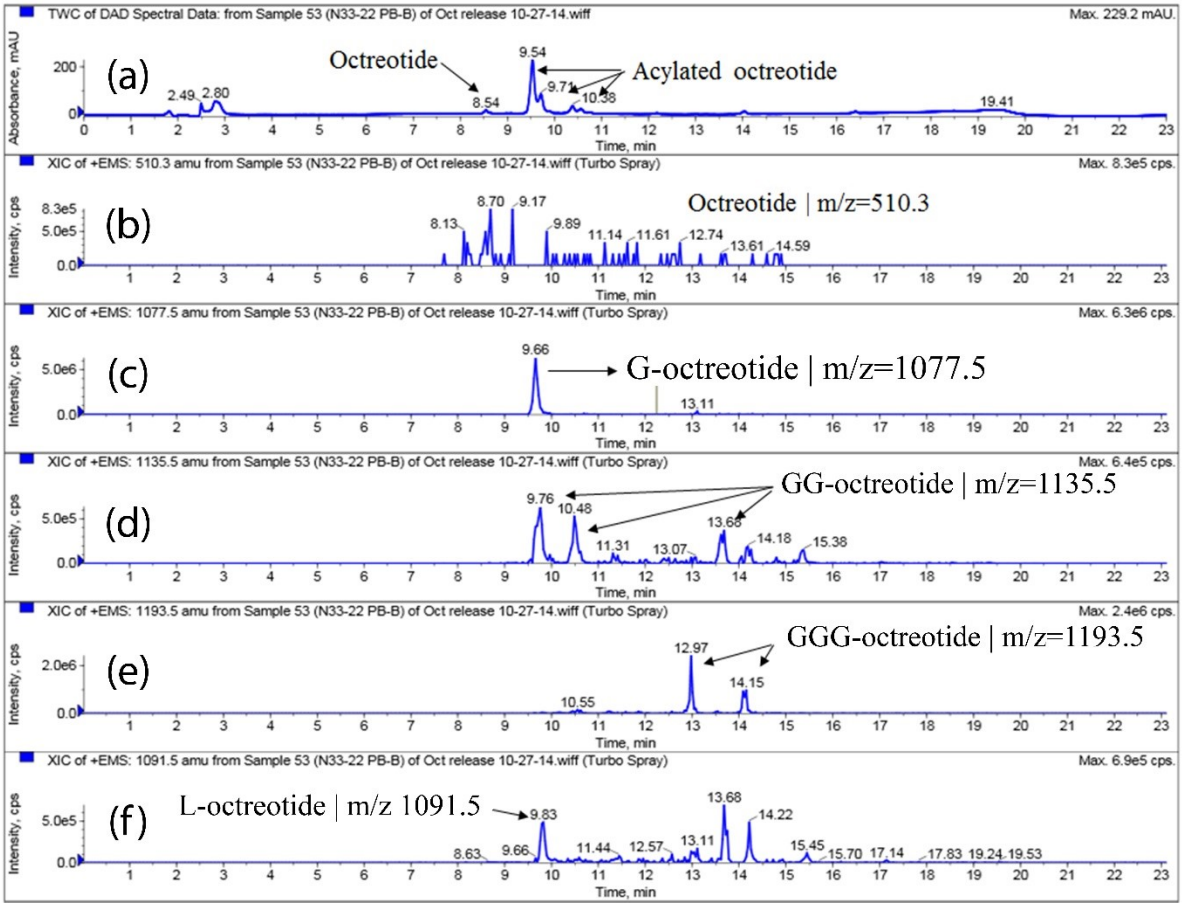

Figure 3-9 UFLC-MS spectrum of release sample (Day 171) from PBBMPs-in-gel. (a) UV chromatogram. Extracted ion chromatogram (EIC) for (b) octreotide, m/z 510.3 (c) Glycoyl-octreotide, m/z 1077.5 (d) Di-glycoyl-octreotide, m/z 1135.5 (e) Tri-glycoyl-octreotide, m/z 1193.5 (f) Lactoyl-octreotide, m/z 1091.5.

A

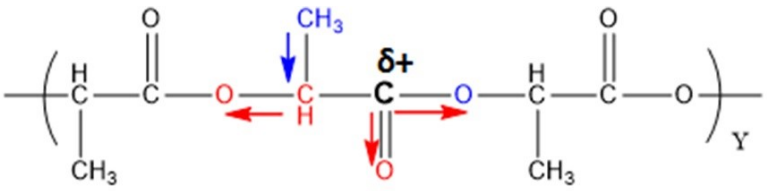

PLA Oligomer

B

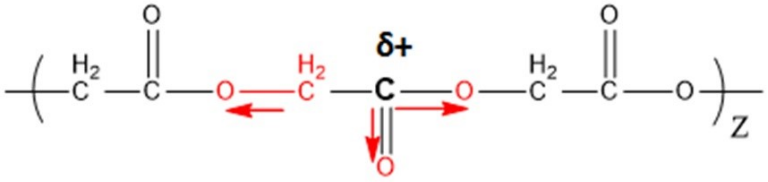

PGA Oligomer

C

PCL Oligomer

Figure 3-10 Schematic depicting electron withdrawal effect of electronegative atoms and electron donating effect of alkyl group responsible for partial positive charge on carbonyl carbon in PLA, PGA and PCL oligomers.

Table 3-6 Summary of octreotide adducts identified using UFLC-MS analysis.

Polymer	Acylated species	M+H/Z	Retention time (min)
TB	C-Octreotide	1133.5	9.9
	CC-Octreotide	1246.8	12.1, 12.4
PBA	L-Octreotide	1091.5	9.8
	LL-Octreotide	1163.2	10.1
	C-Octreotide	1133.5	9.9
	CC-Octreotide	1246.8	ND
PBB	G-Octreotide	1077.5	9.6
	GG-Octreotide	1135.5	9.7, 10.4, 13.6
	GGG-Octreotide	1193.5	12.9, 14.1
	L-Octreotide	1091.5	9.8
	C-Octreotide	1133.5	ND
	CC-Octreotide	1246.8	ND

C- Caprolactoyl, L- Lactoyl, G- Glycoyl, ND- Not detected.
Four samples for TBMPs and nine samples for PBAMPs and PBBMPs, at a month time interval, were selected for analyses.

This observation indicates that the acylation of peptide may also take place in hydrogels matrix apart from the MPs core. The summary of octreotide adducts identified using UFLC-MS analysis is depicted in Table 3-6 along with corresponding observed mass (m/z) and RT.

Only 10% octreotide was acylated for TB polymer despite absence of steric hindrance like in case of PBA. There may be two reasons for this observation. First, it may be due to slow degradation of polymer owing to its semicrystalline nature. It is established that the peptide acylation occurs inside the MPs. The process is facilitated because the area is rich in degraded polymer products and released peptide. Hence, less or negligible acylation of peptide in TP polymer may be attributed to slower degradation of the polymer. In case of PBA and PBB polymers, PLA and PGA blocks degrade at rapid rate than PCL segment resulting in formation of corresponding acylated adducts. Secondly, it might be due to relatively lower reactivity of carbonyl carbon of PCL compared to PLA or PGA segment. Low reactivity could be attributed to hydrophobic effects and/or electron donating inductive effect of alkyl chains adjacent to carbonyl carbon. The carbonyl carbon in PCL may carry less partial positive charge because of electron donating effect of alkyl group (-CH_2-) as depicted in Figure 3-10c. Where as in case of PLA and PGA oligomers, the electron withdrawal effect of electronegative oxygen dominates resulting in stronger partial positive charge on carbonyl carbon making it facile target for nucleophilic attack (Figure 3-10a-b).

CHAPTER 4

4. REVERSIBLE HYDROPHOBIC ION-PARING COMPLEXATION TO MINIMIZE ACYLATION OF OCTREOTIDE DURING LONG-TERM DELIVERY FROM PLGA MICROPARTICLES.

4.1. Materials

Octreotide acetate (D-Phe-Cys-Phe-D-Trp-Lys-Thr-Cys-Thr-ol; M_W 1019.23 Da) was procured from ChinaPeptides Co., Ltd (Shanghai, China). Poly(D, L-lactic-co-glycolide) (50:50, Mw 40-70 kDa), dextran sulfate sodium-salt (Mw 9-20 kDa) and sodium dodecyl sulfate (SDS) were obtained from Sigma Aldrich (St Louis, MO). Dextran sulfate sodium-salt (Mw 36-50 kDa) was obtained from MP Biomedicals (Illkirch, France). MicroBCA™ protein assay kit was purchased from Thermo Scientific (Rockford, IL). All solvents were of analytical reagent grade.

4.2. Methods

4.2.1. Preparation of HIP complex

HIP complex was prepared by simple mixing of aqueous solutions containing ion-pairing agent and octreotide[139]. Briefly, stock solutions of octreotide and ion-pairing agents were prepared in 10 mM citrate buffer at pH 4. Solutions were then mixed in calculated proportions and vortexed. After 3 h, water insoluble complex was separated by centrifugation at 12,000 rpm for 10 min. HIP complex pellet was freeze-dried and stored at -20˚C until further use. Supernatant was analyzed for the amount of free peptide using microBCA™ assay following the protocol provided by the manufacturer [135a]. The percentage of octreotide complexed (complexation efficiency (%CE)), was calculated according to equation 4.1.

$$\% \text{ Complexation efficiency} = (1-Mt/Mo)*100 \qquad \ldots(4.1)$$

Mt = Amount of octreotide in supernatant

Mo = Initial amount of octreotide

4.2.2. Effect of mole ratio of ion-pairing agent to octreotide on complexation efficiency

Three ion-pairing agents, dextran sulfate (9-20kDa, DSA), dextran sulfate (36-50kDa, DSB) and SDS, were employed to prepare HIP complex with octreotide acetate. HIP complex was prepared following a method explained earlier. The solutions were mixed at various mole ratios of ion-pairing agent to octreotide.

4.2.3. Dissociation of HIP complex

HIP complex of octreotide with ion-pairing agents was prepared at optimal mole ratio producing maximum %CE following the method explained earlier. Freeze-dried HIP complex was incubated in an isotonic phosphate buffer saline (IPBS) at pH 7.4 to study the dissociation under simulated physiological condition. Mechanistic studies were carried out to investigate the effects of ionic strength and pH on complex dissociation. HIP complex was incubated in 10 mM phosphate buffer (NaH_2PO_4 (monobasic) and Na_2HPO_4 (dibasic), pH 7.4) containing various strengths of NaCl (10 mM, 100 mM and 154 mM), DDI water and 10 mM citrate buffer (100 mM NaCl, pH 4.2) to delineate the influence of concentration of counter-ions and pH on complex dissociation. Following 30 min incubation, the insoluble complexes were separated by centrifugation at 12,000 RPM for 10 min. Amount of dissociated octreotide in supernatant was quantitated using microBCA™ assay and the percentage of dissociated octreotide was calculated according to equation 4.2.

$$\% \text{ Dissociation} = (Ms/Mi)*100 \qquad \ldots(4.2)$$

Ms = Amount of octreotide in supernatant

Mi = Initial amount of octreotide in HIP complex

4.2.4. Preparation of Microparticles

HIP complexes of octreotide were prepared using ion-pairing agents DSA and DSB at optimal mole ratio following the method described previously. MPs encapsulating HIP-complexed octreotide were prepared by solid/oil/water (S/O/W) emulsion solvent evaporation method. Briefly, oil phase (O) consisted of 100 mg PLGA (50/50, Mw 40-70kDa) in 900 µL DCM. The oil phase was added to a vial containing 10 mg octreotide equivalent HIP complex and vortexed for 2 min. The resulting suspension was tip-sonicated for 30 sec at power output of 2W to form S/O suspension. The suspension was added drop-wise to constantly stirred water phase (5 mL) containing 2% w/v PVA as a stabilizer to form S/O/W emulsion. The resulting emulsion was kept in the hood under constant stirring to evaporate the organic solvent. After 6 h, the resulting MPs were separated by centrifugation at 13,000 RPM for 10 min. MPs were washed with DDI water and centrifuged twice to remove un-entrapped peptide. MPs were suspended in solution containing 2% w/v mannitol for freeze-drying. Freeze-dried particles were then store at -20°C until further use. Ghost MPs without octreotide were also prepared in an identical manner where equivalent amount of ion-pairing agent were suspended in oil phase.

4.2.5. Drug loading (%) and entrapment efficiency (%)

Encapsulation efficiency was determined by UV spectroscopy using Nanodrop™ (Thermo Fisher Scientific Inc.). Briefly, five mg of freeze-dried particles (n = 3) were dissolved in 200 µL DMSO. Ghost MPs containing corresponding ion-pairing agents served as blank. Standard of octreotide were prepared in DMSO ranging from 2.72 to 0.043 mg/mL. UV absorbance was measured at 280 nm. Entrapment efficiency and drug loading were calculated by equation 4.3 and 4.4, respectively.

$$\%EE = (\text{Amount of octreotide in MPs}/\text{Total amount of octreotide})*100 \quad \ldots(4.3)$$

%DL = (Amount of octreotide in MPs/Total weight of MPs)*100 …(4.4)

4.2.6. Scanning electron microscopy of MPs

Scanning electron microscopy (SEM) analysis was performed to analyze particle morphology (size and shape). Freeze-dried MPs were applied to carbon film positioned on an aluminum stub. Surface of particles on carbon film was coated with Au-Pd under centrifugation followed by sample analysis in Phenom Pro desktop scanning electron microscope.

4.2.7. In vitro release of octreotide from MPs-in-gel composite formulation

Freeze-dried MPs were subjected to *In vitro* release study in PBS buffer (pH 7.4) at 37 °C. PLGA MPs encapsulating HIP-complexed octreotide (DSA and DSB) were suspended in 400 µL of thermosensitive gel solution (20 wt%) maintained at 4°C. Pentablock polymer PLA_{250}-PCL_{1250}-PEG_{1500}-PCL_{1250}-PLA_{250} was utilized to prepare thermoreversible gel solution. Preparation and characterization of gelling polymer has been published earlier from our laboratory [132]. Resulting MPs-in-gel suspension was incubated at 37 °C for 2 min to form hydrogel followed by slow addition of 1.5 mL of PBS (pH 7.4) which was pre-incubated at 37 °C. At pre-defined time intervals, 1 mL of clear supernatant was collected and replaced with equal volume of fresh PBS. Release samples were evaluated for native and chemically modified octreotide using ultra-fast liquid chromatography (UFLC) assay. The experiments were carried out in triplicate and plotted as cumulative octreotide released (%) with respect to %EE verses time.

4.2.8. Ultra-fast liquid chromatography assay

See section 3.2.7 for detailed method.

4.2.9. UFLC-MS analysis

See section 3.2.8 for detailed method.

4.3. Result and Discussion

Hydrophobic Ion-Paring (HIP) complexation involves the formation of reversible complex. This process can to increase hydrophobicity of biologics thereby improving entrapment efficiency in polymeric formulations. It has been shown that peptide/protein retains activity and conformational stability with HIP complex in various studies[139-140]. We hypothesize that acylation of peptides can be prevented or minimized by masking the reactive nucleophile amine with reversible HIP complex. HIP complex, formed by charge-charge interaction, may be stable at lower pH and thus prevent the nucleophilic attack of amines on PLGA degradation products inside MPs core (Figure 4-1b). HIP complex may dissociate to release native peptides at physiological pH and in presence of counter ions (Figure 4-1c). A schematic presentation of overall hypothesis is depicted in Figure 4-1. Hence, the aim of our current study was to prepare and characterize HIP complex of octreotide using various ion-pairing agents and evaluate acylation of octreotide during release from PLGA microspheres.

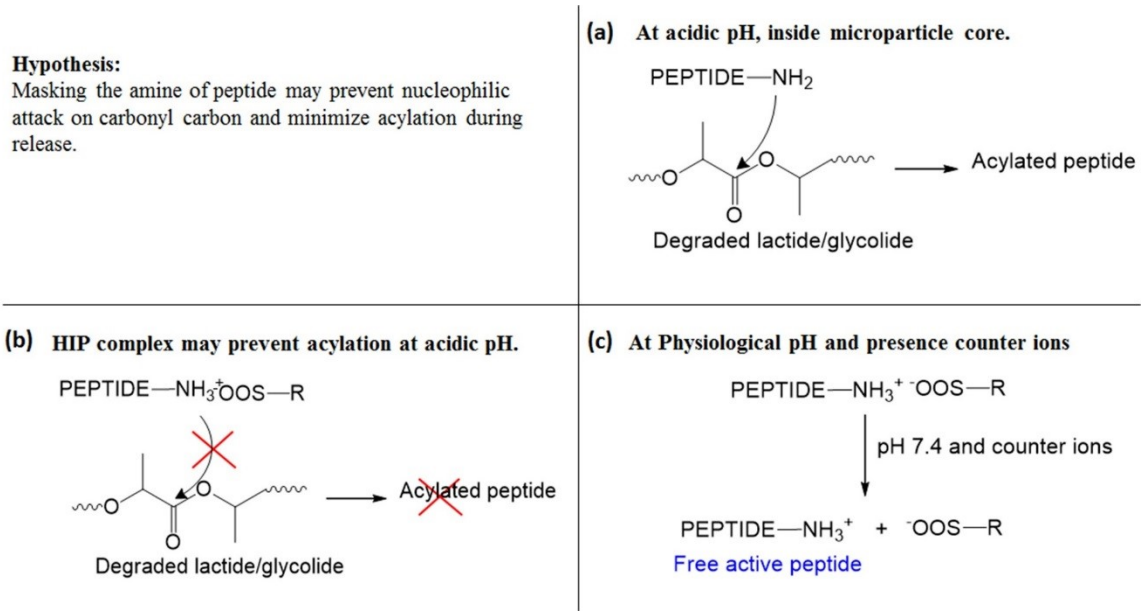

Figure 4-1 (a) chemical derivatization of peptide occurs in MPs core, largely via nucleophilic attack of amine on carbonyl carbon of degraded polymer oligomers. (b) HIP complex may not dissociate at lower pH, preventing acylation. (c) At physiological pH and in presence of counter ions, the HIP complex may dissociate to produce free native peptide.

4.3.1. Preparation of HIP Complex

We investigated SDS and dextran sulfate as the complex forming agents. Dextran sulfate of molecular weights 9-20k and 36-50k Da were examined. Reversible HIP complex was prepared by simple mixing of solutions containing octreotide and ion-pairing agents at low pH. Citrate buffer (pH 4) was selected to dissolve octreotide and ion-pairing agents based on published reports from our laboratory[139a, 139c]. Octreotide has two pKa, 7 and 10.15 associated with amine of lysine and guanidine group of terminal arginine. As a result, a large fraction of amines is ionized at pH 4. The ion-pairing agents have pKa of <2 due to sulfonic acid group, resulting in complete ionization at pH 4. Water insoluble HIP complex is formed via ionic interactions between oppositely charged amine and sulfonate groups. Ionization of charged groups is primarily responsible for aqueous solubility of octreotide and ion-pairing agents. Hence, following charge neutralization, the complex can no longer remain in aqueous solution resulting in precipitation.

4.3.2. Effect of mole ratio of ion-pairing agent to octreotide on complexation efficiency

Stoichiometric balance i.e. charge ratio and corresponding mole ratio of ion-pairing agent to octreotide is an important parameter that may directly influence the efficiency of complex formation. The aim of this experiment was to identify mole ratio producing complete complexation of octreotide to avoid loss of uncomplexed peptide. Effect of mole ratio of ion-pairing agent to octreotide on complexation efficiency is illustrated in Figure 4-2. Mole ratios were selected based on charge ratio of ion-pairing agent to octreotide. For SDS, DSA and DSB, fraction of octreotide complexed reached maximum at mole ratios of 2, 0.028 and 0.009, respectively and nearly all octreotide was complexed. At these optimal mole ratios, the charge ratio also approaches to 1:1 for all ion-pairing agents resulting in near complete binding Figure 4-2.

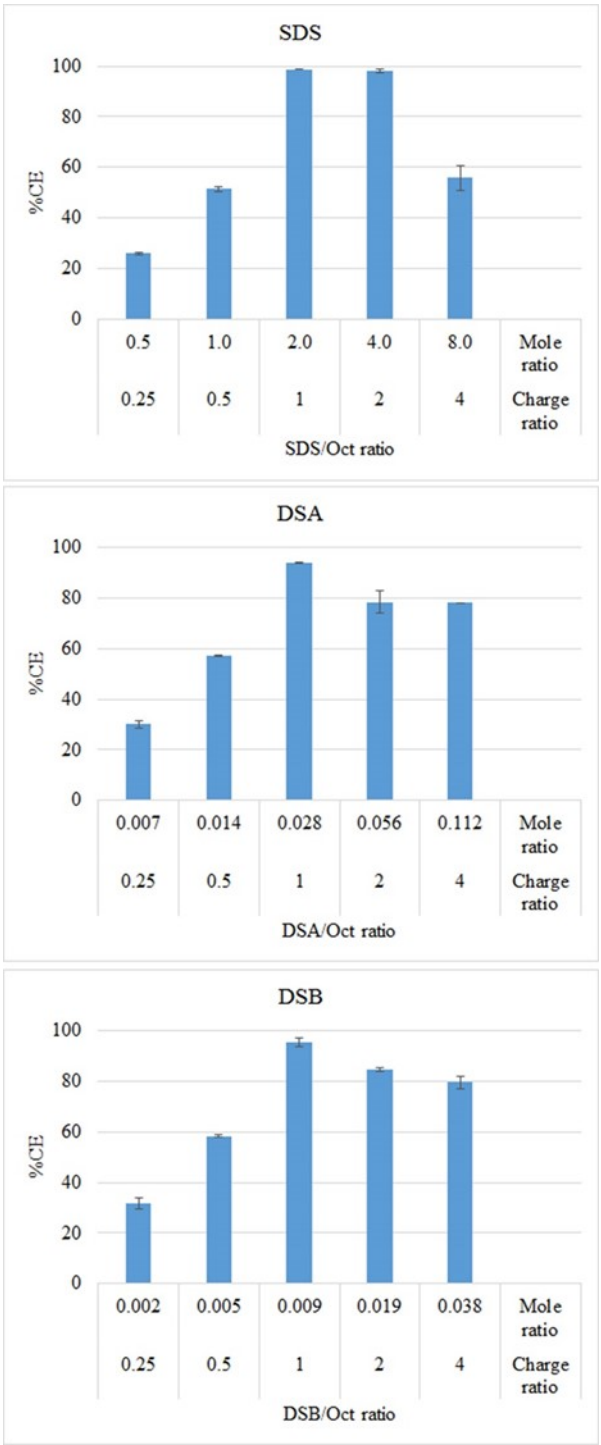

Figure 4-2 Effect of charge/mole ratio of ion-pairing agent/octreotide on % octreotide complexation. Data represented as mean±SD, n=3.

However, fraction of octreotide complexed declined upon further increment in mole ratio. Similar results were observed with lysozyme and IgG-FAB with these ion-pairing agents[139]. This may be due to incomplete charge neutralization in DSA and DSB at higher mole ratio. In case of SDS, it may be attributed to formation of micelles, which subsequently solubilized hydrophobic SDS-oct complex [140].

4.3.3. Dissociation of HIP complex

HIP complexes of octreotide with SDS, DSA and DSB were incubated in IPBS buffer (137 mM NaCl, 2.7 mM KCl, 10 mM Na_2HPO_4, 1.8 mM KH_2PO_4; pH 7.4) and free octreotide in solution was quantified for dissociated octreotide. Dextran sulfate complexes resulted in significantly higher dissociation compared to SDS-oct complex (t-test $p<0.001$) (Figure 4-3). Percent of octreotide dissociated was 90% and 100% with DSA and DSB (t-test, one tailed $p = 0.11$), respectively. Incomplete dissociation (20%) was observed for SDS-oct complex. Similar incomplete dissociation with SDS-IgG-FAB complex has been reported earlier [139c]. HIP complex is governed by electrostatic interactions between opposite charges. Nonetheless, hydrophobic interaction may also play a key role in stabilization of water insoluble complex. If an ionic interaction were the only force responsible for the stabilization of HIP complex, then SDS-oct complex should have dissociated completely. Instead, only a fraction of octreotide was dissociated suggesting the role of hydrophobic interaction in stabilization of SDS-oct complex.

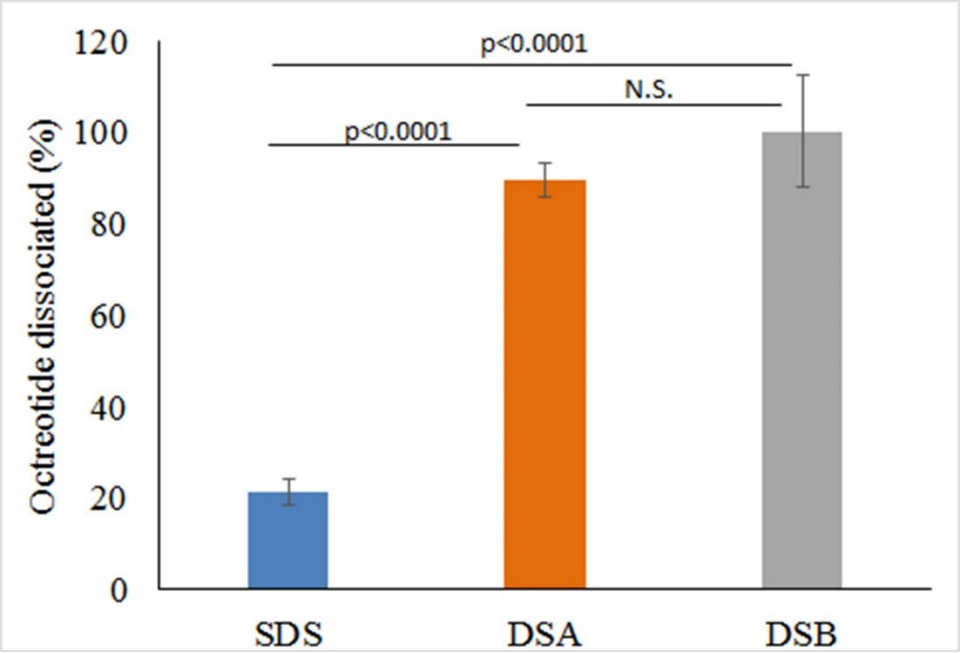

Figure 4-3 Dissociation of SDS-oct, DSA-oct and DSB-oct HIP complex in IPBS buffer at pH 7.4. Data represented as mean±SD, n=3.

For successful application of HIP complex to minimize acylation of peptide, the complex should remain stable at lower pH (Figure 4-1b). Following release, the complex must dissociate completely to produce native peptide (Figure 4-1c). Thus, the dissociation of complex directly affects bioavailability of peptide. Therefore, mechanistic studies were performed to investigate the factors influencing dissociation phenomenon. We examined the influence of concentration of counter ion on dissociation in phosphate buffer (pH 7.4) containing increasing concentration of NaCl. The complex was incubated in DDI water, which acted as a negative control with absence of counter ions. As shown in Figure 4-4, less than 5% octreotide dissociated upon incubation in DDI water because of the absence of counter ions. A proportional increase in fraction of dissociated peptide was observed with an increase in concentration of counter ion at pH 7.4 in phosphate buffer. Dissociation of complex in phosphate buffer (Figure 4-4) and IPBS (Figure 4-3) clearly indicates that the dissociation of complex depends on concentration of counter ions. Again, near complete dissociation was observed in cases of DSA and DSB compared to SDS at 154 mM NaCl. Dissociation of HIP complexes at acidic condition was also studied by incubating complex in 10 mM citrate buffer with 100 mM NaCl at pH 4. Importance of pH on dissociation of complex is evident because a substantially low fraction of complex was dissociated at pH 4 despite presence of counter ions. Based on these results, it can be inferred that HIP complex may be able to mask reactive amines groups in acidic microenvironment inside microparticle core and prevent acylation of peptide (Figure 4-1c).

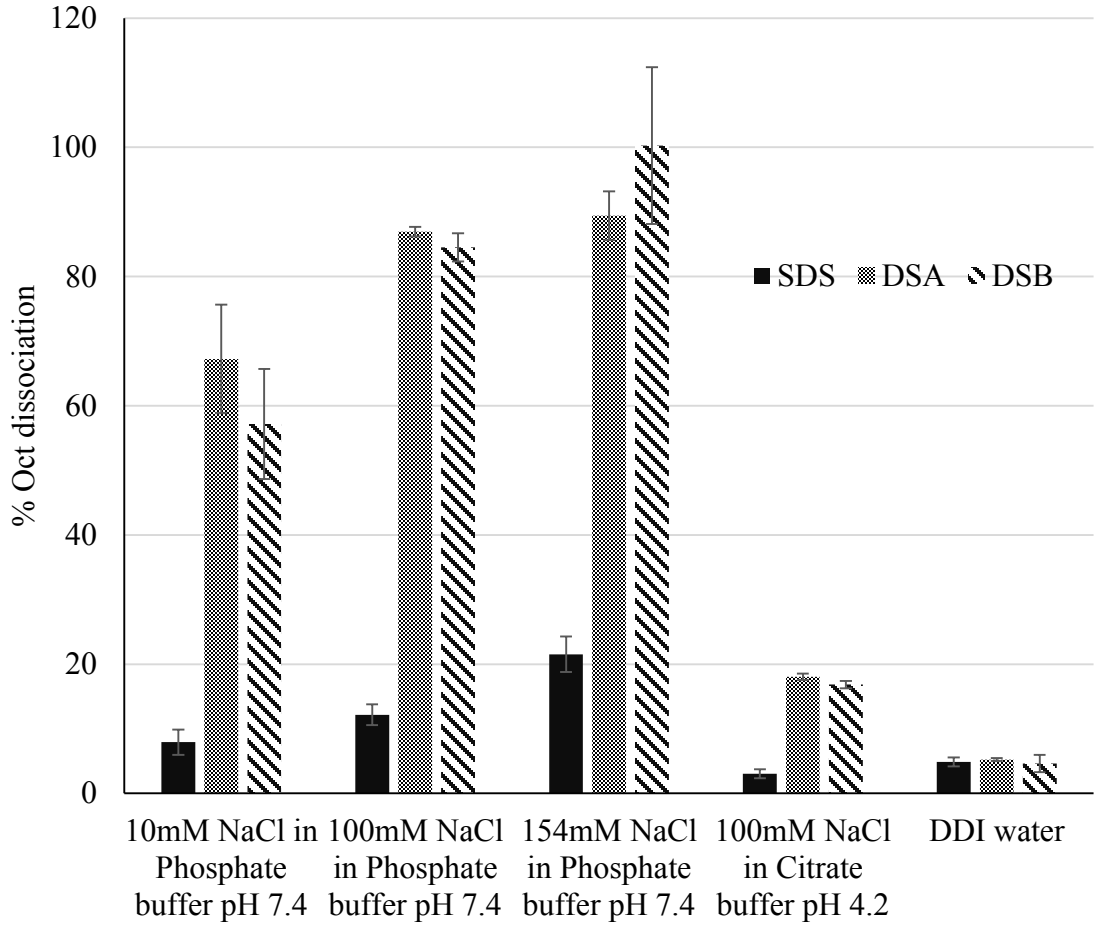

Figure 4-4 Dissociation of SDS-oct, DSA-oct and DSB-oct HIP complex at various ionic strength and pH.

4.3.4. Preparation and characterization of MPs

Ion-pairing agents DSA and DSB were selected for further studies based on the dissociation of complex at simulated physiological condition and stability at low pH. MPs were prepared by S/O/W method and characterized for octreotide loading and encapsulation efficiency following direct method of analysis. PLGA 50/50 at polymer to drug weight ratio of 10:1 was utilized. Excellent entrapment efficiency and drug loading for both DSA and DSB ion-pairing agents were achieved with S/O/W method (Table 4-1). MPs were characterized for particle size and morphology with scanning electron microscopy. MPs were spherical in shape with smooth surfaces (Figure 4-5). DSAMPs were slightly polydispersed and had overall size less than 100 μm. On the other hand, DSBMPs appears to be less polydispersed with a size of 200 μm or less. Larger size of DSBMPs could be attributed to higher molecular weight of DSB (36-50kDa) compared to DSA (9-20kDa), which resulted in larger size DSB-Oct complex.

4.3.5. Mechanism and kinetics of release

In vitro release studies were carried out to investigate the mechanism and kinetics of octreotide release from DSAMPs and DSBMPs in PBS buffer at 37 °C. Samples were analyzed by UFLC to determine the concentration of released peptide (native and acylated). Release profiles depicting the release of total, native and acylated octreotide from DSAMPs and DSBMPs are illustrated in Figure 4-6 and Figure 4-7. Pentablock thermoresponsive polymer was utilized to sustain the release of octreotide. MPs were suspended in an aqueous solution of pentablock polymer (20% w/w), which phase transform to gel at 37 °C to entrap MPs within gel matrix. The hydrogel provides additional diffusion barrier to peptide released from MPs and thus may extend duration of release[132-133].

Table 4-1 Summary of entrapment efficiency and drug loading for DSAMPs and DSBMPs.

Polymer	**Ion-pairing agent**	**Polymer:octreotide weight ratio**	**%EE**	**%DL**
PLGA (50/50)	DSA	10:1	74.7±8.4	7.8±0.3
PLGA (50/50)	DSB	10:1	81.7±6.3	7.9±0.5
Data represented as mean+SD, n = 3.				

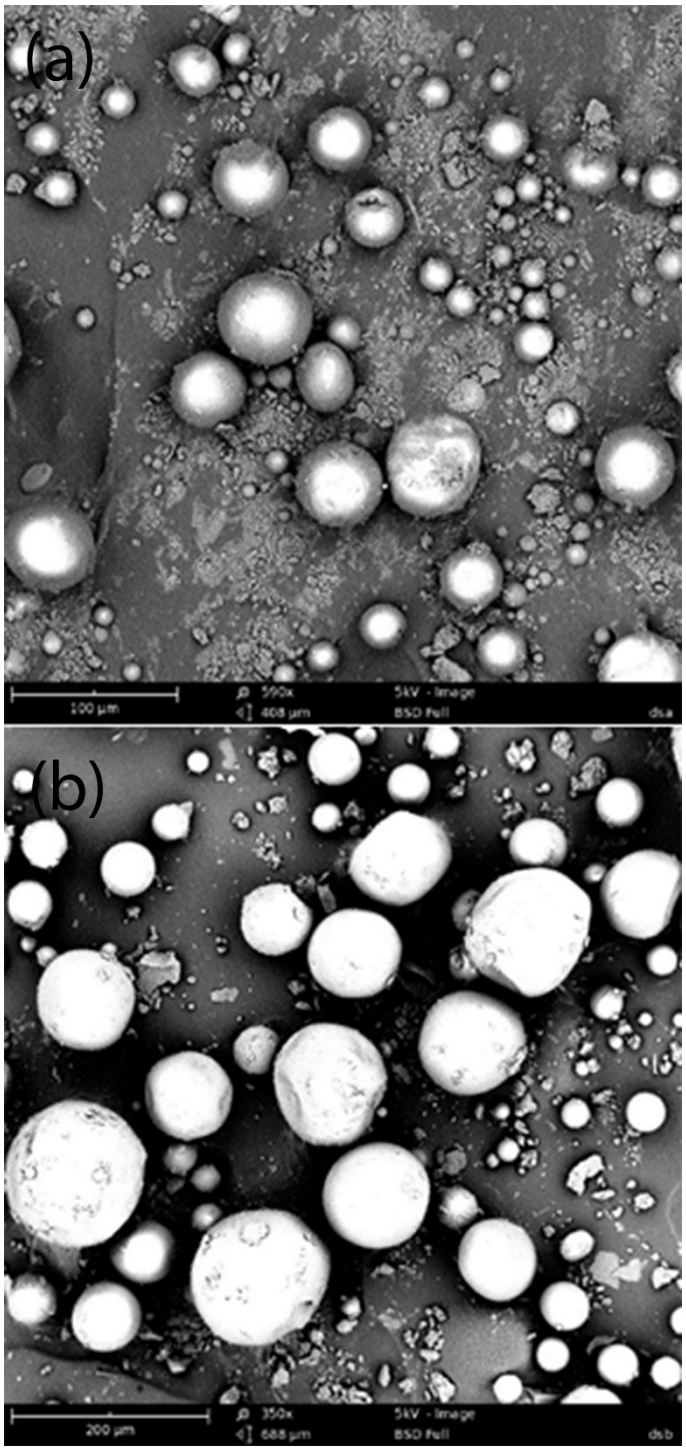

Figure 4-5 Scanning electron micrograph showing surface morphology for (a) DSAMPs and (b) DSBMPs.

DSAMPs and DSBMPs sustained release of octreotide over a period of 55 days. Near complete release was observed for both DSAMPs and DSBMPs. No significant difference in initial burst release was observed for DSAMPs (17.8±1.1%) and DSBMPs (15.6±0.5%) (t-test p = 0.146). Mechanism of release for total octreotide was delineated by fitting the data in mechanistic models including Higuchi, Korsmeyer-Peppas, and Hixson-Crowell models[136-138]. Table 4-2 summarizes the coefficient of determination (R^2) and associated parameter for all the models. Best fit was observed for Korsmeyer-Peppas model based on the R^2 value for both MPs among all three models (Table 4-2). The n-value for both MPs was found to be 0.64 suggesting the release mechanism to be non-Fickian [137]. This mechanism suggests that the release of peptide was both diffusion and degradation controlled. Data was also fitted to zero- and first-order equations to determine the order of release. Process of release was first order kinetics indicated by R^2 values for both DSAMPs and DSBMPs (Table 4-2). First order kinetic suggests that the release rate is proportional to the concentration. As a result, slower release was observed for both MPs in the later phase of release (Figure 4-6 and Figure 4-7). Compared to DSBMPs, release rate was faster for DSAMPs, as indicated by first order rate constant. This result can be attributed to accelerated erosion of polymer matrix due to smaller particle size.

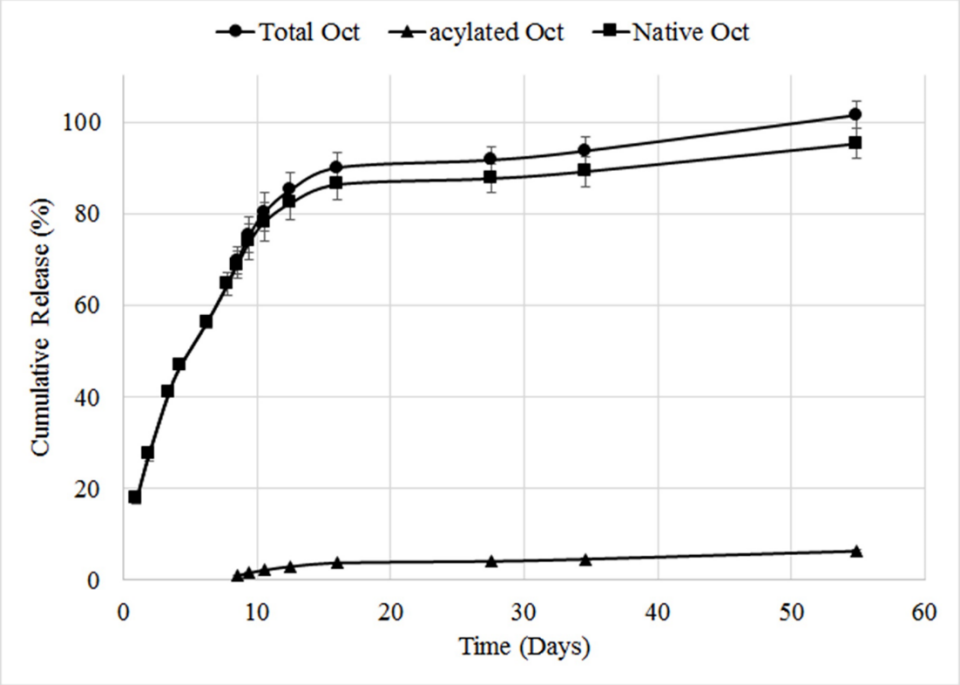

Figure 4-6 *In vitro* release profiles of total, native and acylated octreotide from DSAMPs-in-gel composite formulation.

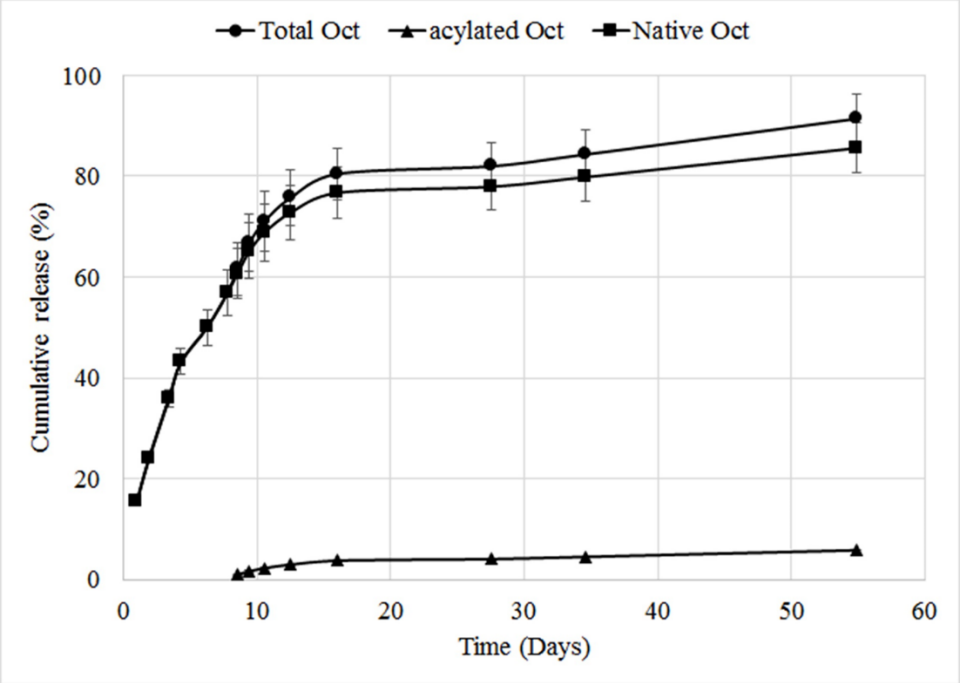

Figure 4-7 *In vitro* release profiles of total, native and acylated octreotide from DSBMPs-in-gel composite formulation.

Table 4-2 Summary of fit for kinetic models and associated parameters for release of octreotide from DSAMPs and DSBMPs in gel formulations.

MPs	Mechanistic and kinetic models						
	Higuchi Model	Korsmeyer-Peppas model		Hixson-Crowell model	Zero Order	First order	
	R^2	R^2	n	R^2	R^2	R^2	Rate constant k (Day^{-1})
DSAMPs	0.5988	0.9964	0.6403	0.7884	0.5821	0.9124	0.107
DSBMPs	0.6224	0.9935	0.6378	0.7582	0.5948	0.8385	0.040

4.3.6. Acylation of peptide during release

Dissociation of HIP complex under acidic pH suggests that peptide complex remains stable at acidic pH inside MPs and may prevent acylation of peptide during release. Amount of native and acylated peptide released from DSAMPs and DSBMPs were quantified by UFLC. Only 6.3% and 5.8% of peptide were acylated for DSAMPs and DSBMPs, respectively. This small amount of acylation may be explained by dissociation of small fraction of peptide at acidic pH (Figure 4-4). Significantly large fractions, 85% from DSMPs and 95% DSAMPs, were chemically intact following the release as we hypothesized. UFLC-MS analysis was performed to identify the peaks associated with native and acylated peptide in the LC chromatogram. UFLC-MS profile for release samples on day 16 from DSAMPs and DSBMPs are represented in Figure 4-8 and Figure 4-9. Native octreotide eluted at 8.89 min in extracted ion-chromatogram as m/z of 510.3 corresponding to peak at 8.67 min in UV chromatogram (Figure 4-8a and Figure 4-9a). Parent ion for native octreotide at m/z 1019.3 was also observed (Data not shown). Presence of 1019.3 and 510.3 m/z suggest that the peptide maintained its native cyclic chemical structure. In both MPs, a very small amount of lactoyl-octreotide (m/z 1091.6, 9.8 min) and glycoyl-octreotide (m/z 1077.7, 9.7 min) adducts were observed as acylated species (Figure 4-8b-d and Figure 4-9b-d), which eluted following native peptide due to higher hydrophobicity. Similar findings have been reported by other investigators [135a].

Table 4-3 depicts the chemically modified species observed in the release samples for DSAMPs and DSBMPs. The observations in Table 4-3 are based on UFLC-MS analysis of release samples on day 1, 9 and 16. The gelling polymer contained polycaprolactone block but caprolactoyl-octreotide (m/z 1133.5) was not detected. Moreover, di-lactoyl and di-glycoyl adducts were not observed.

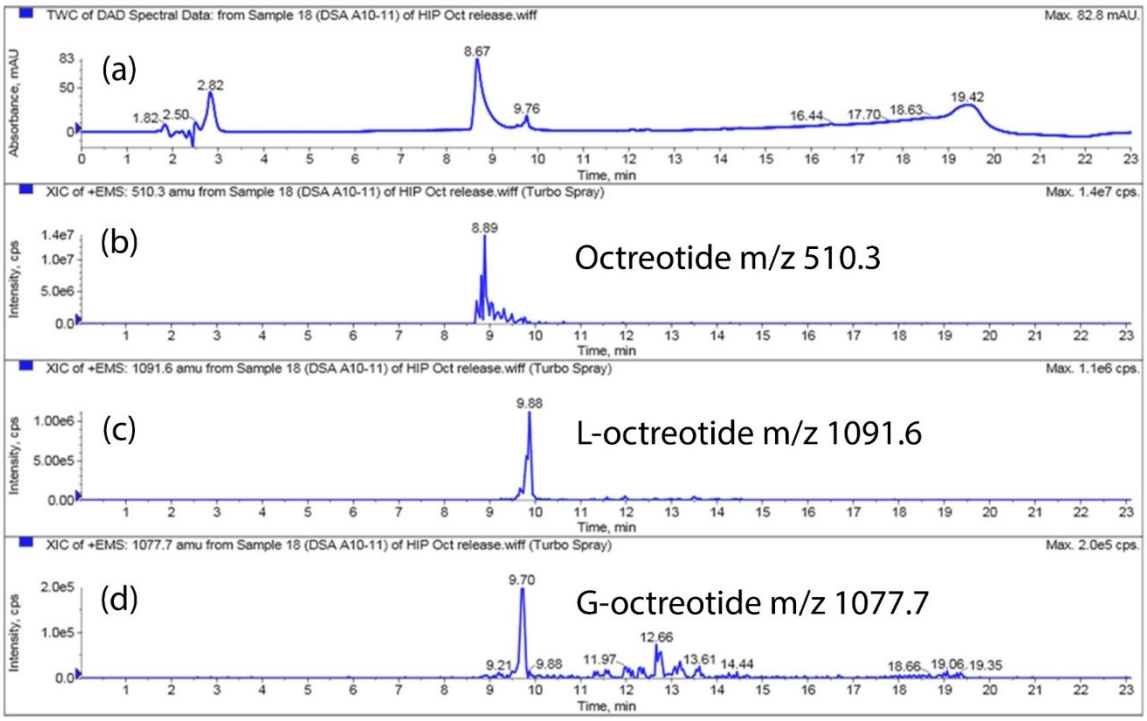

Figure 4-8 UFLC-MS spectrum of release sample (Day 16) from DSAMPs-in-gel. (a) UV chromatogram. Extracted ion chromatogram (EIC) for (b) octreotide, m/z 510.3 (c) Lactoyl-octreotide, m/z 1091.6 and (d) Glycoyl-octreotide, m/z 1077.7.

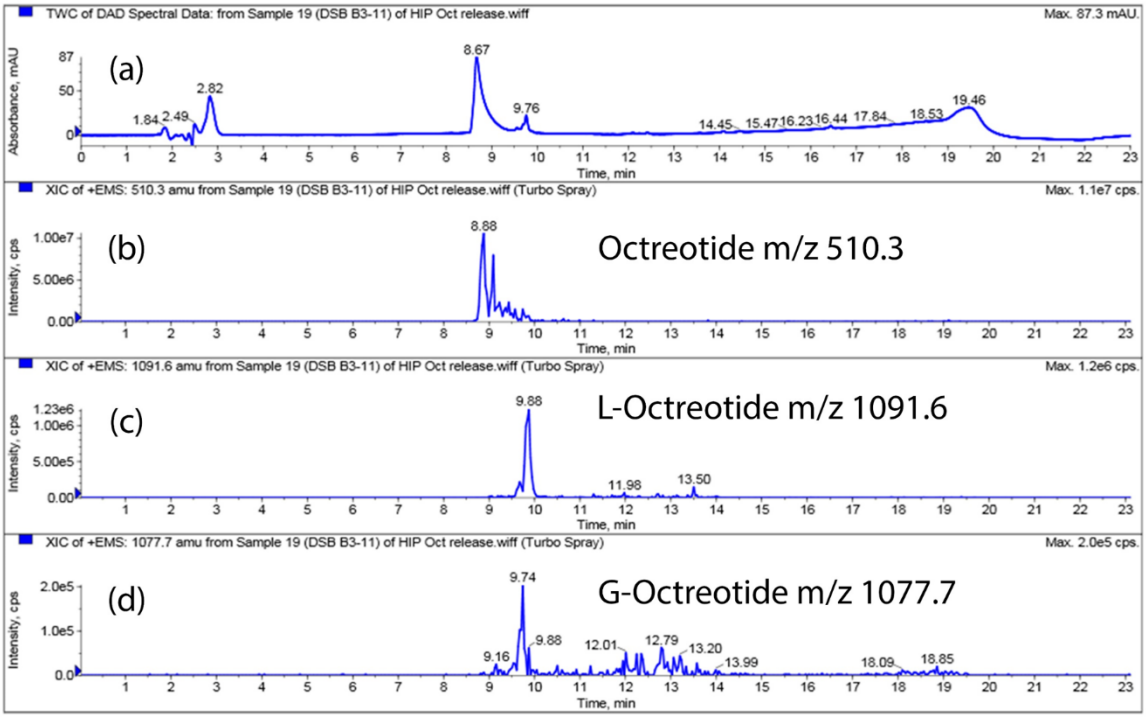

Figure 4-9 UFLC-MS spectrum of release sample (Day 16) from DSBMPs-in-gel. (a) UV chromatogram. Extracted ion chromatogram (EIC) for (b) octreotide, m/z 510.3 (c) Lactoyl-octreotide, m/z 1091.6 and (d) Glycoyl-octreotide, m/z 1077.7.

Table 4-3 Summary of octreotide adducts identified using UFLC-MS analysis in release samples.

MPs	**Acylated species**	**M+H/Z**	**Retention time (min)**
DSAMPs	L-Octreotide	1091.6	9.8
	G-Octreotide	1077.7	9.7
	LL-Octreotide	1163.2	ND
	GG-Octreotide	1135.5	ND
	C-Octreotide	1133.5	ND
DSBMPs	L-Octreotide	1091.6	9.8
	G-Octreotide	1077.7	9.7
	LL-Octreotide	1163.2	ND
	GG-Octreotide	1135.5	ND
	C-Octreotide	1133.5	ND
C- Caprolactoyl, L- Lactoyl, G- Glycoyl, ND- Not detected.			

CHAPTER 5

5. SUMMARY AND RECOMMENDATIONS

5.1. Summary

In order to sustain release of octreotide and minimize its acylation during release from biodegradable systems, we tested two different strategies (a) polymer modification (b) HIP complexation.

In the first strategy, we focused on effect of various polymer compositions on octreotide acylation and duration of release. Effect of polycaprolactone (PCL), polylactic acid (PLA) and polyglycolic acid (PGA) were evaluated. Effect of PLA and PGA on peptide acylation is well established. However, no information is available on effect of PCL on peptide acylation. Octreotide encapsulated MPs with excellent entrapment efficiency were successfully prepared and characterized. MPs-in-gel composite formulation was selected to sustain release of octreotide over period of months. A large fraction of released peptide was acylated during release from lactide-based PBA and glycolide-based PBB polymers. In addition, release of octreotide was incomplete from PBB polymers even after 10 months of release. PB polymers having PLA and PGA segments are less suitable polymer for peptide delivery due to instability of peptide, despite having significantly better entrapment efficiency and duration of release. TB polymer resulted in minimal chemical derivatization of peptide and sustained release of octreotide over a period of three months suggesting TB polymers could be best suited for sustained peptide delivery.

In the second strategy, we tested potential of reversible hydrophobic ion-paring complexation in minimizing acylation of octreotide from polylactide-co-glycolide polymers. Process of HIP complex preparation and characterization has been well established in our

laboratory previously. HIP complex formation with octreotide was very simple and straightforward involving simple mixing of solutions. Complexation efficiency of nearly 100% was achieved with all ion-pairing agents. HIP complex with dextran sulfate was reversible unlike SDS at simulated physiological condition. HIP complex also resulted in excellent encapsulation and loading efficiency in MPs due to increased hydrophobicity. MPs-in-gel composite formulation resulted in sustained release of peptide. More than 95% of released peptide maintained native chemical structure and less than 7% octreotide was acylated with DSA-oct HIP complex. Reversible HIP complex is a viable strategy to maintain chemical stability of peptide during long-term delivery from lactide and glycolide based polymers.

5.2. Recommendations

In present study, we have shown that the PCL based polymers and HIP complex may be suitable means to enhance the stability of peptide during sustained release. However, an individual strategy have certain limitations despite being successful in minimizing peptide acylation during sustained delivery.

PCL based polymers resulted in enhanced stability of peptide during release. However, PCL based TB polymers did not results in high encapsulation efficiency. In addition, PCL polymers exhibits slow degradation, which may result in accumulation of polymer in body. PBA and PBB resulted in significantly high entrapment efficiency and degrade fasters than TB polymers, but the stability of peptide was poor during release. HIP complex resulted in excellent octreotide loading in PLGA polymers. Entrapment efficiency and stability of peptide with HIP complex was very high. However, release profile was biphasic where release rate was very high for first 20 day followed by very slow release rates.

Limitations of these individual approaches may be overcome by combining these approaches. For example, combination of HIP complexation with PBA or PBB polymer MPs. HIP complex can minimize peptide acylation by itself from lactide and glycolide based polymers. PBA and PBB polymers have faster rate of degradation due to low crystallinity and may sustain release of HIP complexed octreotide for longer duration.

APPENDIX

JOHN WILEY AND SONS LICENSE TERMS AND CONDITIONS

Mar 12, 2015

This Agreement between University of Missouri-Kansas City ("You") and John Wiley and Sons ("John Wiley and Sons") consists of your license details and the terms and conditions provided by John Wiley and Sons and Copyright Clearance Center.

License Number	3586550020257
License date	Mar 12, 2015
Licensed Content Publisher	John Wiley and Sons
Licensed Content Publication	Wiley oBooks
Licensed Content Title	Ocular Delivery Using Prodrugs
Licensed Content Author	Deep Kwatra,Ravi Vaishya,Ripal Gaudana,Jwala Jwala,Ashim K. Mitra
Licensed Content Date	Apr 4, 2011
Pages	25
Type of use	Dissertation/Thesis
Requestor type	Author of this Wiley chapter
Format	Print and electronic
Portion	Full chapter
Will you be translating?	No
Title of your thesis / dissertation	EFFECT OF NANOMICELLE SIZE ON TRANS-SCLERAL PERMEABILITY OF DEXAMETHASONE.
Expected completion date	Apr 2015
Expected size (number of pages)	200
Requestor Location	University of Missouri-Kansas City 2464 Charlotte Street KANSAS CITY, MO 64108 United States Attn: Ravi Vaishya
Billing Type	Invoice
Billing Address	University of Missouri-Kansas City 2464 Charlotte Street Kansas City, MO 64108 United States Attn: Ravi Vaishya
Total	0.00 USD
Terms and Conditions	

JOHN WILEY AND SONS LICENSE TERMS AND CONDITIONS

Mar 12, 2015

This Agreement between University of Missouri-Kansas City ("You") and John Wiley and Sons ("John Wiley and Sons") consists of your license details and the terms and conditions provided by John Wiley and Sons and Copyright Clearance Center.

License Number	3586570973368
License date	Mar 12, 2015
Licensed Content Publisher	John Wiley and Sons
Licensed Content Publication	Wiley Interdisciplinary Reviews - Nanomedicine and Nanobiotechnology
Licensed Content Title	Controlled ocular drug delivery with nanomicelles
Licensed Content Author	Ravi D. Vaishya,Varun Khurana,Sulabh Patel,Ashim K. Mitra
Licensed Content Date	Jun 2, 2014
Pages	16
Type of use	Dissertation/Thesis
Requestor type	Author of this Wiley article
Format	Print and electronic
Portion	Full article
Will you be translating?	No
Title of your thesis / dissertation	EFFECT OF NANOMICELLE SIZE ON TRANS-SCLERAL PERMEABILITY OF DEXAMETHASONE.
Expected completion date	Apr 2015
Expected size (number of pages)	200
Requestor Location	University of Missouri-Kansas City 2464 Charlotte Street KANSAS CITY, MO 64108 United States Attn: Ravi Vaishya
Billing Type	Invoice
Billing Address	University of Missouri-Kansas City 2464 Charlotte Street Kansas City, MO 64108 United States Attn: Ravi Vaishya
Total	0.00 USD

SPRINGER LICENSE
TERMS AND CONDITIONS

Mar 12, 2015

This is a License Agreement between University of Missouri-Kansas City ("You") and Springer ("Springer") provided by Copyright Clearance Center ("CCC"). The license consists of your order details, the terms and conditions provided by Springer, and the payment terms and conditions.

All payments must be made in full to CCC. For payment instructions, please see information listed at the bottom of this form.

License Number	3586571495355
License date	Mar 12, 2015
Licensed content publisher	Springer
Licensed content publication	AAPS PharmSciTech
Licensed content title	Novel Dexamethasone-Loaded Nanomicelles for the Intermediate and Posterior Segment Uveitis
Licensed content author	Ravi D. Vaishya
Licensed content date	Jan 1, 2014
Volume number	15
Issue number	5
Type of Use	Thesis/Dissertation
Portion	Full text
Number of copies	5
Author of this Springer article	Yes and you are a contributor of the new work
Order reference number	None
Title of your thesis / dissertation	EFFECT OF NANOMICELLE SIZE ON TRANS-SCLERAL PERMEABILITY OF DEXAMETHASONE.
Expected completion date	Apr 2015
Estimated size(pages)	200
Total	0.00 USD
Terms and Conditions	

Introduction
The publisher for this copyrighted material is Springer Science + Business Media. By clicking "accept" in connection with completing this licensing transaction, you agree that the following terms and conditions apply to this transaction (along with the Billing and Payment terms and conditions established by Copyright Clearance Center, Inc. ("CCC"), at the time that you opened your Rightslink account and that are available at any time at http://myaccount.copyright.com).

Limited License

INFORMA HEALTHCARE LICENSE TERMS AND CONDITIONS

Mar 20, 2015

This is a License Agreement between University of Missouri-Kansas City ("You") and Informa Healthcare ("Informa Healthcare") provided by Copyright Clearance Center ("CCC"). The license consists of your order details, the terms and conditions provided by Informa Healthcare, and the payment terms and conditions.

All payments must be made in full to CCC. For payment instructions, please see information listed at the bottom of this form.

License Number	3593150489079
License date	Mar 20, 2015
Licensed content publisher	Informa Healthcare
Licensed content publication	Expert Opinion on Drug Delivery
Licensed content title	Long-term delivery of protein therapeutics
Licensed content author	Ravi Vaishya, Varun Khurana, Sulabh Patel, et al
Licensed content date	Mar 1, 2015
Volume number	12
Issue number	3
Start Page	415
End Page	440
Type of Use	Dissertation/Thesis
Requestor type	Author
Format	print and electronic
Portion	Full article
Will you be translating?	no
Number of copies	50
Order reference number	None
Title of your thesis / dissertation	EFFECT OF NANOMICELLE SIZE ON TRANS-SCLERAL PERMEABILITY OF DEXAMETHASONE.
Expected completion date	Apr 2015
Estimated Size (pages)	200
Total	0.00 USD
Terms and Conditions	

Informa Healthcare: Terms and Conditions for reuse of Figures, Tables,

REFERENCES

1. Kwatra, D.; Vaishya, R.; Gaudana, R.; Jwala, J.; Mitra, A. K., Ocular Delivery Using Prodrugs. In *Prodrugs and Targeted Delivery*, Wiley-VCH Verlag GmbH and Co. KGaA: 2010; pp 181-205.
2. Dingeldein, S. A.; Klyce, S. D., Imaging of the cornea. *Cornea* **1988,** *7* (3), 170-82.
3. Lacouture, A., [Anatomy-physiology of the eye]. *Rev Infirm* **2006,** (120), 16-7.
4. Edelhauser, H.; Ubels, J., Cornea and sclera. In *Physiology of the eye*, Kaufman, P.; Aam, A., Eds. Moses, RA, Mosby, CV: St. Louis, 2003; pp 47-116.

5. Ambati, J.; Canakis, C. S.; Miller, J. W.; Gragoudas, E. S.; Edwards, A.; Weissgold, D. J.; Kim, I.; Delori, F. C.; Adamis, A. P., Diffusion of high molecular weight compounds through sclera. *Investigative ophthalmology and visual science* **2000,** *41* (5), 1181-5.
6. (a) Sharma, R.; Ehinger, B., Development and structure of retina. In *Physiology of the eye*, Kaufman, P.; Aam, A., Eds. Moses, RA Mosby, CV: St. Louis, 2003; pp 47-116; (b) Cour, M., The retinal pigmented epithelium. In *Physiology of the eye*, Kaufman, P.; Aam, A., Eds. Moses, RA Mosby, CV: St. Louis, 2003; pp 47-116.

7. Andersen, H.; Sander, B., The vitreous. In *Physiology of the eye*, Kaufman, P.; Aam, A., Eds. Moses, RA Mosby, CV: St. Louis, 2003; pp 47-116.

8. Ananthula, H.; Vaishya, R.; Barot, M.; Mitra, A., Bioavailability in ocular pharmacology. In *Duane's Foundations of Clinical Ophthalmology*, W, T.; EA, J., Eds. Lippincott Williams and Wilkins: 2009; Vol. 3.
9. L, S.; Yu, A. B., *Applied Biopharmaceutics and Pharmacokinetics* 4th ed.; McGraw-Hill/Appleton and Lange: 1999.
10. Tiffany, J. M., Tears in health and disease. *Eye 17* (8), 923-926.
11. Ashton, P.; Podder, S. K.; Lee, V. H., Formulation influence on conjunctival penetration of four beta blockers in the pigmented rabbit: a comparison with corneal penetration. *Pharm Res* **1991,** *8* (9), 1166-74.
12. Dursun, D.; Monroy, D.; Knighton, R.; Tervo, T.; Vesaluoma, M.; Carraway, K.; Feuer, W.; Pflugfelder, S. C., The effects of experimental tear film removal on corneal surface regularity and barrier function. *Ophthalmology* **2000,** *107* (9), 1754-60.
13. Lens, A.; Langley, T.; Nemeth, S. C.; Shea, C., *Ocular Anatomy and Physiology* John H. Bond: 1999.
14. Ronald D. Schoenwald, R. L. W., Relationship between steroid permeability across excised rabbit cornea and octanol-water partition coefficients. *Journal of Pharmaceutical Sciences* **1978,** *67* (6), 786-788.
15. Prausnitz, M. R.; Noonan, J. S., Permeability of cornea, sclera, and conjunctiva: a literature analysis for drug delivery to the eye. *J Pharm Sci* **1998,** *87* (12), 1479-88.
16. George M. Grass, J. R. R., Mechanisms of corneal drug penetration II: Ultrastructural analysis of potential pathways for drug movement. *Journal of Pharmaceutical Sciences* **1988,** *77* (1), 15-23.
17. Marshall, W. S.; Klyce, S. D., Cellular and paracellular pathway resistances in the "tight" Cl- -secreting epithelium of rabbit cornea. *J Membr Biol* **1983,** *73* (3), 275-82.
18. Kaur, I. P.; Smitha, R., Penetration enhancers and ocular bioadhesives: two new avenues for ophthalmic drug delivery. *Drug Dev Ind Pharm* **2002,** *28* (4), 353-69.

19. Kaur, I. P.; Kanwar, M., Ocular Preparations: The Formulation Approach. *Drug Development and Industrial Pharmacy* **2002,** *28* (5), 473 - 493.
20. (a) Barsotti, M. F.; Bartels, S. P.; Freddo, T. F.; Kamm, R. D., The source of protein in the aqueous humor of the normal monkey eye. *Investigative ophthalmology and visual science* **1992,** *33* (3), 581-95; (b) Schlingemann, R. O.; Hofman, P.; Klooster, J.; Blaauwgeers, H. G.; Van der Gaag, R.; Vrensen, G. F., Ciliary muscle capillaries have blood-tissue barrier characteristics. *Exp Eye Res* **1998,** *66* (6), 747-54.
21. Anand, B.; Nashed, Y.; Mitra, A., Novel dipeptide prodrugs of acyclovir for ocular herpes infections: Bioreversion, antiviral activity and transport across rabbit cornea. *Curr Eye Res* **2003,** *26* (3-4), 151-63.
22. Hornof, M.; Toropainen, E.; Urtti, A., Cell culture models of the ocular barriers. *Eur J Pharm Biopharm* **2005,** *60* (2), 207-25.
23. Cunha-Vaz, J. G., The blood-retinal barriers system. Basic concepts and clinical evaluation. *Exp Eye Res* **2004,** *78* (3), 715-21.
24. Gardner, T. W.; Antonetti, D. A.; Barber, A. J.; Lieth, E.; Tarbell, J. A., The molecular structure and function of the inner blood-retinal barrier. Penn State Retina Research Group. *Doc Ophthalmol* **1999,** *97* (3-4), 229-37.
25. Stewart, P. A.; Tuor, U. I., Blood-eye barriers in the rat: correlation of ultrastructure with function. *J Comp Neurol* **1994,** *340* (4), 566-76.
26. Cunha-Vaz, J. G., The blood-ocular barriers: past, present, and future. *Doc Ophthalmol* **1997,** *93* (1-2), 149-57.
27. Janoria, K. G.; Gunda, S.; Boddu, S. H.; Mitra, A. K., Novel approaches to retinal drug delivery. *Expert opinion on drug delivery* **2007,** *4* (4), 371-88.
28. Reddy, I. K., *Ocular Therapeutics and Drug Delivery: A Multi-disciplinary Aapproach*. CRC Press: 1995.
29. Ghate, D.; Edelhauser, H. F., Ocular drug delivery. *Expert opinion on drug delivery* **2006,** *3* (2), 275-87.
30. Edman, P., *Biopharmaceutics of Ocular Drug Delivery*. Informa Health Care: 1993.
31. Barar, J.; Javadzadeh, A. R.; Omidi, Y., Ocular novel drug delivery: impacts of membranes and barriers. *Expert opinion on drug delivery* **2008,** *5* (5), 567-81.
32. Hamalainen, K. M.; Kananen, K.; Auriola, S.; Kontturi, K.; Urtti, A., Characterization of paracellular and aqueous penetration routes in cornea, conjunctiva, and sclera. *Investigative ophthalmology and visual science* **1997,** *38* (3), 627-34.
33. Raghava, S.; Hammond, M.; Kompella, U. B., Periocular routes for retinal drug delivery. *Expert opinion on drug delivery* **2004,** *1* (1), 99-114.
34. (a) Van Santvliet, L.; Ludwig, A., Determinants of eye drop size. *Survey of Ophthalmology* **2004,** *49* (2), 197-213; (b) Urtti, A.; Salminen, L., Minimizing systemic absorption of topically administered ophthalmic drugs. *Survey of Ophthalmology* **1993,** *37* (6), 435-456; (c) Shell, J. W., Pharmacokinetics of topically applied ophthalmic drugs. *Survey of Ophthalmology* **1982,** *26* (4), 207-218.
35. (a) Letocha, C. E., Methods for self-administration of eyedrops. *Ann Ophthalmol* **1985,** *17* (12), 768-9; (b) Mishima, S.; Gasset, A.; Klyce, S. D., Jr.; Baum, J. L., Determination of tear volume and tear flow. *Invest Ophthalmol* **1966,** *5* (3), 264-76.
36. Fraunfelder, F. T.; Meyer, S. M., Systemic side effects from ophthalmic timolol and their prevention. *J Ocul Pharmacol* **1987,** *3* (2), 177-84.
37. Gray, R. H., The influence of drop size on pupil dilatation. *Eye* **1991,** *5 (Pt 5)*, 615-9.

38. Duvall, B.; Kershner, R. M., Ophthalmic Medications and Pharmacology. 2nd ed.; Slack Incorporated: 2006.
39. Pinilla, I.; Larrosa, J. M.; Polo, V.; Honrubia, F. M., Subconjunctival injection of low doses of mitomycin C: effects on fibroblast proliferation. *Ophthalmologica* **1998,** *212* (5), 306-9.
40. Ripart, J.; Lefrant, J. Y.; de La Coussaye, J. E.; Prat-Pradal, D.; Vivien, B.; Eledjam, J. J., Peribulbar versus retrobulbar anesthesia for ophthalmic surgery: an anatomical comparison of extraconal and intraconal injections. *Anesthesiology* **2001,** *94* (1), 56-62.
41. Canavan, K. S.; Dark, A.; Garrioch, M. A., Sub-Tenon's administration of local anaesthetic: a review of the technique. *Br J Anaesth* **2003,** *90* (6), 787-93.
42. TRIVEDI, H.; TODKAR, H.; ARBHAVE, V.; BHATIA, P., OCULAR ANAESTHESIA FOR CATARACT SURGERY. *Lancet* **2003,** *3*, 1312-1313,1319.
43. Ebner, R.; Devoto, M. H.; Weil, D.; Bordaberry, M.; Mir, C.; Martinez, H.; Bonelli, L.; Niepomniszcze, H., Treatment of thyroid associated ophthalmopathy with periocular injections of triamcinolone. *Br J Ophthalmol* **2004,** *88* (11), 1380-6.
44. van den Berg, A. A., An audit of peribulbar blockade using 15 mm, 25 mm and 37.5 mm needles, and sub-Tenon's injection. *Anaesthesia* **2004,** *59* (8), 775-80.
45. Vaishya, R. D.; Khurana, V.; Patel, S.; Mitra, A. K., Controlled ocular drug delivery with nanomicelles. *Wiley interdisciplinary reviews. Nanomedicine and nanobiotechnology* **2014,** *6* (5), 422-37.
46. Vaishya, R.; Gokulgandhi, M.; Patel, S.; Minocha, M.; Mitra, A. K., Novel Dexamethasone-loaded nanomicelles for the intermediate and posterior segment uveitis. *AAPS PharmSciTech* **2014**
47. Ribeiro, A.; Sosnik, A.; Chiappetta, D. A.; Veiga, F.; Concheiro, A.; Alvarez-Lorenzo, C., Single and mixed poloxamine micelles as nanocarriers for solubilization and sustained release of ethoxzolamide for topical glaucoma therapy. *Journal of The Royal Society Interface* **2012,** *9* (74), 2059-2069.
48. Pepić, I.; Hafner, A.; Lovrić, J.; Pirkić, B.; Filipović-Grčić, J., A nonionic surfactant/chitosan micelle system in an innovative eye drop formulation. *Journal of Pharmaceutical Sciences* **2010,** *99* (10), 4317-4325.
49. Lin, H.-R.; Chang, P.-C., Novel pluronic-chitosan micelle as an ocular delivery system. *Journal of Biomedical Materials Research Part B: Applied Biomaterials* **2013,** *101B* (5), 689-699.
50. (a) Ho, S.; Clipstone, N.; Timmermann, L.; Northrop, J.; Graef, I.; Fiorentino, D.; Nourse, J.; Crabtree, G. R., The mechanism of action of cyclosporin A and FK506. *Clinical immunology and immunopathology* **1996,** *80* (3 Pt 2), S40-5; (b) Di Tommaso, C.; Como, C.; Gurny, R.; Möller, M., Investigations on the lyophilisation of MPEG–hexPLA micelle based pharmaceutical formulations. *European Journal of Pharmaceutical Sciences* **2010,** *40* (1), 38-47.
51. Pepić, I.; Jalšenjak, N.; Jalšenjak, I., Micellar solutions of triblock copolymer surfactants with pilocarpine. *International journal of pharmaceutics* **2004,** *272* (1–2), 57-64.
52. Ribeiro, A.; Sandez-Macho, I.; Casas, M.; Alvarez-Perez, S.; Alvarez-Lorenzo, C.; Concheiro, A., Poloxamine micellar solubilization of alpha-tocopherol for topical ocular treatment. *Colloids and surfaces. B, Biointerfaces* **2013,** *103*, 550-7.
53. (a) Di Tommaso, C.; Como, C.; Gurny, R.; Moller, M., Investigations on the lyophilisation of MPEG-hexPLA micelle based pharmaceutical formulations. *European journal of pharmaceutical sciences : official journal of the European Federation for Pharmaceutical Sciences* **2010,** *40* (1), 38-47; (b) Di Tommaso, C.; Torriglia, A.; Furrer, P.; Behar-Cohen, F.;

Gurny, R.; Moller, M., Ocular biocompatibility of novel Cyclosporin A formulations based on methoxy poly(ethylene glycol)-hexylsubstituted poly(lactide) micelle carriers. *International journal of pharmaceutics* **2011,** *416* (2), 515-24; (c) Di Tommaso, C.; Bourges, J. L.; Valamanesh, F.; Trubitsyn, G.; Torriglia, A.; Jeanny, J. C.; Behar-Cohen, F.; Gurny, R.; Moller, M., Novel micelle carriers for cyclosporin A topical ocular delivery: in vivo cornea penetration, ocular distribution and efficacy studies. *Eur J Pharm Biopharm* **2012,** *81* (2), 257-64; (d) Di Tommaso, C.; Valamanesh, F.; Miller, F.; Furrer, P.; Rodriguez-Aller, M.; Behar-Cohen, F.; Gurny, R.; Moller, M., A novel cyclosporin a aqueous formulation for dry eye treatment: in vitro and in vivo evaluation. *Invest Ophthalmol Vis Sci* **2012,** *53* (4), 2292-9.
54. Tu, J.; Pang, H.; Yan, Z.; Li, P., Ocular permeability of pirenzepine hydrochloride enhanced by methoxy poly(ethylene glycol)-poly(D, L-lactide) block copolymer. *Drug development and industrial pharmacy* **2007,** *33* (10), 1142-50.
55. Lin, H. R.; Chang, P. C., Novel pluronic-chitosan micelle as an ocular delivery system. *Journal of biomedical materials research. Part B, Applied biomaterials* **2013,** *101* (5), 689-99.
56. Rafie, F.; Javadzadeh, Y.; Javadzadeh, A. R.; Ghavidel, L. A.; Jafari, B.; Moogooee, M.; Davaran, S., In vivo evaluation of novel nanoparticles containing dexamethasone for ocular drug delivery on rabbit eye. *Curr Eye Res* **2010,** *35* (12), 1081-9.
57. Gupta, A. K.; Madan, S.; Majumdar, D. K.; Maitra, A., Ketorolac entrapped in polymeric micelles: preparation, characterisation and ocular anti-inflammatory studies. *International journal of pharmaceutics* **2000,** *209* (1-2), 1-14.
58. Qu, X.; Khutoryanskiy, V. V.; Stewart, A.; Rahman, S.; Papahadjopoulos-Sternberg, B.; Dufes, C.; McCarthy, D.; Wilson, C. G.; Lyons, R.; Carter, K. C.; Schatzlein, A.; Uchegbu, I. F., Carbohydrate-based micelle clusters which enhance hydrophobic drug bioavailability by up to 1 order of magnitude. *Biomacromolecules* **2006,** *7* (12), 3452-9.
59. Kim, H.; Choi, J. S.; Kim, K. S.; Yang, J. A.; Joo, C. K.; Hahn, S. K., Flt1 peptide-hyaluronate conjugate micelle-like nanoparticles encapsulating genistein for the treatment of ocular neovascularization. *Acta biomaterialia* **2012,** *8* (11), 3932-40.
60. Liaw, J.; Chang, S. F.; Hsiao, F. C., In vivo gene delivery into ocular tissues by eye drops of poly(ethylene oxide)-poly(propylene oxide)-poly(ethylene oxide) (PEO-PPO-PEO) polymeric micelles. *Gene therapy* **2001,** *8* (13), 999-1004.
61. Kuwano, M.; Ibuki, H.; Morikawa, N.; Ota, A.; Kawashima, Y., Cyclosporine A formulation affects its ocular distribution in rabbits. *Pharm Res* **2002,** *19* (1), 108-11.
62. Luschmann, C.; Herrmann, W.; Strauss, O.; Luschmann, K.; Goepferich, A., Ocular delivery systems for poorly soluble drugs: an in-vivo evaluation. *International journal of pharmaceutics* **2013,** *455* (1-2), 331-7.
63. Civiale, C.; Licciardi, M.; Cavallaro, G.; Giammona, G.; Mazzone, M. G., Polyhydroxyethylaspartamide-based micelles for ocular drug delivery. *International journal of pharmaceutics* **2009,** *378* (1-2), 177-86.
64. Luschmann, C.; Tessmar, J.; Schoeberl, S.; Strau, O.; Luschmann, K.; Goepferich, A., Self-assembling colloidal system for the ocular administration of cyclosporine a. *Cornea* **2014,** *33* (1), 77-81.
65. Pepic, I.; Lovric, J.; Filipovic-Grcic, J., Polymeric Micelles in Ocular Drug Delivery: Rationale, Strategies and Challenges. *Chemical and Biochemical Engineering Quarterly* **2012,** *26* (4), 365.
66. Aliabadi, H. M.; Lavasanifar, A., Polymeric micelles for drug delivery. *Expert opinion on drug delivery* **2006,** *3* (1), 139-62.

67. Chi, S. C.; Yeom, D. I.; Kim, S. C.; Park, E. S., A polymeric micellar carrier for the solubilization of biphenyl dimethyl dicarboxylate. *Archives of pharmacal research* **2003,** *26* (2), 173-81.
68. Gong, C.; Wei, X.; Wang, X.; Wang, Y.; Guo, G.; Mao, Y.; Luo, F.; Qian, Z., Biodegradable self-assembled PEG-PCL-PEG micelles for hydrophobic honokiol delivery: I. Preparation and characterization. *Nanotechnology* **2010,** *21* (21), 215103.
69. Kim, S.; Park, K., 19 Polymer Micelles for Drug Delivery.
70. Chien, Y., *Novel Drug Delivery Systems*. Marcel Dekker Inc.: 1982.
71. Amrite, A. C.; Kompella, U. B., Size-dependent disposition of nanoparticles and microparticles following subconjunctival administration. *J Pharm Pharmacol* **2005,** *57* (12), 1555-63.
72. Pepic, I.; Jalsenjak, N.; Jalsenjak, I., Micellar solutions of triblock copolymer surfactants with pilocarpine. *International journal of pharmaceutics* **2004,** *272* (1-2), 57-64.
73. Vadlapudi, A. D.; Cholkar, K.; Vadlapatla, R. K.; Mitra, A. K., Aqueous Nanomicellar Formulation for Topical Delivery of Biotinylated Lipid Prodrug of Acyclovir: Formulation Development and Ocular Biocompatibility. *Journal of ocular pharmacology and therapeutics : the official journal of the Association for Ocular Pharmacology and Therapeutics* **2013**.
74. Mitra, A. K.; Velagaleti, P. R.; Natesan, S., Ophthalmic Compositions Comprising Calcineurin Inhibitors or mTOR Inhibitors. Google Patents: 2011.
75. Velagaleti PR, A. E., Khan IJ, Gilger BC, and Mitra AK, Topical delivery of hydrophobic drugs using a novel mixed nanomicellar technology to treat diseases of the anterior and posterior segments of the eye. *Drug Delivery Today* **2010,** *10* (4), 42-47.
76. (a) Gaudana, R.; Ananthula, H. K.; Parenky, A.; Mitra, A. K., Ocular drug delivery. *AAPS J* **2010,** *12* (3), 348-60; (b) HariKrishna Ananthula; Ravi Vaishya; Megha Barot; Mitra, A., Bioavailability. Tasman W; EA, J., Eds. Philadelphia: Lippincott Williams and Wilkins: 2009.
77. (a) Tang, D. L.; Song, F.; Chen, C.; Wang, X. L.; Wang, Y. Z., A pH-responsive chitosan-b-poly(p-dioxanone) nanocarrier: formation and efficient antitumor drug delivery. *Nanotechnology* **2013,** *24* (14), 145101; (b) Gu, Q.; Xing, J. Z.; Huang, M.; He, C.; Chen, J., SN-38 loaded polymeric micelles to enhance cancer therapy. *Nanotechnology* **2012,** *23* (20), 205101; (c) Zhang, Z.; Mei, L.; Feng, S. S., Paclitaxel drug delivery systems. *Expert opinion on drug delivery* **2013,** *10* (3), 325-40; (d) Sun, M.; Su, X.; Ding, B.; He, X.; Liu, X.; Yu, A.; Lou, H.; Zhai, G., Advances in nanotechnology-based delivery systems for curcumin. *Nanomedicine* **2012,** *7* (7), 1085-100.
78. Inokuchi, Y.; Hironaka, K.; Fujisawa, T.; Tozuka, Y.; Tsuruma, K.; Shimazawa, M.; Takeuchi, H.; Hara, H., Physicochemical properties affecting retinal drug/coumarin-6 delivery from nanocarrier systems via eyedrop administration. *Investigative ophthalmology and visual science* **2010,** *51* (6), 3162-70.
79. Nussenblatt, R. B., The natural history of uveitis. *Int Ophthalmol* **1990,** *14* (5-6), 303-8.
80. (a) Gaudana, R.; Jwala, J.; Boddu, S. H.; Mitra, A. K., Recent perspectives in ocular drug delivery. *Pharm Res* **2009,** *26* (5), 1197-216; (b) Taylor, S. R.; Isa, H.; Joshi, L.; Lightman, S., New developments in corticosteroid therapy for uveitis. *Ophthalmologica* **2010,** *224 Suppl 1*, 46-53; (c) Lowder, C.; Belfort, R., Jr.; Lightman, S.; Foster, C. S.; Robinson, M. R.; Schiffman, R. M.; Li, X. Y.; Cui, H.; Whitcup, S. M., Dexamethasone intravitreal implant for noninfectious intermediate or posterior uveitis. *Arch Ophthalmol* **2011,** *129* (5), 545-53.

81. Robert H Janigian Jr; Jr, R. H. J. Uveitis Evaluation and Treatment http://emedicine.medscape.com/article/1209123-overview (accessed 06/25/2013).
82. (a) Saraiya, N. V.; Goldstein, D. A., Dexamethasone for ocular inflammation. *Expert Opin Pharmacother* **2011,** *12* (7), 1127-31; (b) Couch, S. M.; Bakri, S. J., Intravitreal triamcinolone for intraocular inflammation and associated macular edema. *Clin Ophthalmol* **2009,** *3*, 41-7.
83. Kim, S. H.; Lutz, R. J.; Wang, N. S.; Robinson, M. R., Transport barriers in transscleral drug delivery for retinal diseases. *Ophthalmic Res* **2007,** *39* (5), 244-54.
84. Vaishya, R. D.; Gokulgandhi, M.; Patel, S.; Minocha, M.; Mitra, A. K., Novel dexamethasone-loaded nanomicelles for the intermediate and posterior segment uveitis. *AAPS PharmSciTech* **2014,** *15* (5), 1238-51.
85. (a) Park, S. H.; Choi, B. G.; Joo, M. K.; Han, D. K.; Sohn, Y. S.; Jeong, B., Temperature-Sensitive Poly(caprolactone-co-trimethylene carbonate)−Poly(ethylene glycol)−Poly(caprolactone-co-trimethylene carbonate) as in Situ Gel-Forming Biomaterial. *Macromolecules* **2008,** *41* (17), 6486-6492; (b) Gou, M.; Men, K.; Shi, H.; Xiang, M.; Zhang, J.; Song, J.; Long, J.; Wan, Y.; Luo, F.; Zhao, X.; Qian, Z., Curcumin-loaded biodegradable polymeric micelles for colon cancer therapy in vitro and in vivo. *Nanoscale* **2011,** *3* (4), 1558-67.
86. (a) Kalyanasundaram, K.; Thomas, J. K., Environmental effects on vibronic band intensities in pyrene monomer fluorescence and their application in studies of micellar systems. *Journal of the American Chemical Society* **1977,** *99* (7), 2039-2044; (b) Basu Ray, G.; Chakraborty, I.; Moulik, S. P., Pyrene absorption can be a convenient method for probing critical micellar concentration (cmc) and indexing micellar polarity. *Journal of Colloid and Interface Science* **2006,** *294* (1), 248-254.
87. Gagarinova, V. M.; Alferov, V. P.; Kuznetsov, V. P.; Ostrovskaia, S. A.; Lapis, G. A.; Piskareva, N. A., [Human leukocytic interferon as an agent for emergency prevention of influenza and other acute respiratory diseases in children's preschool institutions]. *Pediatriia* **1990,** (11), 74-8.
88. Gaudana, R.; Parenky, A.; Vaishya, R.; Samanta, S. K.; Mitra, A. K., Development and characterization of nanoparticulate formulation of a water soluble prodrug of dexamethasone by HIP complexation. *Journal of microencapsulation* **2011,** *28* (1), 10-20.
89. (a) Boddu, S. H.; Jwala, J.; Vaishya, R.; Earla, R.; Karla, P. K.; Pal, D.; Mitra, A. K., Novel nanoparticulate gel formulations of steroids for the treatment of macular edema. *Journal of ocular pharmacology and therapeutics : the official journal of the Association for Ocular Pharmacology and Therapeutics* **2010,** *26* (1), 37-48; (b) Choi, S. H.; Park, T. G., Hydrophobic ion pair formation between leuprolide and sodium oleate for sustained release from biodegradable polymeric microspheres. *International journal of pharmaceutics* **2000,** *203* (1-2), 193-202; (c) Duvvuri, S.; Gaurav Janoria, K.; Mitra, A. K., Effect of polymer blending on the release of ganciclovir from PLGA microspheres. *Pharm Res* **2006,** *23* (1), 215-23.
90. ChemAxon http://www.chemicalize.org/structure/#!mol=honokiolandsource=calculate (accessed 7/8/13).
91. Palmer, D.; Levina, M.; Douroumis, D.; Maniruzzaman, M.; Morgan, D. J.; Farrell, T. P.; Rajabi-Siahboomi, A. R.; Nokhodchi, A., Mechanism of synergistic interactions and its influence on drug release from extended release matrices manufactured using binary mixtures of polyethylene oxide and sodium carboxymethylcellulose. *Colloids and surfaces. B, Biointerfaces* **2013,** *104*, 174-80.

92. Earla, R.; Boddu, S. H.; Cholkar, K.; Hariharan, S.; Jwala, J.; Mitra, A. K., Development and validation of a fast and sensitive bioanalytical method for the quantitative determination of glucocorticoids--quantitative measurement of dexamethasone in rabbit ocular matrices by liquid chromatography tandem mass spectrometry. *Journal of pharmaceutical and biomedical analysis* **2010,** *52* (4), 525-33.
93. Vaishya, R.; Khurana, V.; Patel, S.; Mitra, A. K., Long-term delivery of protein therapeutics. *Expert opinion on drug delivery* **2014**, 1-26.
94. (a) America, P. R. a. M. o. *Biologic Medicines in Development*; February 7, 2013, 2013; (b) Davison, D. B., The Number of Human Genes and Proteins. Nano Science and Technology Institute: 2002; pp. 6-11. http://www.nsti.org/procs/ICCN2002/1/T11.02.
95. (a) Valkov, E.; Sharpe, T.; Marsh, M.; Greive, S.; Hyvonen, M., Targeting protein-protein interactions and fragment-based drug discovery. *Topics in current chemistry* **2012,** *317*, 145-79; (b) Thiel, P.; Kaiser, M.; Ottmann, C., Small-molecule stabilization of protein-protein interactions: an underestimated concept in drug discovery? *Angewandte Chemie* **2012,** *51* (9), 2012-8.
96. Voet, A.; Zhang, K. Y., Pharmacophore modelling as a virtual screening tool for the discovery of small molecule protein-protein interaction inhibitors. *Current pharmaceutical design* **2012,** *18* (30), 4586-98.
97. Su, J.; Mazzeo, J.; Subbarao, N.; Jin, T., Pharmaceutical development of biologics: fundamentals, challenges and recent advances. *Therapeutic delivery* **2011,** *2* (7), 865-71.
98. Rathore, A. S., Roadmap for implementation of quality by design (QbD) for biotechnology products. *Trends in biotechnology* **2009,** *27* (9), 546-53.
99. (a) Kaltashov, I. A.; Bobst, C. E.; Abzalimov, R. R.; Wang, G.; Baykal, B.; Wang, S., Advances and challenges in analytical characterization of biotechnology products: mass spectrometry-based approaches to study properties and behavior of protein therapeutics. *Biotechnology advances* **2012,** *30* (1), 210-22; (b) Gilg, D.; Riedl, B.; Zier, A.; Zimmermann, M. F., Analytical methods for the characterization and quality control of pharmaceutical peptides and proteins, using erythropoietin as an example. *Pharmaceutica acta Helvetiae* **1996,** *71* (6), 383-94.
100. Office, C. B. *Research and Development in the Pharmaceutical Industry*; 2006.
101. Pharmaceutical Research and Manufacturers of America, P. *Key Industry and PhRMA Facts*; Pharmaceutical Research and Manufacturers of America, PhRMA: 2013.
102. Jiskoot, W.; Randolph, T. W.; Volkin, D. B.; Middaugh, C. R.; Schoneich, C.; Winter, G.; Friess, W.; Crommelin, D. J.; Carpenter, J. F., Protein instability and immunogenicity: roadblocks to clinical application of injectable protein delivery systems for sustained release. *Journal of pharmaceutical sciences* **2012,** *101* (3), 946-54.
103. Vaishya, R. D.; Khurana, V.; Patel, S.; Mitra, A. K., Controlled ocular drug delivery with nanomicelles. *Wiley Interdisciplinary Reviews: Nanomedicine and Nanobiotechnology* **2014**, n/a-n/a.
104. (a) Aungst, B. J., Intestinal permeation enhancers. *Journal of pharmaceutical sciences* **2000,** *89* (4), 429-42; (b) Gupta, S.; Jain, A.; Chakraborty, M.; Sahni, J. K.; Ali, J.; Dang, S., Oral delivery of therapeutic proteins and peptides: a review on recent developments. *Drug delivery* **2013,** *20* (6), 237-46 *review on recent development in oral protein delivery; (c) Park, K.; Kwon, I. C.; Park, K., Oral protein delivery: Current status and future prospect. *Reactive and Functional Polymers* **2011,** *71* (3), 280-287.

105. (a) Sakagami, M., Systemic delivery of biotherapeutics through the lung: opportunities and challenges for improved lung absorption. *Therapeutic delivery* **2013,** *4* (12), 1511-25 *Protein delivery through lungs. ; (b) Pisal, D. S.; Kosloski, M. P.; Balu-Iyer, S. V., Delivery of therapeutic proteins. *Journal of pharmaceutical sciences* **2010,** *99* (6), 2557-2575.
106. Sabaté, E., Adherence to Long-Term Therapies - Evidence for Action. World Health Organization: 2003. http://apps.who.int/medicinedocs/en/d/Js4883e/.
107. Yandrapu, S.; Kompella, U. B., Development of sustained-release microspheres for the delivery of SAR 1118, an LFA-1 antagonist intended for the treatment of vascular complications of the eye. *Journal of ocular pharmacology and therapeutics : the official journal of the Association for Ocular Pharmacology and Therapeutics* **2013,** *29* (2), 236-48.
108. Koenig, J., Does process excellence handcuff drug development? *Drug discovery today* **2011,** *16* (9-10), 377-81.
109. Wang, L.; Liu, Y.; Zhang, W.; Chen, X.; Yang, T.; Ma, G., Microspheres and microcapsules for protein delivery: strategies of drug activity retention. *Current pharmaceutical design* **2013,** *19* (35), 6340-52 *A comprehensive review focusing on strategies for protein activity retention.
110. Degim, I. T.; Celebi, N., Controlled delivery of peptides and proteins. *Current pharmaceutical design* **2007,** *13* (1), 99-117.
111. Sinha, V. R.; Trehan, A., Biodegradable microspheres for protein delivery. *Journal of controlled release : official journal of the Controlled Release Society* **2003,** *90* (3), 261-80.
112. Bittner, B.; Morlock, M.; Koll, H.; Winter, G.; Kissel, T., Recombinant human erythropoietin (rhEPO) loaded poly(lactide-co-glycolide) microspheres: influence of the encapsulation technique and polymer purity on microsphere characteristics. *European journal of pharmaceutics and biopharmaceutics : official journal of Arbeitsgemeinschaft fur Pharmazeutische Verfahrenstechnik e.V* **1998,** *45* (3), 295-305.
113. Johnson, O. L.; Cleland, J. L.; Lee, H. J.; Charnis, M.; Duenas, E.; Jaworowicz, W.; Shepard, D.; Shahzamani, A.; Jones, A. J.; Putney, S. D., A month-long effect from a single injection of microencapsulated human growth hormone. *Nature medicine* **1996,** *2* (7), 795-9.
114. Genta, I.; Perugini, P.; Pavanetto, F.; Maculotti, K.; Modena, T.; Casado, B.; Lupi, A.; Iadarola, P.; Conti, B., Enzyme loaded biodegradable microspheres in vitro ex vivo evaluation. *Journal of controlled release : official journal of the Controlled Release Society* **2001,** *77* (3), 287-95.
115. Fattal, E.; Couvreur, P.; Pecquet, S., [Oral tolerance induced by poly (lactide-co-glycolide) containing B lactoglobulin]. *Annales pharmaceutiques francaises* **2002,** *60* (1), 44-9.
116. Zhou, S.; Deng, X.; He, S.; Li, X.; Jia, W.; Wei, D.; Zhang, Z.; Ma, J., Study on biodegradable microspheres containing recombinant interferon-alpha-2a. *The Journal of pharmacy and pharmacology* **2002,** *54* (9), 1287-92.
117. Yeh, M. K., The stability of insulin in biodegradable microparticles based on blends of lactide polymers and polyethylene glycol. *Journal of microencapsulation* **2000,** *17* (6), 743-56.
118. Takenaga, M.; Yamaguchi, Y.; Kitagawa, A.; Ogawa, Y.; Mizushima, Y.; Igarashi, R., A novel sustained-release formulation of insulin with dramatic reduction in initial rapid release. *Journal of controlled release : official journal of the Controlled Release Society* **2002,** *79* (1-3), 81-91.
119. (a) Kang, C. E.; Baumann, M. D.; Tator, C. H.; Shoichet, M. S., Localized and sustained delivery of fibroblast growth factor-2 from a nanoparticle-hydrogel composite for treatment of spinal cord injury. *Cells, tissues, organs* **2013,** *197* (1), 55-63; (b) Sulabh Patel, R. V., Gyan

Prakash Mishra, Viral Tamboli, Dhananjay Pal, and Ashim K. Mitra, Tailor-made Pentablock Copolymer Based Formulation for Sustained Ocular Delivery of Protein Therapeutics. *Journal of drug delivery* **2014,** *In press*.
120. Mitra, A. K.; Mishra, G. P., Pentablock Polymers. Google Patents: 2011.
121. Sulabh P Patel, R. D. V., Dhananjay Pal, Ashim K. Mitra, Novel Pentablock Copolymer-Based Nanoparticulate Systems for Sustained Protein Delivery. *AAPS PharmSciTech* **2014**.
122. Lee, R. J.; Springer, M. L.; Blanco-Bose, W. E.; Shaw, R.; Ursell, P. C.; Blau, H. M., VEGF gene delivery to myocardium: deleterious effects of unregulated expression. *Circulation* **2000,** *102* (8), 898-901.
123. Geng, H.; Song, H.; Qi, J.; Cui, D., Sustained release of VEGF from PLGA nanoparticles embedded thermo-sensitive hydrogel in full-thickness porcine bladder acellular matrix. *Nanoscale research letters* **2011,** *6* (1), 312.
124. Feelders, R. A.; Hofland, L. J.; van Aken, M. O.; Neggers, S. J.; Lamberts, S. W.; de Herder, W. W.; van der Lely, A. J., Medical therapy of acromegaly: efficacy and safety of somatostatin analogues. *Drugs* **2009,** *69* (16), 2207-26.
125. (a) De Martino, M. C.; Hofland, L. J.; Lamberts, S. W., Somatostatin and somatostatin receptors: from basic concepts to clinical applications. *Progress in brain research* **2010,** *182*, 255-80; (b) Modlin, I. M.; Latich, I.; Kidd, M.; Zikusoka, M.; Eick, G., Therapeutic options for gastrointestinal carcinoids. *Clinical gastroenterology and hepatology : the official clinical practice journal of the American Gastroenterological Association* **2006,** *4* (5), 526-47.
126. Chanson, P.; Timsit, J.; Harris, A. G., Clinical pharmacokinetics of octreotide. Therapeutic applications in patients with pituitary tumours. *Clinical pharmacokinetics* **1993,** *25* (5), 375-91.
127. (a) Ghassemi, A. H.; van Steenbergen, M. J.; Barendregt, A.; Talsma, H.; Kok, R. J.; van Nostrum, C. F.; Crommelin, D. J.; Hennink, W. E., Controlled release of octreotide and assessment of peptide acylation from poly(D,L-lactide-co-hydroxymethyl glycolide) compared to PLGA microspheres. *Pharm Res* **2012,** *29* (1), 110-20; (b) Ibrahim, M. A.; Ismail, A.; Fetouh, M. I.; Gopferich, A., Stability of insulin during the erosion of poly(lactic acid) and poly(lactic-co-glycolic acid) microspheres. *Journal of controlled release : official journal of the Controlled Release Society* **2005,** *106* (3), 241-52; (c) Murty, S. B.; Goodman, J.; Thanoo, B. C.; DeLuca, P. P., Identification of chemically modified peptide from poly(D,L-lactide-co-glycolide) microspheres under in vitro release conditions. *AAPS PharmSciTech* **2003,** *4* (4), E50.
128. (a) Ghalanbor, Z.; Korber, M.; Bodmeier, R., Protein release from poly(lactide-co-glycolide) implants prepared by hot-melt extrusion: thioester formation as a reason for incomplete release. *International journal of pharmaceutics* **2012,** *438* (1-2), 302-6; (b) Zhang, Y.; Schwendeman, S. P., Minimizing acylation of peptides in PLGA microspheres. *Journal of controlled release : official journal of the Controlled Release Society* **2012,** *162* (1), 119-26; (c) Na, D. H.; Youn, Y. S.; Lee, S. D.; Son, M. W.; Kim, W. B.; DeLuca, P. P.; Lee, K. C., Monitoring of peptide acylation inside degrading PLGA microspheres by capillary electrophoresis and MALDI-TOF mass spectrometry. *Journal of controlled release : official journal of the Controlled Release Society* **2003,** *92* (3), 291-9; (d) Lucke, A.; Fustella, E.; Tessmar, J.; Gazzaniga, A.; Gopferich, A., The effect of poly(ethylene glycol)-poly(D,L-lactic acid) diblock copolymers on peptide acylation. *Journal of controlled release : official journal of the Controlled Release Society* **2002,** *80* (1-3), 157-68.
129. Qi, F.; Yang, L.; Wu, J.; Ma, G.; Su, Z., Microcosmic Mechanism of Dication for Inhibiting Acylation of Acidic Peptide. *Pharm Res* **2015**.

130. Wang, J.; Wang, B. M.; Schwendeman, S. P., Characterization of the initial burst release of a model peptide from poly(D,L-lactide-co-glycolide) microspheres. *Journal of controlled release : official journal of the Controlled Release Society* **2002,** *82* (2-3), 289-307.
131. Patel, S. P.; Vaishya, R.; Pal, D.; Mitra, A. K., Novel Pentablock Copolymer-Based Nanoparticulate Systems for Sustained Protein Delivery. *AAPS PharmSciTech* **2014**.
132. Patel, S. P.; Vaishya, R.; Yang, X.; Pal, D.; Mitra, A. K., Novel thermosensitive pentablock copolymers for sustained delivery of proteins in the treatment of posterior segment diseases. *Protein and peptide letters* **2014,** *21* (11), 1185-200.
133. Tamboli, V.; Mishra, G. P.; Mitra, A. K., Novel pentablock copolymer (PLA-PCL-PEG-PCL-PLA) based nanoparticles for controlled drug delivery: Effect of copolymer compositions on the crystallinity of copolymers and in vitro drug release profile from nanoparticles. *Colloid and polymer science* **2013,** *291* (5), 1235-1245.
134. Patel, S. P.; Vaishya, R.; Mishra, G. P.; Tamboli, V.; Pal, D.; Mitra, A. K., Tailor-made pentablock copolymer based formulation for sustained ocular delivery of protein therapeutics. *Journal of drug delivery* **2014,** *2014*, 401747.
135. (a) Na, D. H.; Murty, S. B.; Lee, K. C.; Thanoo, B. C.; DeLuca, P. P., Preparation and stability of poly(ethylene glycol) (PEG)ylated octreotide for application to microsphere delivery. *AAPS PharmSciTech* **2003,** *4* (4), E72; (b) Lucke, A.; Gopferich, A., Acylation of peptides by lactic acid solutions. *Eur J Pharm Biopharm* **2003,** *55* (1), 27-33.
136. Higuchi, T., Mechanism of Sustained-Action Medication. Theoretical Analysis of Rate of Release of Solid Drugs Dispersed in Solid Matrices. *J Pharm Sci* **1963,** *52*, 1145-9.
137. Korsmeyer, R. W.; Gurny, R.; Doelker, E.; Buri, P.; Peppas, N. A., Mechanisms of solute release from porous hydrophilic polymers. *International journal of pharmaceutics* **1983,** *15* (1), 25-35.
138. Hixson, A. W.; Crowell, J. H., Dependence of Reaction Velocity upon surface and Agitation. *Industrial and Engineering Chemistry* **1931,** *23* (8), 923-931.
139. (a) Gaudana, R.; Gokulgandhi, M.; Khurana, V.; Kwatra, D.; Mitra, A. K., Design and evaluation of a novel nanoparticulate-based formulation encapsulating a HIP complex of lysozyme. *Pharmaceutical development and technology* **2013,** *18* (3), 752-9; (b) Gaudana, R.; Khurana, V.; Parenky, A.; Mitra, A. K., Encapsulation of Protein-Polysaccharide HIP Complex in Polymeric Nanoparticles. *Journal of drug delivery* **2011,** *2011*, 458128; (c) Patel, A.; Gaudana, R.; Mitra, A. K., A novel approach for antibody nanocarriers development through hydrophobic ion-pairing complexation. *Journal of microencapsulation* **2014,** *31* (6), 542-50.
140. Shi, K.; Cui, F.; Yamamoto, H.; Kawashima, Y., Investigation of drug loading and in vitro release mechanisms of insulin-lauryl sulfate complex loaded PLGA nanoparticles. *Pharmazie* **2008,** *63* (12), 866-71.

VITA

Ravi D. Vaishya was born on 18th June 1986, in Ahmedabad, Gujarat, India. He completed his Bachelor of Pharmacy from Hemchandracharya North Gujarat University in 2007. After completion of his B. Pharm. degree, he joined the Interdisciplinary Ph.D. program at UMKC in January 2008 to pursue a Ph.D. degree in Pharmaceutical Science and Chemistry. He is an active member of American Association of Pharmaceutical Scientists (AAPS), Association of Research in Vision and Ophthalmology (ARVO) and Pharmaceutical Sciences Graduate Student Association (PSGSA). He served as the Treasurer of PSGSA student chapter, UMKC, for one year. He completed his doctoral studies in April 2015 under the guidance of Dr. Ashim K. Mitra. He has authored/co-authored several peer reviewed publications and book chapters, and has presented his work in a number of international and national conferences such as AAPS, ARVO and PGSRM.